Early Age and Durability Study of the Bond Strength on the Interface between UHPC – HSC

by

Li Xin Tan

A Thesis

Submitted to the Faculty of Graduate Studies of

The University of Manitoba

in partial fulfilment of the requirements for the degree of

MASTER OF SCIENCE

Department of Civil Engineering

University of Manitoba

Winnipeg, Manitoba

Abstract

This thesis explores the bond performance of the interface between UHPC and high strength concrete. The aim of the experimental work is to define some of the transverse shear transfer parameters, such as the cohesion and friction coefficient at the interface between the shear key filler material and adjacent precast box beams on bridge design.

The four test methods used to quantify the short- and long-term bond performance include the direct tension, pull off, slant shear and bi-shear tests. The study emphasizes on evaluating the interfacial bond performance between the materials using small-scale specimens. The variables in the experiments consist of the age of UHPC, the exposure to the freeze-thaw cycles as well as number of cyclic loadings. A total of five interface parameters were evaluated, namely, the roughness average, mean texture depth, mean profile depth, true surface area and interfacial area ratio on direct tension test specimens. The Mohr-Coulomb's and Carol's approaches were adopted to construct the failure envelope and the experimental results were subsequently used to estimate the cohesion and friction coefficients at the bond interface.

The overall interface bond performance of the small-scale specimens was satisfactory. The direct tensile and slant shear strength exceeded the minimum bond strength as specified in ACI 546 (2006). The correlation between the interface parameters, modes of failure and direct tensile strength showed mixed results. Further research will be needed to establish the relationship between the variables.

Acknowledgements

I would like to express my deepest gratitude to my advisor, Dr. Dagmar Svecova for the guidance and being unconditionally supportive throughout the project.

I would like to thank Dr. Ali Semendary, Dr. Chad Klowak, Dan Szara, Sam Abraha and Geoff Cao for the technical assistance and sharing valuable insight. Thank you for all the hard work and commitment to make this project a success.

I would also like to acknowledge and thank Dr. Graziano Fiorillo and Dr. Amir Ghatefar for being in the advisory committee.

Thanks to Manitoba Infrastructure for providing us the opportunity to take on this research project and a very special thanks to Evangeline Murison for going the extra mile to help with the project. I would also like to thank Lafarge for accommodating our requests and assisting with the test specimen's placement.

Table of Contents

List of Figures

List of Tables

1. Introduction

Over the last few decades, the application of ultra-high performance concrete (UHPC) in bridges and structures has been increasing significantly due to its exceptional mechanical and long-term durability properties. Common applications of UHPC in North America include superstructure connections in the bridge overlay and shear key system, as well as the rehabilitation of infrastructures (Harris et al. 2014, Haber et al. 2018). The implementation of UHPC in the shear keys of the bridges leads to the elimination of post-tensioning tie and rods, while at the same time enables shear, moment, axial tension and axial compression forces to be transferred between adjacent beams or girders (Yuan and Graybeal 2016). In Canada, 110 bridges were constructed from year 2009 to 2019 using UHPC either as components, connections or repair materials (Federal Highway Administration 2019); only three bridges with UHPC connections were constructed in Manitoba in 2014 and 2019.

Although researchers have extensively explored the potential and compatibility of UHPC in bridge design, there is no design specification or standard test method currently available that assesses and/or quantify the performance of the designed cementitious material. The lack of information regarding the UHPC material properties and compatibility with other concrete materials may further hinder the material selection process for designers.

1.1. Overview and Background

In collaboration with the provincial regulatory body, Manitoba Infrastructure (MI), the University of Manitoba undertook the research project to address some of the knowledge gap that was required in designing bridge shear key. This project involved constructing and instrumenting,

along with material testing of the first precast box girder bridge in Manitoba that used UHPC as a filler material in shear key design.

WSP engineering consulting firm was the industry partner for this project and has provided the detailed precast box girder and UHPC shear key bridge design. A comprehensive monitoring system was proposed and implemented to study the static and dynamic structural behaviour of the conglomerated high strength concrete (HSC) precast box girder connected longitudinally with UHPC shear keys and lap splice dowel bars.

1.2. Scope and Objectives

The main objective of this research was to investigate the bond interface performance between the UHPC and the precast box beam bridge shear keys under varied load conditions. To successfully attain the objective of this project, the experimental work was divided into two phases:

1. Small-scale specimens preparation and testing
    a. Cast small-scale specimens at the Lafarge precast fabricating plant and bridge construction site.
    b. Tested specimens at the at the W.R. McQuade Structures Laboratory at the University of Manitoba.
    c. Defined the parameters affecting the bond performance.
2. Bridge capacity evaluation
    a. Installed strain gauges and thermocouples within the bridge components.

b. Collected strain and temperature data periodically from the bridge data acquisition system.
c. Compared the experimental strain from laboratory test results with the on-site strain gauge readings and evaluated if interface at the bridge was cracked.

The second phase of the project was not within the scope of study in this thesis.

The two main parts in the first phase of the experimental program included examining of the shear keys short-term performance, investigating the bond strength of the interface between precast concrete and UHPC material with different modes of failure, as well as determining the durability performance at the bond interface.

The goal for this research is to provide bridge designers with shear key design parameters such as the cohesion values and shear, as well as to obtain a better understanding of the UHPC behaviour and its compatibility with HSC.

1.3. Thesis Organization

This thesis consists of five chapters, that is: the introduction, literature review, experimental program, results and discussion and finally, the conclusions and recommendations. Below are the details of the organization:

- Chapter 1 introduces the project and defines its scope and objectives.
- Chapter 2 provides related analysis and findings from previous research.
- Chapter 3 outlines the process and procedure of the experimental program.
- Chapter 4 delivers the results and data analysis from the experiments.

- Chapter 5 presents the conclusions and recommendations drawn from the experimental program.

2. Literature Review

The following literature review presents the existing research related to the evaluation of the performance of UHPC used in various applications – focusing on the shear key interface bond performance under different loading conditions. Emphasis was given to the load transfer mechanism in precast box girder in bridge design, test method and types of stresses in the adjacent beam interface, interface bond performance between UHPC and several cementitious materials, and the durability study on the bond interface between UHPC and other concrete materials.

2.1. Load Transfer Mechanism and the Interfacial Stresses in Box Beam Bridges

In the past, cementitious grout was commonly used in the keyway of precast concrete box beam. However, as reported by several researchers, longitudinal cracks in the grout materials as well as in the interface between the precast members and keyway were frequently observed (Gulyas et. al 1995, Lall et al. 1998, Miller et al. 1995). Every so often the leaking keyways have caused premature bridge deterioration due to salt attack and subsequently the keyway lost its bond with the precast girders. The failing of the joints did not only diminish the efficiency of load transfer between individual precast girders, but it also accelerated the corrosion in the steel reinforcement (Huckelbridge et al. 1995).

To tackle the issue, transverse post tensioning duct and tie coupled with the use of grout materials in both full-depth and partial-depth shear keys was introduced. The compression force

from transverse post tensioning along the sides of the beams was expected to reduce the possible cracking in the grout material due to shear and bending induced by material shrinkage, moving traffic loads (Hanna et. al 2009), as well as mitigating tensile stresses across the joint (Russell 2011). El-Remaily et al. (1996) and Hanna et al. (2009) have also suggested that the transverse post tensioning of the beam diaphragms was the main transverse load distribution path for the live loads (Yuan and Graybeal 2016).

Initially, this type of construction method was very well received by the industry due to its ease and speedy construction (Grace et. al 2012, Yuan and Graybeal 2016). As time went by, similar issues with the longitudinal shear keys degradation were observed for this type of bridge configuration. The cracking and debonding of the shear keys have led to premature bridge deterioration and reduced its practicability and efficiency due to compromised load transfer between the adjacent beams.

Gulyas et al. (1995) and Grace et al. (2012) have reported that the transverse post tensioning stress on the diaphragms of the box beam girders can be dissipated along the transverse width of the bridge, resulting in nonuniform pressure on the sides of the box beams and high stresses localized at the end spans. Instead of implementing the transverse post-tensioned duct and tie, the effectiveness of the transverse load distribution of the box beam bridges was highly dependent on the bond between the grout and the adjacent box beams.

2.1.1. Geometry Design and Properties of UHPC Shear Keys in Box Beam Bridges

Although bridge shear keys are widely used for joining adjacent bridge components to ensure monolithic behaviour, there is no established standardized shear key design guidance.

There are two clauses in the AASHTO (2017) standard that have specified the longitudinal joint dimensions and grout material strength if used in precast concrete bridges. Clause 5.12.2.3.2 specifies the depth of the shear transfer joints should not be less than 7 in (178 mm) and shall be modelled and analyzed as hinges without moment resistance. Also, the code specifies the minimum compressive strength of the nonshrinking grout shear key fillers to be 5.0 ksi (34.5 MPa) within 24 hours. For longitudinal joints resisting flexural forces, AASHTO (2017) Clause 5.12.2.3.3 specifies the shear key depth greater than 5 in (127 mm) and filled with nonshrinkage mortar of 5 ksi (34.5 MPa) minimum compressive strength within 24 hours. When transverse post-tensioning is required at longitudinal joints, Clause 5.12.2.3.3c specifies the minimum value to be 0.25 ksi (1.7 MPa). Post-tensioning of the precast components is encouraged to ensure monolithic bridge behaviour. As reported by Yuan et al. (2018), there is no specification on the design detail of the shear keys, nor is the calculation of the transverse forces provided in AASHTO (2017).

JSCE (2007) indicates that cracks are often observed when mortar is used in the joint due to shrinkage and creep. Therefore, the small width of mortar joints between 10 and 60 mm should be used. As for concrete joint, the width of the shear key shall be designed by taking into consideration the tensile reinforcement. JSCE (2007) references Figure 2-1 when designing the shear keys.

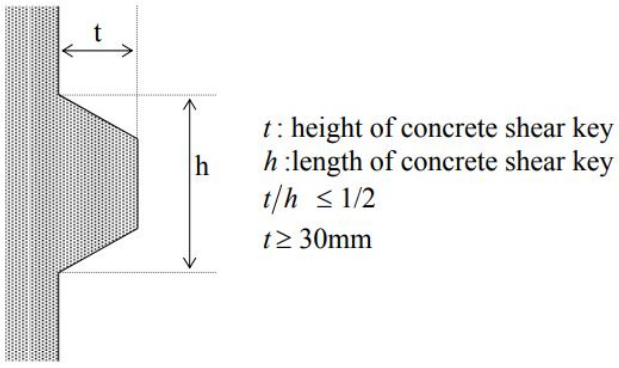

Figure 2-1 JSCE 2007 shear key dimensions

Federal Highway Administration (2014) demonstrated the first successful prestressed box beam bridge in the US to use UHPC as filler material in the shear keys. The design of the shear keys for the 18.6 m span bridge conformed with AASHTO (2017) specification of 7 in (178 mm) in height, 6 in (152 mm) wide and with dowel bars protruding 4.75 in (121 mm) outside of the concrete on both sides of the precast box girder. There was no transverse post-tensioning and cast-in-place top slab that conventionally ensures proper load transfer between adjacent girders.

Yuan et al. (2018) investigated the performance of post-tensioned, full- and partial-depth conventional grouted connections, as well as the transversely reinforced, full- and partial-depth UHPC shear keys of box beam bridge. The conventional grouted connections were coupled with transverse post-tensioning, while no transverse post-tensioning was applied to the UHPC shear keys. The surface of the UHPC shear key was treated by painting retarder and exposing the aggregate, while the conventional grouted connection surface was sandblasted. The partial-depth UHPC shear key was 7 in (178 mm) deep and 6 in (152 mm) wide with 1.5 in (38 mm) opening. The top full-depth UHPC shear key is 6.813 in (173 mm) deep, 5.25 in (133 mm) wide, with 0.75 in (19 mm) top and bottom opening. The bottom shear key is 8.63 in (219 mm) deep,

5.25 in (133 mm) wide with the top opening connected to the bottom opening of the top shear key. The study has found that both partial and full-depth UHPC shear key did not crack during the thermal and loading cycles. The moment distribution and differential deflection of both partial- and full-depth UHPC shear key were comparable to the conventional grout connections with the same boundary conditions. The partial-depth UHPC shear key was found to suffice the performance requirements.

Hussein et al. (2018) evaluated the optimum shape and size of UHPC filled shear keys in adjacent high strength box girder bridges, by taking into account both the economical aspect and structural performance. The authors have evaluated 14 different shapes and sizes of shear keys using finite element modelling and compared them to the results obtained from experimental results. The authors have established an optimum shear key shown in Figure 2-2, that exhibited good flexural and direct tension performance. The width and height of the shear key were found to significantly affect the direct shear performance, while the flexural capacity of the shear key was highly affected by its height. The cross-sectional area of the shear key did not affect the direct tension, flexural nor the direct shear performance of the shear key.

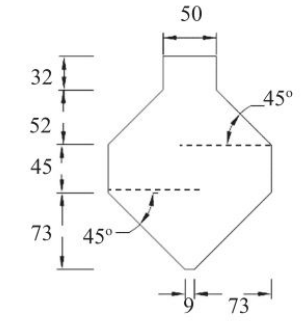

Figure 2-2 Optimum shear key (Hussein et al. 2018)

2.1.2. Shear Design Expressions from Codes and Standards

The main shear transfer mechanism along the plane interface is controlled by cohesion, friction and aggregate interlock. The shear transfer capacity of concrete depends on the compressive force on the shear plane, surface roughness, compressive strength of the concrete and confining forces from shear reinforcement (AASHTO 2017, JSCE 2007, CSA S6 2019). As the roughness of an interface decreases, the interlocking effect decreases, and friction becomes the controlling factor. In JSCE (2007) Clause 9.2.2.5, states that the effect of surface roughness is smaller in HSC because the strength of the aggregate is the limiting factor to the ultimate concrete strength.

The Canadian Standards Association (CSA) assumes load transfers from adjacent beams through transverse shear, and flexural rigidity is neglected (Yuan et al. 2018). CSA Canadian Highway Bridge Design (S6), Clause 8.9.5.1 indicates that the shear resistance of a shear plane shall be maintained by the cohesion and friction of the materials, and cracks are assumed to be occurring on the shear plane. The interface shear transfer can be calculated as:

Equation 2-1 $$v_r = \lambda_1 \emptyset_c (c + \mu\sigma) + \emptyset_s \rho_v f_y \cos\alpha_f$$

Where λ_1 is the concrete density dependant parameter, $\emptyset_c$ is the concrete resistance factor, c is the cohesion value, μ is the friction coefficient, σ is the counterbalanced compressive stress acted on the interface due to the tension in the reinforcement induced by the perpendicular interface separation, $\emptyset_s$ is the steel resistance factor, ρ_v is the area of vertical reinforcement and concrete cross sectional area ratio, f_y is the steel reinforcement yielding strength and α_f is the angle between the shear reinforcement and the shear plane. The first part of the equation

represents the friction and cohesion of the surface as a function of the material properties and the surface treatment of interface contact point, while the latter part of the equation is derived from dowel action of the shear reinforcement. Table 2-1 presents the coefficients of friction and cohesion based on the surface preparation of the concrete.

Table 2-1 Coefficient of friction and cohesion factor on different surfaces (CSA S6 2019)

Parameters	Concrete placed against clean surface of a hardened concrete	Concrete placed against clean and roughened surface to amplitude of 5 mm with spacing of 15 mm of a hardened concrete	Concrete placed monolithically
c (MPa)	0.25	0.50	1.00
μ	0.60	1.00	1.40

AASHTO (2017) specifies the interface shear reinforcements to extend both sides of the interface to a development length that is enough to achieve the yield stress. The nominal interface shear resistance is provided as follows:

Equation 2-2 $$V_{ni} = cA_{cv} + \mu\left(A_{vf}f_y + P_c\right)$$

Equation 2-3 $$For\ V_{ni} \leq K_1 f'_c A_{cv}$$

Equation 2-4 $$V_{ni} \leq K_2 A_{cv}$$

Where V_{ni} is the nominal interface shear resistance in kip, A_{cv} is the area of concrete of the point of contact, P_c is the compressive force normal to the shear plane, K_1, K_2 are limiting factors for the interface shear resistance in ksi and the rest of the variables are as defined previously. The code assumes that the confining force exerted on the concrete by the interface shear reinforcement is directly proportional to the friction coefficient. The K_1 factor is defined to prevent crushing or shearing of aggregate on the shear plane, while K_2 in Equation 2-4 takes into

account of the variability of the K_1 factor. Table 2-2 presents the cohesion and friction coefficients on the concrete surfaces as listed in AASHTO (2017).

Table 2-2 Coefficient of friction and cohesion factor on different concrete surfaces (AASHTO 2017)

Parameters	Cast-in-place concrete slab placed against clean and roughened to 0.25 in (6.35 mm) amplitude concrete girder surface	Normal weight concrete cast monolithically	Lightweight concrete placed monolithically, or against clean and roughened to 0.25 in (6.35 mm) amplitude concrete surface	Normal weight concrete placed against clean and roughened to 0.25 in (6.35 mm) amplitude concrete surface	Concrete placed against not roughened, clean concrete surface	Concrete anchored to clean and free of paint as-rolled structural steel
c in ksi (MPa)	0.28 (1.93)	0.40 (2.76)	0.24 (1.65)	0.24 (1.65)	0.075 (0.52)	0.025 (0.17)
μ	1.0	1.4	1.0	1.0	0.6	0.7
K_1 in ksi (MPa)	0.3 (2.07)	0.25 (1.72)	0.25 (1.72)	0.25 (1.72)	0.2 (1.38)	0.2 (1.38)
K_2 in ksi (MPa)	1.8 (12.41) for normal weight & 1.3 (8.96) for lightweight concrete	1.5 (10.34)	1.0 (6.89)	1.5 (10.34)	0.8 (5.52)	0.8 (5.52)

Santos and Júlio (2012) compiled the shear-friction research studies on concrete-to-concrete interface presented by previous researchers from 1960 to 2009. The shear-friction theory only applies to the interface shear strength that was assumed to be controlled by the surface cohesion, dowel action and friction. The authors identified several design codes in the Europe and North America, such as the Eurocode 2 Design of Concrete Structures, ACI 318 Building Code Requirements for Structural Concrete, CSA A23.3 Design of Concrete Structures and AASHTO LRFD Bridge Design Specification. They utilized the shear-friction theory with three assumptions: (1) shear forces are transferred by friction, (2) all tensile forces on the interface are absorbed by the steel reinforcement, and (3) concrete tensile strength is neglected. Depending on the design codes, the coefficient of cohesion and friction are assessed based on the different classification of the concrete surface roughness. In the compilation of the literature review, the effect of concrete curing conditions and concrete strength differential were often not included in the design approaches – such as the ACI 318, AASHTO LRFD and Eurocode 2 – for shear-friction and/or cohesion between two concretes.

Espeche and León (2011) presented a criterion to estimate the bond strength between old and new concrete based on the failure envelope developed using the theory of plasticity. The three main parameters for constructing the failure envelope included the interfacial tensile strength (f'_t), friction angle ($\emptyset'$) and cohesion (c'). In-situ tests, pure shear and, shear and compression tests, and direct and indirect tension tests were commonly used in assessing the parameters of the failure criterion. Table 2-3 shows the $\emptyset'$ is the determining parameter of the sliding failure criterion, and it was estimated based on the roughness of the surface.

Table 2-3 Quantitating friction angle to degree of roughness (Espeche and Leon 2011)

Roughness Degree	Surface Treatment Description	$\emptyset'(°)$
Low	Natural wooden mould, saw-cut surface	37-40
Medium	Sandblasted, steel brushed	43-46
High	Splitting, waterjetting, hammering with energy control	50-53

The authors also presented the Mohr-Coulomb's (Equation 2-5 and Equation 2-6) and Carol's (Equation 2-7 to Equation 2-9) approach to estimate the cohesion and friction coefficient. Equation 2-5 also presents the simple relationship between shear, normal stress, cohesion and friction angle without the tension influence from the dowel bars. The Mohr-Coulomb's approach took into account the shear and normal stresses from slant shear test and the cohesion value was taken as the tensile test value, while the Carol's approach utilized the cracked envelope with the assumption of no tensile stress being applied when the interface was subjected to low normal compression stress. The Carol's approach used the shear and normal stress values from slant shear tests, and direct shear value. The ratio of the predicted cohesion values and splitting tensile strength using the Carol's failure criterion were between 1.75 and 2.0.

Equation 2-5 $$\tau = c - \sigma \tan \emptyset$$

Equation 2-6 $$\mu = \tan \emptyset$$

Equation 2-7 $$\tau = \sqrt{(c - \sigma \tan \emptyset)^2 - (c - f'_t \tan \emptyset)^2}$$

Equation 2-8 $$c = \left(\frac{2 - \sin \emptyset}{\cos \emptyset}\right) f'_t \text{ for } \emptyset > 30°$$

Equation 2-9 $$c = \sqrt{3} f'_t \text{ for } \emptyset \leq 30°$$

Where τ is the shear stress at the interface, σ is the normal stress at the interface (negative value for compression) and the other variables are defined previously.

Zanotti and Randl (2019) performed various tests to evaluate the bond performance between normal strength concrete (NSC) and HSC with and without fiber reinforcement. The tests conducted included direct and splitting tensile, pull off, slant shear and direct shear tests. The Carol's failure criterion approach yielded consistent ratio of extrapolated cohesion value and direct shear strength for the specimens, in the range of 0.84 and 0.96.

2.1.3. Interface Roughness

The friction coefficient is a function of the angle of friction with the shear plane, and it depends on the degree of surface roughness of the interface between the two cementitious materials. The surface roughness controls the perpendicular interface separation as indicated in most of the design codes and standards (AASHTO 2017, JSCE 2007, CSA S6 2019, ACI 318 2014). Particularly, ACI 318 (2014) and AASHTO (2017) have specified 0.25 in (6 mm) amplitude, and CSA specifies 5 mm amplitude as one of the criteria for characterizing the cohesion and friction coefficient for intentionally roughened concrete surface to ensure effective horizontal shear transfer. Nonetheless, without further information, the sole requirement for determining the friction coefficient and cohesion value of the concrete surfaces based on amplitude can be inconsistent. Parameters such as the macro and micro texture of materials between the two bonding materials are frequently mentioned to have an significant impact on the concrete bond performance.

Perez et al. (2009) have indicated several profile parameters, such as the arithmetical mean deviation (roughness average, R_a), mean spacing between profile peaks at the mean line, ratio of real surface and projected surface (I_{ss}), profile depth excluding extreme elevation and mean angle of the profile to evaluate the bond performance between NSC and repair material. The optical profilometry utilized has 0.55 mm/pixel x 0.55 mm/pixel resolution. According to the authors, the R_a and I_{ss} were some of the more common parameters to evaluate the concrete profile roughness. Their test results have showed that neither R_a nor I_{ss} correlated well with the direct tensile strength, and the direct tension bond performance was most likely to be affected by the micro-roughness compared to macro-roughness.

Santos and Júlio (2013) compiled the roughness evaluation methods for concrete surfaces. The roughness parameters studied were the R_a root-mean-square roughness, mean and maximum peak height, mean and maximum valley depth, mean and maximum peak-to-valley height and total roughness height. Although R_a is the most used roughness parameter in quantifying the surface roughness, it is not an accurate nor a proper quantitative tool to evaluate the surface condition of a material. As shown in Figure 2-3, the three roughness profiles produced the same R_a values – materials with different surfaces may exhibit similar R_a value. The methods of assessment reviewed included quantitative and qualitative evaluations. The quantitative evaluation methods included the sand patch test, outflow meter, mechanical stylus, circular track meter, digital surface roughness meter, microscopy, slit-island method, roughness gradient method, photogrammetric method, shadow profilometry, processing of digital image (PDI) method, 2D laser roughness analyzer (LRA) method and 3D laser scanning method, while the

qualitative evaluation methods included the concrete surface profiles visual inspection, ultrasound method and air leakage method. Quantitative evaluation methods are preferred to the qualitative evaluation methods. The current design code adopts qualitative assessment method such as visual inspection, which is subjective and can differ from person to person. It is known that the concrete-to-concrete bond performance is more dependent on the micro-texture than the macro-texture; the optical and electron microscopy, and laser based profilometer are methods of analysis that can accurately measure the internal micro texture of the concrete.

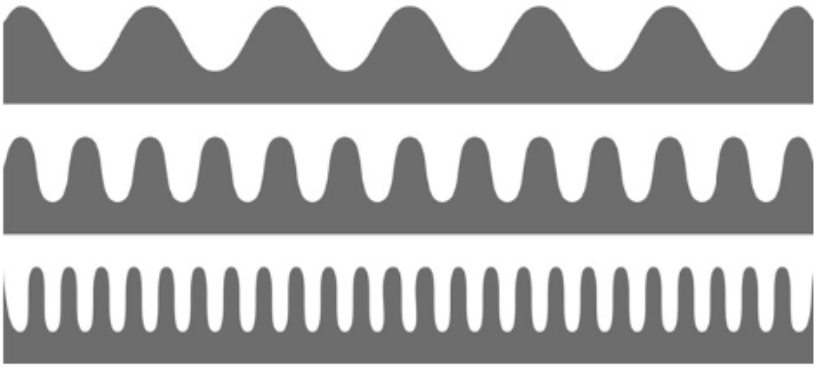

Figure 2-3 Types of surface profile with same R_a (Santos and Julio 2013)

As presented by Liu (2015), the author examined the feasibility of replacing the use of 2D amplitude parameters such as MPD and root mean square roughness, with 3D surface parameters to analyze pavement texture. It was found that the combination of simulated MTD, skewness and kurtosis can be used to quantify the road friction and pavement sound intensity noise. One of the field tests revealed R^2 values of 0.71 and 0.53 between simulated MTD and skewness, and pavement sound intensity noise and friction, respectively.

2.2. Bond Interface Studies: UHPC/High Performance Concrete Compatibility

UHPC is typically used as material for precast connections in building and bridge construction. The evaluation of bond performance between UHPC and several types of material is critical to ensure adequate material application. The modulus of elasticity differential in the material was deemed to be one of the main issues that could potentially cause irregular stress distribution. However, the high mechanical performance of UHPC is seen to be capable of compensating for this effect (Haber and Graybeal 2018).

Due to the low binder to water ratio, UHPC is prone to early age shrinkage, surface drying and cracking as the water evaporates rapidly from the surface. It was commonly known that early age longitudinal cracking at the shear key is contributed by material shrinkage induced high tensile strain – causing vertical separation at the bond interface of the bridge longitudinal connection (De la Varga et al. 2018). Yoo et al. (2013) have conducted a study on the early age performance of UHPC. The parameters in the study included the early age setting, shrinkage and tensile characteristics of the cementitious materials. The authors have defined the time zero for UHPC autogenous shrinkage as the time when the penetration resistance of the concrete reaches 1.5 MPa, which was also 0.6 hours after the initial setting time, and 2.1 hours before final setting time. The autogenous shrinkage measured from time zero to day 15 was 613 με, which was translated to approximately 24.5 MPa tensile stress with 40 GPa tensile elastic modulus. The first crack in the UHPC was observed at 40% of the post cracking strength which was around 8 MPa.

Sprinkel and Ozyildirim (2000) performed pull off tensile tests on 16 types of high performance concrete overlays. The types of high performance overlays were constructed using combination

of different proportion from the following materials: silica fume, slag, class F fly ash, latex-modified concrete, Rheocrete corrosion-inhibiting admixture (CIA), Armtex CIA, ACI topical treatment, Darex CIA, Postrite topical treatment, shrinkage-reducing admixture, polyolefin fibers, steel fibers and polypropylene fibers. The bond strength of the materials that is estimated by using the pull off test can be considered very good if the value is between 1.7 MPa and 2.1 MPa, and excellent if the value exceeds 2.1 MPa.

Carbonell Muñoz et al. (2014) have reported that the bond performance of UHPC on saturated NSC with brushed, sandblasted, grooved and aggregate exposed surfaces have exceeded the recommended bond strength capacities by ACI 546 (2006) as listed in Table 2-4. The saturated concrete provides water for further hydration in the UHPC, and therefore, strengthening the bond performance at the transition zone. The slant shear and pull off tests were performed in accordance with ASTM C882 (2012) and ASTM C1583 (2004), respectively. Both of the results showed positive outcome, where in most cases specimens achieved ACI 546-06 requirements.

Table 2-4 Slant shear and direct tensile bond strength characterization (ACI 546 2006)

Test Method	Bond strength on day 1 (MPa)	Bond strength on day 7 (MPa)	Bond Strength on day 28 (MPa)
Slant Shear	2.8 – 6.9	6.9 – 12	14 – 21
Direct Tensile	0.5 – 1	1 – 1.7	1.7 – 2.1

Hussein et al. (2016) have reported the adhesion value of UHPC with smooth (cut) surface HSC, cohesion value of UHPC with midrough (sandblasted) surface and rough surface (exposed aggregate) of HSC, using the direct tension test in accordance with ASTM C1404 (1998 (2003)). The term: “cohesion” or “adhesion” used in the paper depended on the failure location of the

specimens: failure loads recorded for specimens that have failed at the bond interface were denoted by “adhesion”, while the other types of failure were identified as cohesion failure. As shown in Table 2-5, the friction coefficients were then back calculated using the Mohr-Coulomb theory. It was observed that the bond interface of some of the midrough and rough specimens failed in the HSC instead of directly at the bond interface, indicating that the interface bond strength is higher than the material strength. The authors have deduced the reason for obtaining higher bond strength using the direct tension test in the study compared to the pull off tests as presented by Carbonell et al. (2013) and Tayeh et al. (2014) was that the tensile stress applied was partially dissipated as shear stress on the epoxy between the molds and the specimens. Hence, the actual load carried by the specimens was lower than the load applied, consequently resulting to a higher ultimate direct tensile strength recorded.

Table 2-5 Adhesion, cohesion and friction coefficients obtained from the study (Hussein et al. 2016)

Interface Roughness	Adhesion (MPa)	Cohesion (MPa)	Friction Coefficient
Smooth	3.02	-	0.44
Midrough	-	5.01	1.09
Rough	-	5.63	1.44

De la Varga et al. (2018) presented some of the techniques used in improving the shrinkage and bond performance of concrete of 55 MPa compressive strength and UHPC. The shrinkage of the material was evaluated in sealed and drying conditions. A total of approximately 450 με shrinkage over six-month period was observed in both of the conditions in the UHPC. Pull off tests with three surface roughness were performed to assess the materials’ tensile bond performance. An average of 3.85 MPa bond strength was recorded during the testing of the high aggregate

exposure level. The authors have indicated three main reasons for the high tensile strength observed: less air entrapped in the interface between the UHPC and concrete due to highly flowable material properties, fine particle material composition that led to particle packing and dense microstructure, and lower level of shrinkage. The pull off bond strength obtained with low level of aggregate exposure was 90 % of the bond strength of specimens with high level of aggregate exposure.

Haber et al. (2018) conducted flexural beam and pull off tests on different classes of UHPC and 43 MPa precast concrete with exposed aggregate surface to evaluate the bond performance between the two materials. Both of the tests were performed on day 7 and 14 after the UHPC was cast. The only mode of failure observed in the flexural beam tests was failure in the precast concrete, with average tensile stress of 3.64 MPa and 3.9 MPa on day 7 and day 14, respectively. The average bond strength on day 7 in the pull off test was 2.76 MPa, and 2.84 MPa on day 14. The authors have found that the age of UHPC has no significant effect on the bond strength.

Semendary et al. (2019) investigated the direct tensile bond performance between UHPC and HSC with compressive strength of 56 MPa. The tests were performed on smooth, as cast and exposed aggregate HSC surfaces. The average of the tensile strength of the exposed aggregate interface specimens for days 3, 5, 7, 28 and 91 were 1.37 MPa, 1.72 MPa, 1.79 MPa, 2.32 MPa and 2.23 MPa respectively. The mode of failure observed in the first four tests was partial interface failure (PIF) with concrete debonding and aggregate fracture, while only the aggregate fracture and substrate failure occurred on day 90. The tensile strength of the specimens can be related to the percentage of the exposed aggregate at the interface. The average tensile strength

of the smooth and as-cast specimens was 1.7 MPa and 2.0 MPa, respectively, which is approximately 80 % the tensile strength of the exposed aggregate specimens.

Semendary and Svecova (2020a) investigated some of the factors affecting the UHPC bond performance between HSC and NSC, that includes the types of tests, age of UHPC, types of substrate and the interface conditions. The exposed aggregates surface texture on the specimens has a mean profile depth of 2.39 mm and 1.96 mm on the NSC and HSC specimens, respectively. The test results from the experiments showed using crushed stone in HSC has increased the bond strength in the direct tension tests. A larger increase in bond strength was observed between UHPC day 3 and day 7. The saturated interface conditions improved the consistency of the results for the pull off tensile strength on day 28. No conclusion was drawn on the effect of interface conditions in bi-shear tests due to large coefficient of variation and small sample size. While the slant shear test results showed that the interface conditions have no significant effect on the bond strength, the authors have indicated that the geometry and material properties of the slant shear test specimens are more likely to affect the bond performance.

Semendary and Svecova (2020b) performed pull off, bi-shear and slant shear tests to analyze the effect of UHPC age on the bond performance with HSC. In the pull of tests, the mode of failure shifted from UHPC failure on day 3, to bond interface failure on day 7 and to HSC failure on day 14 and 28. A gradual increase in mean pull off strength from 1.9 MPa to 3.6 MPa was observed. Mixed mode of failure was observed in the bi-shear tests and no trend in the mean bi-shear test results was observed. The minimal displacement of the specimens recorded during the bi-shear tests indicated that abrupt failure has occurred. The slant shear tests showed increase in bond

strength with the increase of UHPC age, as well as shifting from UHPC failure on day 2 to HSC failure for the rest of the tests. The cohesion obtained in the experiments ranged between 3.2 MPa and 6.5 MPa, with the lowest occurring on day 2 and the highest occurring on day 7. The friction coefficient obtained based on pull off data ranges between 1.37 and 1.52, while it is between 1.07 and 1.37 based on bi-shear test results. The values well exceeded the values provided by AASHTO LRFD – 1.65 MPa and 1 for cohesion and friction coefficients, respectively.

2.3. Durability Studies

As mentioned in the study by Grace et. al (2012), not only were the longitudinal cracks observed on bridge deck results from live loads, the stresses induced from differential temperature also play a significant role in the deterioration of the shear keys.

UHPC is widely known for its superior mechanical and durability properties that is contributed from particle packing, low water to binder ratio and dense microstructure. As reported by Haber et al. (2018), the five UHPC materials that were investigated showed high resistance to the freeze-thaw (FT) cycles – little to no drop in the relative modulus of elasticity and mass loss in the material was observed after 600 FT cycles assessed in accordance with ASTM C666 Procedure A with specimens submerging in a water bath temperature cycling between -18 ºC and 4 ºC.

As reported by Zhou and Qiao (2018), UHPC is more durable than conventional concrete and hence, short term conditioning does not have adverse effects on the material. The authors have found that the decreasing trend of the tangent modulus of elasticity of UHPC initialized after 300 to 600 cycles and the peak tensile strength started to decrease after 600 cycles.

Hasnat and Ghafoori (2021) investigated the compressive strength, splitting tensile strength and mass loss of 30 non-proprietary UHPC materials after 70 FT cycles. In the literature review provided, the authors have summarized some of the recent FT research performed using either proprietary or non-proprietary UHPC. Most of the tests showed no degradation or only marginal mass loss was observed in the specimens even after 1500 FT cycles. In the study, the specimens underwent temperature cycling between -18 °C and 20 °C, with 18 hours halt at the minimum and maximum temperature for every cycle. The test results showed an average of 25 % increase in compressive strength, 18 % in splitting tensile strength and 0.27 % mass loss after 70 FT cycles.

Although UHPC possesses superior durability properties, the difference in the coefficient of thermal expansion between UHPC and other concrete materials poses a potential risk to the durability at the interface. It may lead to a reduction of interface bond strength as a result of the thermal movement. However, at this time, very little research work is available in literature specifically on the FT interface bond performance between UHPC and other cementitious materials.

In a previous study conducted by Lee et al. (2005), a reduction of 6 % in compressive strength in reactive powder concrete (RPC) after 1000 FT cycles in air in accordance with ASTM C666 with temperature cycles ranging between -18 ºC to 4 ºC, and 16 % reduction in high strength material (HSM) were observed using 3-in (76 mm) concrete cube specimens. The slant shear test was performed to evaluate the slant shear strength between two RPC materials, as well as the bond strength between HSM and regular concrete. The test results have indicated drop of 27 % in slant

shear strength of HSM/RC specimens after undergoing 600 FT cycles and 1 % drop in slant shear strength in RPC/RPC specimens.

Carbonell Muñoz (2012) performed splitting tensile tests after 300, 600 and 900 FT cycles to study the UHPC – NSC interface bond performance. The FT cycles were conducted in accordance with ASTM C666 Procedure B, that includes freezing the specimens in air at-18 ºC and thawing them in the water at 4 ºC. The authors have found that no mass loss was observed, and the relative dynamic modulus of the specimens has increased after 300 FT cycles. The splitting tensile strength of the specimens remained unaffected even after 900 FT cycles.

2.4. Summary

The literature review provided a brief insight into the development of the use of UHPC in longitudinal connection in bridge construction and the bond interaction between the concrete materials. The connections between adjacent beams are of the essence in ensuring effective load transfer between adjacent beams. The use of UHPC as filler material in shear keys without additional transverse post-tensioning duct and ties was seen to be a feasible approach in enhancing the overall structural performance due to its outstanding mechanical properties. However, the current codes and guidelines have not provided standardized test methods to evaluate the fatigue, tensile, shear and, combination of both shear and compression bond performance of this designed material. With the improvement in concrete technology, it is necessary to probe further into the load transfer assessment methods in the current code provisions. In addition, some of the important topics such as the influence of temperature and cyclic loading on the HSC-UHPC bond interface performance were not widely discussed in

available literature. Successful implementation of UHPC in bridge shear keys can only be achieved if the bridge is able to withstand the load combinations and outdoor exposures that it is subjected to.

3. Experimental Program

3.1. Introduction

The focus of this study is on the behaviour of UHPC as filler material in shear keys in adjacent prestressed box beam bridges. The UHPC shear keys are monitored from the time of casting for the duration of this project – which is approximately 2 years. This thesis will focus on the bond between UHPC and the substrate as it changes with time and applied stress. The bridge of interest is located at Provincial Road (PR) No. 422, spanning over the Little Morris River at Morris, Manitoba.

The following sections outline the materials used in this experimental program, as well as the procedures that were carried out in order to successfully prepare the specimens to achieve the research objectives. The details of the program presented include specimen preparation methods, description of various testing procedures and data analysis.

3.2. Little Morris Bridge Precast Box Beam Fabrication and Construction

3.2.1. Precast Box Beams

The adjacent precast box beams were fabricated at Lafarge Precast plant in Winnipeg, Manitoba from May 15th 2019 to June 7th 2019. After fabrication, the precast box beams were transported and assembled on the site. For reference, the beams and shear keys were numbered one to eight, from west to east as shown in Figure 3-1. The bridge consists of eight precast box beams with width of 1200 mm and depth of 1200 mm, each. Together, the precast box beams are all

connected with shear keys and dowel bars as means of transferring load between adjacent beams. The total length of the simply supported span of the box beam was 30.14 m.

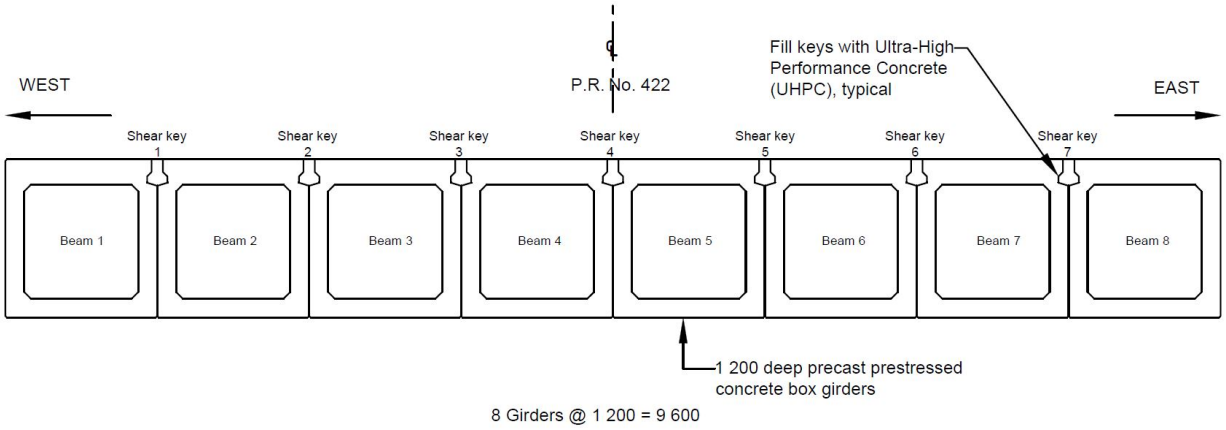

Figure 3-1 Box beam cross section

The formwork used to create the shear key was treated with retarder before casting to ensure that the surface of the shear keys have exposed aggregates after power washing the next day. During the construction of the precast box beams, Lafarge has taken specimens from the second, sixth and eleventh batch of the concrete to test for compressive strength test. The slump flow and air content for each concrete batch were verified by a quality control inspector at the plant. The results of the tests provided by Lafarge are tabulated and can be found in Appendix 1.

Figure 3-2 Casting of precast concrete beam girder at Lafarge

The finished precast box beam underwent steam curing for 12 to 18 hours after casting to ensure required strength was developed. After reaching the release strength of 35 MPa to 45 MPa, the prestressed strands were flame cut and the box beam was then transferred to the yard. Then, the shear key interfaces were power washed to expose the aggregates. The box beams were kept in a tent outside of the plant and they were wrapped with wet burlap to continue with its curing. The precast box beams were kept in the tent for at least two days before they were transferred out to the yard for temporary storage. Table 3-1 provides the date each beam was cast.

Table 3-1 Casting dates for the beams

Casting Date	Beam
May 15th, 2019	2
May 21st, 2019	4
May 23rd, 2019	5
May 27th, 2019	7
May 29th, 2019	6
May 31st, 2019	3
June 5th, 2019	8
June 7th, 2019	1

3.2.1.1. Precast Concrete Specimens

During the construction of the beams, eight 102 mm x 203 mm cylinders and eight 152 mm x 305 mm cylinder specimens were cast with the construction of each precast box beam using the HSC material from that beam. The specimens were prepared, cast, and tested in accordance with the ASTM C39 (2018), ASTM C469 (2014) and ASTM C496 (2017) for compressive strength, modulus of elasticity and splitting tensile strength, respectively. After casting, the specimens were then capped and placed under the finished box beam for 12 to 18 hours. After that, they were demolded at the same time as the box beams were demolded. The specimens were then transferred to the water tank for further curing as shown in Figure 3-3 together with the Lafarge concrete specimens. The cylinders were transported back to the University of Manitoba W.R. McQuade Structure Lab after one day, and they stayed in the curing room until the next test took place. The 102 mm x 203 mm cylinders were used to test for the compressive strength, modulus of elasticity and Poisson's ratio of the concrete, while the 152 mm x 305 mm cylinders were used to test for the splitting tensile strength of the concrete. The modulus of elasticity was obtained from stress-strain curves recorded during compression testing of the 102 mm x 203 mm cylinders using Equation 3-1. This modulus of elasticity together with the strain recorded for each beam at the bridge was used to calculate the actual stress in the box beam girders.

Equation 3-1 $$\sigma = E\varepsilon$$

Where E is the modulus of elasticity obtained from lab tests in MPa, σ is the stress in MPa and ε is the strain measured in the box girders.

Figure 3-3 Water tank for concrete cylinder curing

As far as the material compositions and proportions are concerned, no known information was shared by the precast fabricating plant.

3.2.2. Shear Keys

Longitudinal shear keys in bridges are designed to transfer shear between adjacent beams and ensure monolithic structural behavior. The details of the shear key dimensions implemented in the project are shown in Figure 3-4. Dowel bars were placed along the shear keys with 175 mm spacing and staggered at 87.5 mm with 125 mm extension from each side of the box beams. The dowel bars selected for the project were 15M ChromX 9000 Series high strength and corrosion resistant rebar.

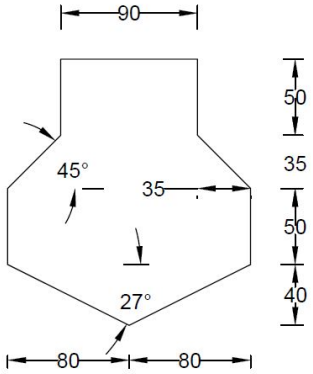

Figure 3-4 Shear key dimension

Figure 3-5 Dowel bars arrangement within the bridge shear key

The shear keys were filled with commercially available UHPC material provided by Lafarge – Ductal JS 1000. The raw materials for the UHPC include Larfage Ductal Premix, water, CHRYSO®Fluid Premia 150 superplasticizer and micro steel fibres with nominal size 0.2 mm x 14 mm. The materials were mixed on site with two mixers under the supplier's supervision. A total of 32 batches with total volume of 4.8 m^3 of UHPC mix were made to cast the shear keys at the bridge site. The average static flow of the material was recorded to be 205 mm to 225 mm, and the material achieved an average dynamic flow of 215 mm to 235 mm. The flow tests were

carried out by the supplier in accordance with ASTM C230 (2014). The fresh material properties of UHPC can be found in Appendix 2.

UHPC material for Shear Key 7 was mixed and cast on the 30th of July 2019, while the rest of the shear keys were mixed and cast on the 1st of August 2019. Before the pouring of UHPC, the surfaces of the shear keys on the precast concrete beams were sprayed with water to ensure saturated surface condition. Two wheelbarrows were used for transferring the UHPC from the mixer to the shear keys. Once the shear keys were filled up, a plywood was used to cover the surface of the shear keys for curing. There was no external compaction provided during the pouring of UHPC at site. Figure 3-6 depicts the process of casting the shear keys on site.

(a) (b) (c)

Figure 3-6 Shear keys casting process: (a) mixing of the materials; (b) filling of the shear keys; (c) shear keys covered with plywood

3.2.2.1. UHPC Specimens

Similarly, a total of 45-76 mm x 152 mm cylinders and 30-102 mm x 203 mm cylinders were cast simultaneously with the pouring of Shear Key 3, 4, 5 and 7 at the Little Morris bridge construction site. The 76 mm x 152 mm cylinders were tested for compressive strength and the 102 mm x 203

mm cylinders were tested for the modulus of elasticity in accordance with ASTM C1856 (2017). Amongst the specimens taken, 18 of the 76 mm x 152 mm cylinders and nine of the 102 mm x 203 mm cylinders were cast on site with Shear Key 7 on 30th of July 2019. The rest of the specimens were cast on the 1st of August 2019 with the remaining shear keys. The UHPC specimens were transported back to the university the next day after casting. Approximately 10% of the cylinders cast (three of the 76 mm x 152 mm cylinders and two of the 102 mm x 203 mm cylinders) on the 30th of July 2019 were not of good quality due to the worn-out cylinders that were expanded on the openings of the molds and consequently affecting the shape of the final products. Therefore, they were not tested for compressive strength and modulus of elasticity.

3.3. Small-Scale Bond Specimen Test Methods

The main objective of the small-scale tests was to compare the strain from the field measurement with the values obtained from laboratory testing of the small bond specimens. In addition to this, the effect of temperature cycling on the bond performance between the two materials was studied. Four different test methods, namely, direct tension, pull off, bi-shear and slant shear were used to investigate the bond performance at the precast concrete-UHPC shear key interface.

To ensure that the small-scale specimens in this study were representative of the materials used in the bridge, the first portion of each specimen was cast together with the bridge beams in the precast plant, while the UHPC portion of each specimen was poured together with the shear keys at the bridge construction site. The first portion of the bond specimen was cast using HSC from the beams during casting of Beam 4 and 5 at the precast plant, while the other portion was cast with UHPC in Shear Key 3 to 5 during the pouring of the UHPC at the bridge construction site. The

three shear keys were adjacent to the Beams 4 and 5. The specimens that were tested for the early-age bond performance were cast together with Beam 5, while the test specimens subjected to temperature cycling were cast together with Beam 4. The exposed aggregate surface of HSC was prepared the same way as the bridge components to ensure that the specimens were the best representation of the materials used on the bridge. The two materials were cured under the same conditions as the precast box beam and UHPC shear keys. The bond tests were performed on day 1, 5, 7, 14, 28, and 91 after casting the UHPC, and the evaluation of bond performance in the durability test was performed after the specimens underwent 60, 120 and 180 temperature cycles. Details of these cycles will be discussed in a separate section.

3.3.1. Preparation of the Small-Scale Bond Test Specimens

3.3.1.1. Precast Concrete Portion of Bond Specimens

The HSC portion of the specimens was hand-filled, and a pencil vibrator was utilized to compact the bi-shear and pull off test specimens; while on the other hand, the direct tension and slant shear specimens were rodded to achieve adequate compaction.

After placing HSC into its respective mold, the finished surface of the direct tension and slant shear test specimens were painted with retarder. The slant shear test specimens were cast in molds that were placed on an angled wooden rack, hence, creating the 60° interface angle with respect to the horizontal direction. The HSC of the direct tension specimens were fabricated using 76 mm by 152 mm cylinders and then saw cut to 76 mm in height.

Conversely, 2-inch thick polystyrene foams were cut to the size of the bi-shear and pull off test UHPC portion of the specimen molds. The foams were painted with chemical retarder and were inserted on the bottom of the wood molds prior to the pouring of HSC to expose the aggregate on the surface of the concrete. Figure 3-7 shows the molds lying beside the box beam ready for casting at the precast concrete plant.

Figure 3-7 Pull off and bi-shear test specimen molds with inserted foams painted with retarder before casting

All specimens were placed underneath the precast box beams after casting to ensure that the specimens were exposed to similar curing conditions. The specimens were then demolded after 12 to 18 hours and power-washed to create exposed aggregate surface roughness as shown in Figure 3-8. It was observed that the surface texture of the direct tension test specimens varied between specimens taken from Beam 5 and Beam 4. Hence, a pavement scanner (LS-40 Pavement Surface Analyzer) was used to analyse the surface roughness and texture of the test specimens.

The small-scale bond specimens were stored and cured together with the precast box beam in the tent, covered with wet burlap for seven to nine days before they were transported out to the yard of the precast concrete plant. The demolded bond test specimens were then kept outdoor, under the same conditions as the precast box beams for 22 to 24 days before they were transported back to the University of Manitoba. The HSC portion of the bond specimens were then placed back into the full molds after approximately 26 to 41 days of casting. Figure 3-9 depicts the bond test specimens that were placed back into their molds and were ready to be overlaid with UHPC material.

(a) (b) (c)

Figure 3-8 Exposed aggregate surfaces (a) bi-shear; (b) direct tension; (c) slant shear specimens

(a) (b) (c)

Figure 3-9 HSC portion of the specimens in (a) pull off and bi-shear; (b) direct tension; (c) slant shear molds

3.3.1.2. UHPC Portion of Bond Specimens

The small-scale specimens were transported to the bridge site on the 29th of July 2019, and UHPC was cast on the 1st of August 2019. Before casting the UHPC portion of the specimens, the exposed aggregate surface of HSC was sprayed with water to ensure that the surfaces of the specimens were saturated. The specimens were hand-filled, and no external compaction applied during the pouring of UHPC. The process of casting the small-scale specimens was identical to the casting of the shear keys on the bridge.

After casting, the finished surface of the pull-off test and bi-shear test specimens were covered with polyethylene sheets and, specimens in cylinders were capped to cure as shown in Figure 3-10. The specimens were cured outdoor, at the bridge construction site for a day before they were moved back to the University of Manitoba. The specimens stored outside of the W.R. Heavy

Structure Lab throughout the program were uncovered. Table 3-2 presents a summary of test specimens cast for the entire duration of this program.

Figure 3-10 Specimens covered with poly after casting UHPC

Table 3-2 Summary of the Specimens Cast

Test Specimens	Specimen Dimensions (inches (mm))	Total Number of Specimens
HSC Compressive Strength	4 x 8 (102 x 203) cylinders	64
HSC Modulus of Elasticity	6 x 12 (152 x 305) cylinders	64
UHPC Compressive Strength	3 x 6 (76 x 152) cylinders	42
UHPC Modulus of Elasticity	4 x 8 (102 x 203) cylinders	32
Direct Tension	3 x 6 (76 x 152) cylinders	80
Pull Off	7 x 13 x 6 (178 x 330 x 152) prisms	32
Bi-Shear	6 x 6 x 6 (152 x 152 x 152) cubes	82
Slant Shear	3 x 6 (76 x 152) cylinders	80

3.3.2. Interface Bond Performance Assessments

3.3.2.1. Direct Tension Test

The direct tension test specimens were 76 mm x 152 mm cylinders, as shown in Figure 3-11. An O-ring was placed on the interface between the HSC and UHPC during the sample preparation process. Two pieces of threaded steel pipes were glued onto each end of the cylinder using epoxy.

The glued specimens were left to cure for one to two days before testing. The direct tension test was performed in the Instron DX-300 hydraulic machine. A tensile load of 1 mm/min was applied to the specimen perpendicular to the bond interface until failure as indicated in ASTM C1404 (1998 (2003)). Although ASTM C1404 (1998 (2003)) was withdrawn without replacement due to limited usage by the industry and researchers, it is still deemed to provide valuable information on the forced interface failure under tensile load.

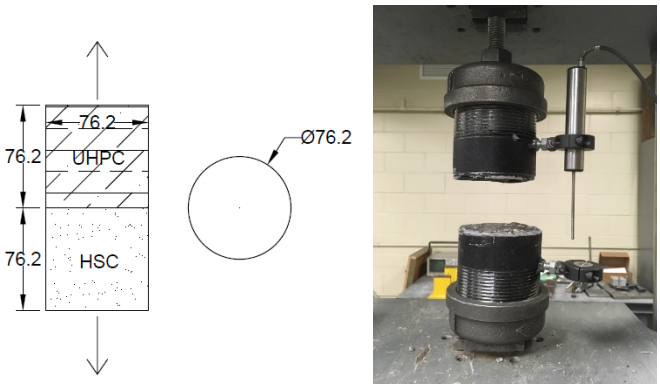

Figure 3-11 Direct tension test specimen details

3.3.2.2. Pull Off Test

For the pull off tests, a 330 mm x 178 mm x 152 mm HSC slab with 51 mm UHPC overlay was cast as indicated in Figure 3-12. The UHPC surface of the slab was partially drilled with three 51 mm diameter cores 76 mm into the substrate depth of the slab. After grinding the top surface of the slab, a 51 mm diameter steel disc was glued on the surface of the pre-cut cores using epoxy. The epoxy was allowed to cure for 1 to 2 days before testing. The pull off tests were performed in accordance with ASTM C1583 (2017). During the test, the test machine – Proceq DY, applied 35 ± 15 kPa/s constant tensile load to the steel disc until failure and the ultimate load was recorded.

The tensile strength of the direct tension and pull off tests was determined by dividing the maximum tensile load by the cross-sectional area of the 51 mm diameter drilled core.

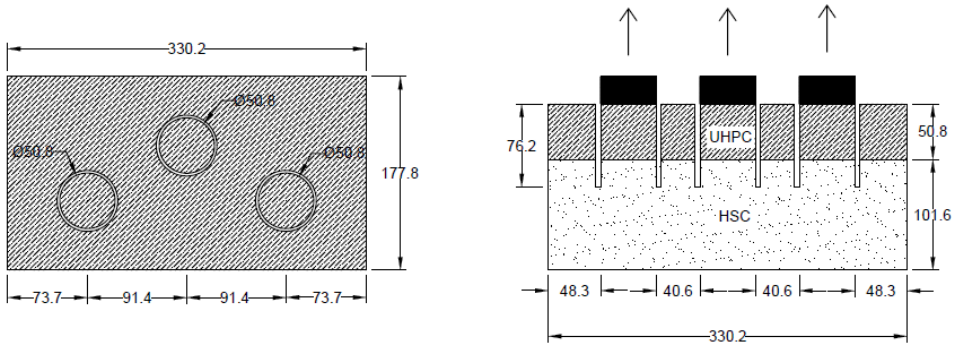

(a) (b)

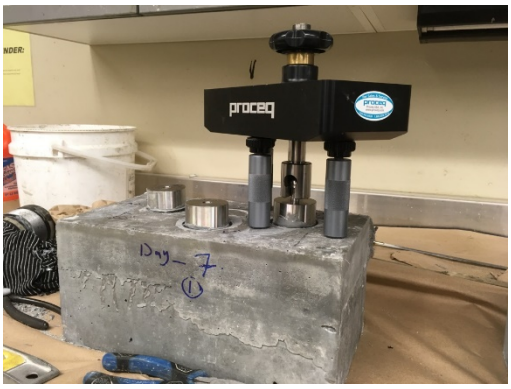

(c)

Figure 3-12 Pull off test specimens (a) position of the cores in plan view; (b) side view dimensions; (c) test performed

3.3.2.3. Slant Shear Test

A 76 mm x 152 mm cylindrical specimen for slant shear test is shown in Figure 3-13. The specimens were cast and tested in in accordance with ASTM C882-13a (2015) with both HSC and UHPC. The specimen's preparation included grinding the end surfaces of the slant shear cylinders were ground to a flat surface. During the tests, compressive load was applied on the end surfaces

until failure. The first specimens for each set of tests were loaded until failure under load control at 40 lb/sec according to ASTM standard, which is also equivalent to 66 kN/min. The rest of the specimens from the same group were loaded with displacement control that were back calculated using the duration and ultimate failure load from the first test. Deriving from Mohr's circle and equilibrium of forces, the normal and shear stresses acting on the inclined interface of the test specimens can be calculated as,

Equation 3-2 $$\sigma_0 = \frac{P}{A}$$

Equation 3-3 $$\sigma_n = \sigma_0 \, sin^2\theta$$

Equation 3-4 $$\tau_n = 0.5 \, \sigma_0 \sin 2\theta$$

Where σ_0 is the shear strength on the slanted surface, P was the maximum compressive force recorded, A was the cross-sectional area of the specimen, σ_n was the normal stress on the slant surface and τ_n was the shear stress on the slant surface.

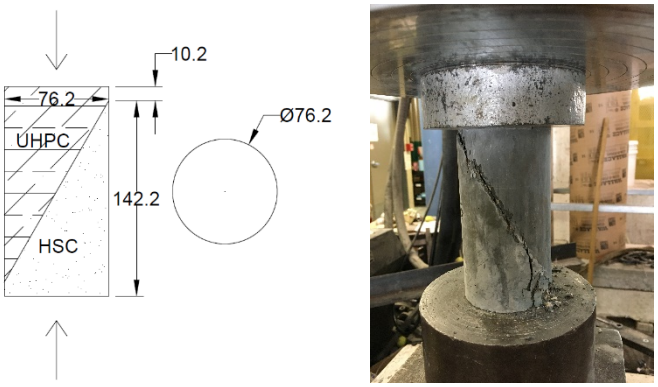

Figure 3-13 Slant shear test specimen details

3.3.2.4. Bi-Shear Test

A cube with side dimension of 152 mm as shown in Figure 3-14 was cast for bi-shear test. Three steel plates (51 mm x 32 mm x 152 mm) were used to align with the HSC and UHPC bonded

interface, and compressive load was applied onto the top of the steel plate until failure. The load rate used was identical to the one used for the slant shear tests. The purpose of steel plates in the setup was for pushing (shearing) off the middle section of the bi-shear specimens. Since both surfaces along the sides of the steel plates were subjected to compressive load applied, the bi-shear shear strength can be expressed as follows,

Equation 3-5 $$Shear\ Strength = \frac{P}{2 \times A}$$

Where P is the load identified on the load-stroke graph where the first sudden drop of load occurred and cross-sectional area of one side of the cube, A.

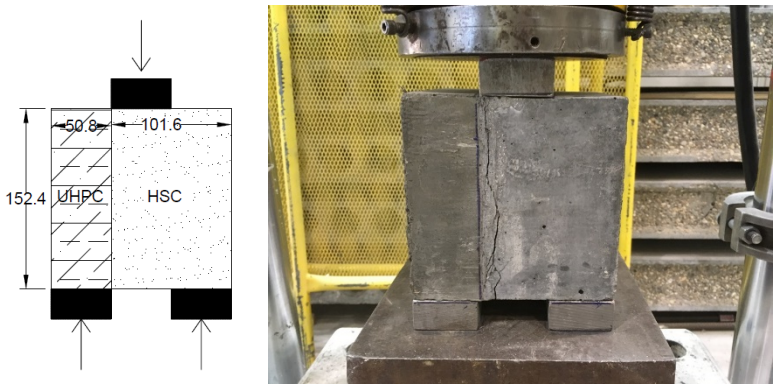

Figure 3-14 Bi-shear test specimen details

3.3.2.5. Durability Test

The actual temperature fluctuation in Manitoba was taken into consideration and the experimental program explored how temperature cycles affect the material behaviour.

According to Prairie Climate Centre (2019), the average freeze-thaw (FT) cycles from 1976 to 2005 was 64.1 per year and an average of 56.6 cycles per year is projected from 2051 to 2080.

As shown in the light blue plot in Figure 3-15, the annual FT cycles in Winnipeg was predicted to be decreasing over the years. For the purpose of this study, 60 FT cycles per year were assumed.

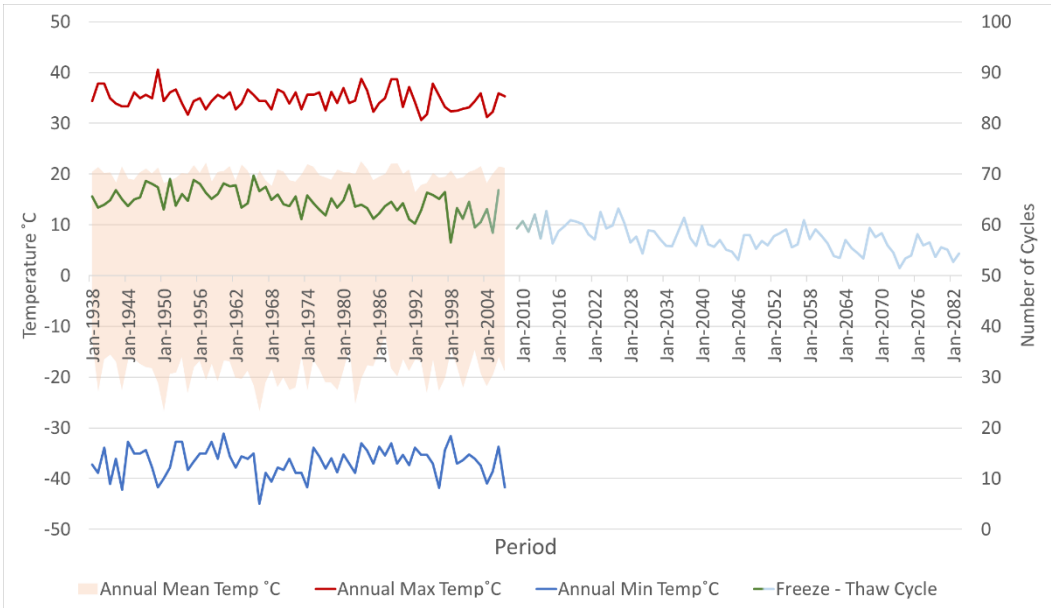

Figure 3-15 Annual temperature and number of FT cycles in Winnipeg

The experiment procedure was designed to simulate the one, two and three year(s) of repeated FT cycles in the area. The small-scale bond specimens taken from Beam 4 were divided into three groups of exposure: 60 cycles, 120 cycles and 180 cycles. The details of the chamber setup were as follows:

- Rate of temperature fluctuation: 4 °C per hour
- Minimum temperature: -20 °C
- Maximum temperature: 20 °C
- Relative humidity: 50%
- Maintaining the minimum and maximum temperature for two hours for every cycle

The initial intend for the chamber setup was to complete one cycle per day, and the chamber was to be left on running for 180 days in total for 180 thermal cycles. The 60 and 120 cycles specimens were taken out during the two hours break at the maximum temperature after completing their respective cycles. The chamber broke down twice and it has stopped working for 16 days in between the first 60 cycles. Table 3-3 shows the timeline of the temperature cycles applied. In addition, a set of specimens were left outdoor for a year after they were transported back from the bridge site. They served as control test when compared to the other tests.

Table 3-3 Timeline of the temperature cycling

Number of temperature cycles	Start date	End date
Control	-	-
60 (1 year exposure)	January 10th, 2020	March 25th, 2020
120 (2 years exposure)	March 27th, 2020	May 27th, 2020
180 (3 years exposure)	June 26th, 2020	August 25th, 2020

The HSC used in these specimens was from the same batch as Beam 4 that was cast on 21st of May 2019. The UHPC portion of the specimens was cast at the bridge construction site during the pouring of UHPC. As reported previously, the specimens were cured together with the beams and shear keys after casting to minimize possible discrepancies between the bridge components and the test specimens. The test methods employed in this study included the direct tension, pull off, bi-shear and slant shear tests.

Following completion of the thermal cycling, the specimens were tested in two regimes. In the first regime, the tests were conducted in room temperature, and during the second regime the bi-shear and slant shear tests only were conducted in an environmental chamber at -20 °C. This was due to the limitation of the application of epoxy needed for the tension tests under extreme

cold temperature; it can only be used in temperatures higher than 4° C. Table 3-4 presents a summary of number of test specimens used in this section of the experimental program.

Table 3-4 Total number of specimens for each test performed in the experiment

Test Specimens	Specimen Dimensions in Inches (mm)	Total Number of Specimens	
		Tested at room temperature	Tested at -20°C
Direct Tension	3 x 6 (76 x 152) cylinders	16	-
Pull Off	7 x 13 x 6 (178 x 330 x 152) prisms	17	-
Bi-Shear	6 x 6 x 6 (152 x 152 x 152) cubes	16	12
Slant Shear	3 x 6 (76 x 152) cylinders	16	12

3.3.2.6. Fatigue Testing on Direct Tension Specimens

The test specimens used to perform the fatigue test were the direct tension specimens that were previously subjected to 180 FT cycles as mentioned in Section 3.3.2.5. The test specimens were loaded under cyclic loading in the MTS testing machine to test for its fatigue performance.

The specimen preparation included grinding the end surfaces to achieve a perfectly flat surface before attaching a 1.25 in (32 mm) thick pucks with threaded screw hole using an epoxy. Figure 3-16 shows the fatigue test setup in the lab.

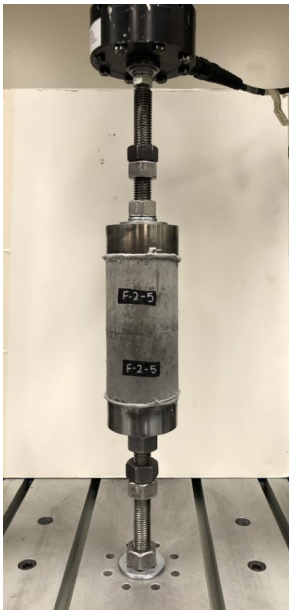

Figure 3-16 Fatigue test specimens loaded in the MTS machine

The test parameters are defined in Table 3-5. The fatigue loading consists of maximum one million reversed fatigue cycles applied at a rate of 1 Hz. The specimens that have not failed under the cyclic loading were tested for the direct tensile strength. The tension load applied during the loading cycles was approximately 88 % of the average direct tensile bond strength obtained in Section 4.5.1.1. In compression, the load was equal to 2 % of the HSC compressive strength. The direct tension loading rate applied in the tensile test was 1 mm/min. The total number of the cycles, direct tensile strength and the modes of failure were recorded and discussed in Section 4.7.

Table 3-5 Fatigue test parameters

Frequency (Hz)	Max. tension (kN)	Max. compression (kN)
1	14.00	13.00

3.4. Parameters Used for Determination of Roughness

A total of 80 profiles of the HSC exposed aggregate surface of the direct tension test specimens from both beams were scanned and analyzed. The 3D texture of the direct tension test specimens was recorded using the LS-40 Pavement Surface Analyzer. The scanner was developed by the Measurement Instrument Technology (HyMIT, 2013), based on the principle of laser triangulation in elevation measurement (Acosta et al. 2006). The scanner provides 3D surface data with pixels of 2048 x 2448 over a 100 mm x 100 mm surface, which gives the texture height resolution in the transverse and longitudinal direction of 41 µm/pixel and 49 µm/pixel, respectively. An example of the elevation profile generated is shown in Figure 3-17. The numerical results produced were further analyzed using different texture parameters such as the roughness average (R_a), mean texture depth (MTD) from sand patch method, mean profile depth (MPD), true surface area and interfacial area ratio. These parameters will be described in the sections that follow.

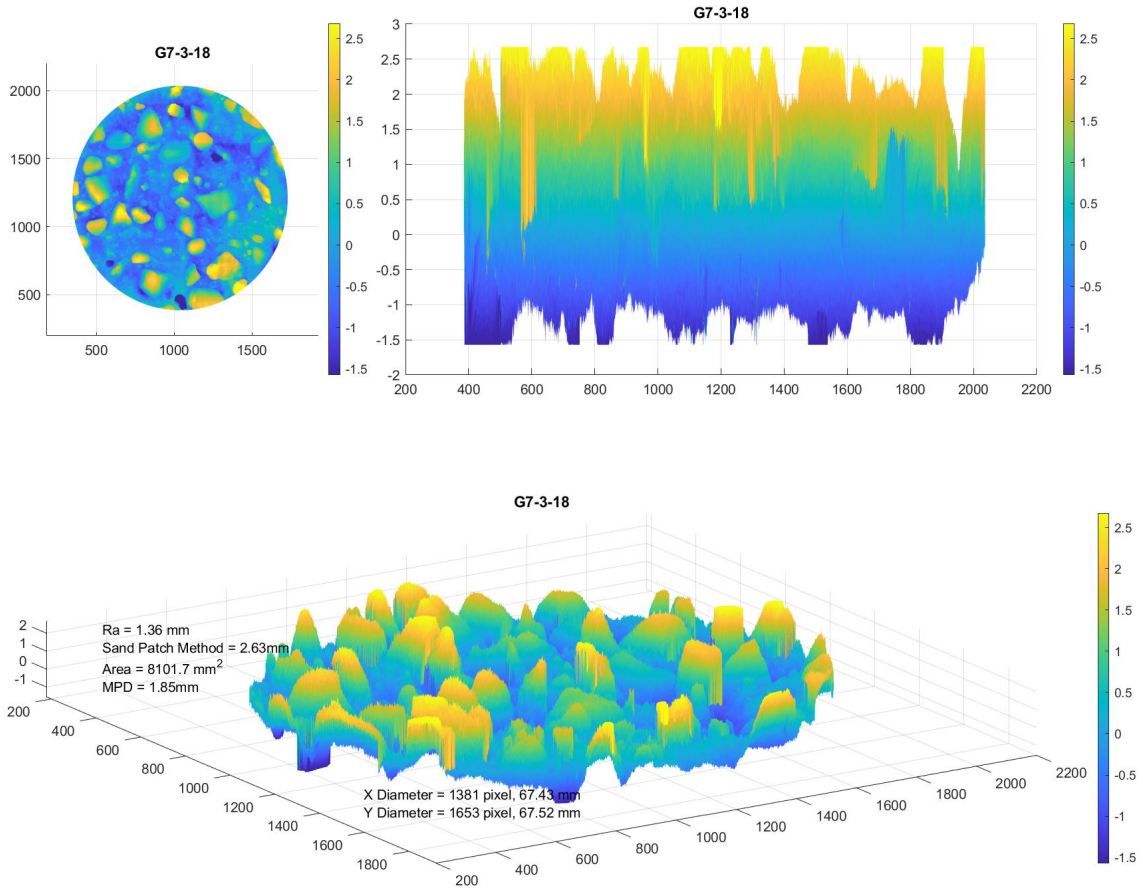

Figure 3-17 Example of the plan, side and perspective projection of the specimen surface generated from MATLAB

3.4.1. Roughness Average (R_a)

As mentioned in Section 2.1.3, R_a was used in many resources to classify the surface profile. The data from the surface scan came in a matrix of elevations for each pixel. To determine the R_a, the average elevation of the specimen was calculated for each column of the data matrix. Then, average R_a in the columns was determined by dividing the summation of the absolute difference of each elevation and the average elevation of the column by the number of points taken into

consideration. The same procedure was used in the transverse direction. Finally, the average value of both directions was determined to be the actual R_a. Equation 3-6 to Equation 3-8 provided are the numerical expression of the R_a calculation.

Equation 3-6 $$For\ the\ longitudinal\ direction,\ R_{ac} = \frac{\sum_{j=1}^{m}\sum_{i=1}^{n}|z_i - \bar{z}_j|}{k}$$

Equation 3-7 $$For\ the\ transverse\ direction,\ R_{ar} = \frac{\sum_{i=1}^{n}\sum_{j=1}^{m}|z_j - \bar{z}_i|}{k}$$

Equation 3-8 $$R_a = \frac{R_{ac} + R_{ar}}{2}$$

Where z is the elevation of the corresponding pixel, i and j are the row and column number, respectively, m is the total number of columns, n is the total number of rows and k is the total number of points taken into consideration.

3.4.2. Sand Patch Method

The sand patch method is commonly used in characterizing the road pavement texture. The original sand patch method requires spreading a constant volume of sand over the area of interest, and the mean texture depth (MTD) can be calculated by dividing the sand volume by the area of the circular surface. The resulted value shall be equal to the MTD of the pavement macrotexture. The detailed procedure of the sand patch method can be found in ASTM E 965 – 15 (2019).

In this study, a similar approach was taken with some modification to the procedure. Instead of conducting the physical measurements, MATLAB was used to analyze the MTD of the surfaces of the specimens. To do so, an assumed volume of cylinder ($h_{max}\pi r^2$) was capped on the specimen

surface profile and the elevation of the cylinder was calculated to be the maximum distance between the maximum and the minimum elevations of the surface profile. Adopted from Liu (2015), the summation of the volume per pixel from both directions were calculated by assuming a rectangular pyramid for each elevation recorded. The MTD was calculated by dividing the volume of the capped surface by the plane surface area of the specimen profiles as described in Equation 3-10.

Equation 3-9 $$V_{cap} = h_{max}\pi r^2 - \sum_{j=1}^{m}\sum_{i=1}^{n}\frac{1}{3}az_{ij}$$

Equation 3-10 $$MTD = \frac{V_{cap}}{\pi r^2}$$

Where h_{max} is the maximum elevation difference between the highest and the lowest point, r is the radius of the scanned profile, a is the area between i and j point and the rest of the variables are as defined previously.

3.4.3. Mean Profile Depth (MPD)

Another common practice in the pavement surface analysis is to calculate the MPD of the surfaces. ASTM E1845 (2015) covers the calculation procedures for MPD from a pavement surface. The standard has stated that segments of 100 mm shall be analyzed to determine the MPD. With each segment, the baseline is divided into two, and for each half segment, a maximum peak is obtained within the baseline. The average of the two peaks minus the profile average results in the mean segment depth. The MPD can be obtained by averaging the mean segment depth for all segments of the surface profiles as can be seen in Figure 3-18.

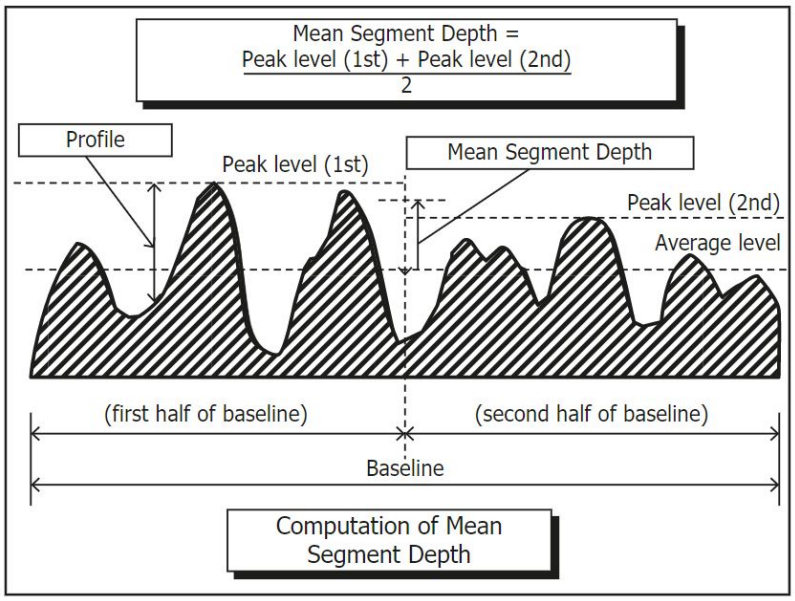

Figure 3-18 Mean segment depth calculation (ASTM E1845 2015)

A modified version of the mean profile depth calculation was utilized due to the small circular profile of the specimens in this study. Instead of using a baseline of 100 mm, the profile was analyzed by dividing the number of rows of the matrix into two. For each column, two peak levels were selected, and the mean profile depth of the corresponding column was equal to the average profile height of the two peak levels minus the average profile elevation of the column. The MPD in the longitudinal direction of the specimen was calculated by averaging the mean segment depth from all the columns. The same procedure was implemented in the transverse direction. The final MPD was calculated by averaging the MPD from both directions as shown in Equation 3-11. The variables are as defined previously.

Equation 3-11 $$MPD = \frac{\left(\frac{\sum_{j=1}^{j=m}\frac{\left(z_{max,j1}-z_{max,j2}\right)}{2}-\bar{z}_j}{m}+\frac{\sum_{i=1}^{i=n}\frac{\left(z_{max,i1}-z_{max,i2}\right)}{2}-\bar{z}_i}{n}\right)}{2}$$

3.4.4. True Surface Area

The true surface area was calculated to determine the area in contact between the two bonding materials. The hypothesis that was used was that the larger the effective contact area, the stronger the bond between two materials (Bissonnette et al. 2012). For a given surface in 3D space, the true surface area in the region can be calculated using Equation 3-12.

Equation 3-12 $$True\ Surface\ Area = \int_R \sqrt{\left(\frac{\delta z}{\delta x}\right)^2 + \left(\frac{\delta z}{\delta y}\right)^2 + 1}\ dA$$

Where R is the region of the surface, $\frac{\delta z}{\delta x}$ is the derivative of z in the transverse direction, $\frac{\delta z}{\delta y}$ is the derivative of z in the longitudinal direction. Equation 3-13 was derived by substituting the derivative of z and double integration with the elevation of the corresponding point and the dimensions of the pixels, respectively. A symmetric difference was used in finding the slopes of the elevation for a better accuracy in predicting the true surface area.

Equation 3-13

$$True\ surface\ Area = \left(\left(\sqrt{slope\ of\ z\ in\ column^2 + slope\ of\ z\ in\ row^2 + 1}\right) \times 0.049 \times 0.041\right)$$

$$slope\ of\ z\ in\ columns = \frac{z_{j+1} - z_{j-1}}{2 \times 0.041}$$

$$slope\ of\ z\ in\ rows = \frac{z_{i+1} - z_{i-1}}{2 \times 0.049}$$

3.4.5. Interfacial Area Ratio

Due to data processing, the individual plane surface area of the cylinders considered in the true surface area may vary. The interfacial area ratio was expressed to quantify the true surface area contributed by the surface profile on a unique region. The ratio can be calculated as follows:

Equation 3-14 $$Interfacial\ area\ ratio = \frac{True\ Surface\ Area - Plane\ Surface\ Area}{Plane\ Surface\ Area}$$

4. Results and Analysis

The following sections feature the results obtained from the research program and their analysis.

4.1. Test Specimen Naming Convention

In the following results and analysis sections, the specimens were labeled based on either the UHPC age, temperature treatment or fatigue parameters applied in the study.

In the UHPC early age bond study, the first two letters refer to the test method, the following numbers refer to the UHPC age in day(s), and the numbers at the end are the specimen's identifier. DT, PO, SS and BS refer to direct tension, pull off, slant shear and bi-shear tests, respectively. For example, "DT-1-1" is the specimen 1 direct tension test on day 1 and "BS-14-37" is the specimen 37 bi-shear test on day 14.

For the durability study, the first two letters, "FT" refer to freeze-thaw cycles. The following numbers refer to the number of free-thaw cycles that the specimens were subjected to. Then, the last letter, "C" refers to the specimens that were tested in the chamber with surrounding temperature of -20 °C. For example, specimen "FT-120" is a specimen that underwent 120 freeze-thaw cycles and was tested at room temperature, whereas "FT-180-C" is a specimen that underwent 180 freeze-thaw cycles and was tested at -20 °C.

The naming convention for the fatigue tests uses three characters. The first "F" refers to fatigue test, the following number refers to the test configuration and the last number is the specimen number; "F-2-1" refers to first specimen tested with the second test configuration.

4.2. Mechanical Properties of Precast Concrete

To quantify the mechanical properties of the precast concrete in this research program, four tests were carried out at the structure's laboratory at the University of Manitoba, namely the compression test, splitting tensile test, modulus of elasticity test and Poisson's ratio test.

Not all specimens were tested for the modulus of elasticity, Poisson's ratio and splitting tensile strength. Beams 1 and 2 were chosen because they have the lowest and the highest compressive strength, respectively from the data provided by Lafarge; while the compressive strength of Beam 4 and 6 represented the middle values in the Lafarge test results provided. Specimens from Beam 5 were tested for splitting tensile strength because the material of the small-scale specimens was taken from the same beam.

Three 102 mm x 203 mm cylinders were loaded to approximately 40 % of their ultimate capacity to test for their modulus of elasticity and Poisson's ratio before reloading them to failure in compression. A compressometer – extensometer ring shown in Figure 4-1 was used to record the changes in length and diameter of the cylinders. According to ASTM C469 (2014), the modulus of elasticity and Poisson's ratio can be calculated according to Equation 4-1 and Equation 4-2, respectively.

Equation 4-1 $$E = \frac{S_2 - S_1}{\varepsilon_2 - \varepsilon_1}$$

Equation 4-2 $$\mu = \frac{\varepsilon_{t2} - \varepsilon_{t1}}{\varepsilon_2 - \varepsilon_1}$$

Where S_1 is the stress corresponding to the longitudinal strain ε_1 of 0.00005, S_2 is the stress corresponding to the 40 % of the ultimate load, ε_2 is the longitudinal strain corresponding to S_2,

ε_{t2} is the transverse strain at mid-height of the specimen corresponding to S_2 and ε_{t1} is the transverse strain at mid-height of the specimen corresponding to S_1, μ is the Poisson's ratio.

Figure 4-1 Modulus of elasticity test

The cylinder specimens from precast concrete Beam 5 were tested for compressive strength on 6th of August 2019 (i.e., 83 days after casting), while the rest of the specimens were tested for compressive strength and modulus of elasticity after 118 to 148 days after casting. A summary of the test results as well as the day 28 compressive strengths values provided from Lafarge and lab tests were tabulated in Table 4-1. Detailed test results and the stress-strain graphs for the modulus of elasticity can be found in Appendix 1 and 3.

Table 4-1 Summary of the HSC material properties

Girder	Average Compressive Strength from U of M lab (MPa)	Lafarge Day 28 Average Compressive Strength (MPa)	Average Modulus of Elasticity (MPa)	Poisson's Ratio	Splitting Tensile Strength (MPa)
1	75.7	74.5	36,700	0.28	5.52
2	86.9	88.1	40,000	0.26	5.52
3	71.9	86.2	N/A	N/A	N/A
4	70.8	77.2	36,700	0.26	5.15
5	73.9	80.2	N/A	N/A	4.79
6	75.6	81.4	37,400	0.27	5.66
7	86.3	77.4	N/A	N/A	N/A
8	73.6	84.0	N/A	N/A	N/A

Figure 4-2 shows the box plot of compressive strength of concrete in each girder and differentiates between the strength obtained at the University of Manitoba and in Lafarge laboratory. The blue dots represent data form the laboratory at the University of Manitoba, while the orange dots represent strengths obtained in Lafarge laboratory. The compressive strength of specimens tested at University of Manitoba lab was lower than the day 28 compressive strength provided by the Lafarge precast plant for all the girders except for the girder 7 as presented in Figure 4-2. Four outliers were observed in the box plots – 42.4 MPa and 51.5 MPa in girder 1, 46.3 MPa in girder 4 and 49 MPa in girder 7. The outliers indicated that the compressive strength obtained were outside of the 1.5 times the interquartile range of their recorded strength. These values were deemed to be due to material variability and were excluded in the average compressive strength listed in Table 4-1.

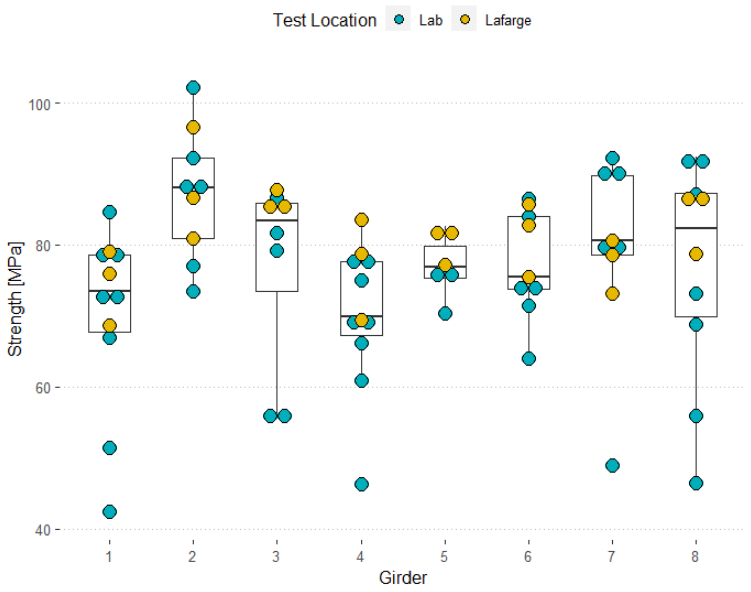

Figure 4-2 Compressive strength for HSC tested in the lab and at Lafarge for each box girder

The data from Lafarge also showed that it was more consistent and has lower spread compared to the University of Manitoba lab results. The specimens from the precast plant were cured by submerging the specimens in a water tank up until the day of testing, while the University of Manitoba lab specimens were only cured in the water tank for a day after demolding, and they were placed in the curing room after. Possible loss of moisture and damage may have occurred while travelling, even though proper precautions have been taken, such as covering the specimens with poly sheets and placing foams in between cylinders to minimize the collisions between the specimens.

4.3. Mechanical Properties of UHPC

The summary of the test results for the compressive strength and modulus of elasticity of the UHPC at different age is provided in Table 4-2. The average values were obtained from testing three to five cylinders, depending on the consistency of the test results obtained. Table 4-2 shows

that on average, the compressive strength from the first batch was lower than the second batch. This is especially true for day 1 to day 14 tests. The first day compressive strength of the UHPC cast on July 30 was only 34 % of the first day compressive strength of the batch cast on August 1st. The reason for this could be the cement that were used on site during the casting of Shear Key 7 was older material that was left over from the contractor's previous project.

Table 4-2 Mechanical properties of UHPC

Date of Casting	UHPC Age (days)	Average Compressive Strength (MPa)	Average Modulus of Elasticity (MPa)
30-Jul	1	14.7	16400
30-Jul	3	106.3	42300
30-Jul	7	138.2	N/A
30-Jul	14	146.4	N/A
30-Jul	28	164.4	N/A
01-Aug	1	43.5	28300
01-Aug	5	125.1	43400
01-Aug	7	135.0	45600
01-Aug	14	167.9	51000
01-Aug	28	152.7	50400
01-Aug	91	164.2	58700

It should be noted that two of the specimens from the second batch that were tested on the 14th day after casting were tested twice. The machine was shut off manually after a drastic drop in the load was observed. Although cracks were observed, the specimen did not shatter, and the materials were held by the steel fibers when taken out from the loading machine. Therefore, the specimens were put back into the machine and loaded until failure as presented in Figure 4-3. The ultimate compressive strength of the material was recorded as the maximum load capacity of the specimens.

Figure 4-3 Typical UHPC failure

Similar to the HSC, the modulus of elasticity of the UHPC is computed by loading the 102 mm x 203 mm cylinders in compression to approximately 40% of the ultimate strength. The strain in the cylinders were recorded using a compressometer – extensometer ring shown in Figure 4-1, and the modulus of elasticity was calculated using Equation 4-1

$$E = \frac{S_2 - S_1}{\varepsilon_2 - \varepsilon_1}$$ Equation 4-1.

4.4. Small-Scale UHPC Early Age Bond Test

The strength and failure mode of the specimens were tabulated and discussed in the following sections. The modes of failure can be categorized into three main modes: failure in the HSC material, failure in UHPC material and partial interface failure (PIF) between UHPC and HSC. The mode of failure of the specimens provided evidence for the quality of the bond between the two specimens. For the most part, specimens that have failed in the HSC material indicate that the bond strength of the two materials was stronger than the strength of the materials and vice versa. It should be highlighted that only the specimens that have failed in the interface between the two materials are considered for calculating the bond strength. The detailed results for each test can be found in the Appendix 5 to 8.

4.4.1. Tensile Test

4.4.1.1. Direct Tension

Throughout the experiment, a total of 30 direct tension test specimens were prepared and tested to study the direct tension bond interface performance between the two materials. The tests were performed on UHPC age day 5, 7, 14, 28 and 91. The direct tension test was not conducted on the first day after UHPC casting because the specimens could not be transported to the University of Manitoba and prepared for testing. The UHPC portion of the specimens was not fully cured on the first day after casting and transporting it could lead to internal damage and premature failure during test setup. Therefore, the tests only started on the fifth day after casting.

The summary of the test results can be found in Table 4-3. The following results do not consider the specimens that failed due to epoxy debonding.

Table 4-3 Summary of the direct tension tests

UHPC Age (days)	Number of Specimens	Average Tensile Strength (MPa)	STD (MPa)	COV
5	5	3.6	0.7	19 %
7	3	3.9	0.5	13 %
14	6	3.9	0.7	18 %
28	6	2.5	0.8	30 %
91	6	2.9	0.6	20 %

STD – Standard Deviation
COV – Coefficient of Variation

As shown in Table 4-3, the average tensile strengths reported were highest on day 7 and day 14. The low standard deviation between 0.5 MPa and 0.8 MPa showed conformity between the tests performed on the same day.

The boxplots in Figure 4-4 depict the relationship between the direct tensile strength of the specimens at the day of testing. Other than the two of the test results, 1.6 MPa and 1.64 MPa obtained on day 28 were slightly lower than the ACI 546 (2006) direct tensile minimum required strength on day 28 of 1.7 to 2.1 MPa, the rest of the specimens showed excellent tensile strength in the tests conducted. A 36 % decrease in average tensile strength was recorded from day 14 to 28. The box plot shows that there was a large spread in the distribution of the strength that were obtained on day 28. However, none of the low strength values were 1.5 times the interquartile range, and therefore they were not considered outliers. The mean strength values for both days 28 and 91 were lower than the values obtained on days 5 to 14. The significant drop in the average tensile strength on day 28, also exceeded the range of reported strength ranges by other researchers. Haber et al. (2018) reported 25 % drop and Zhang et al. (2020) reported 1.5 % to 2.7 % drop in direct tensile pull off bond strength on day 14 and day 28, respectively.

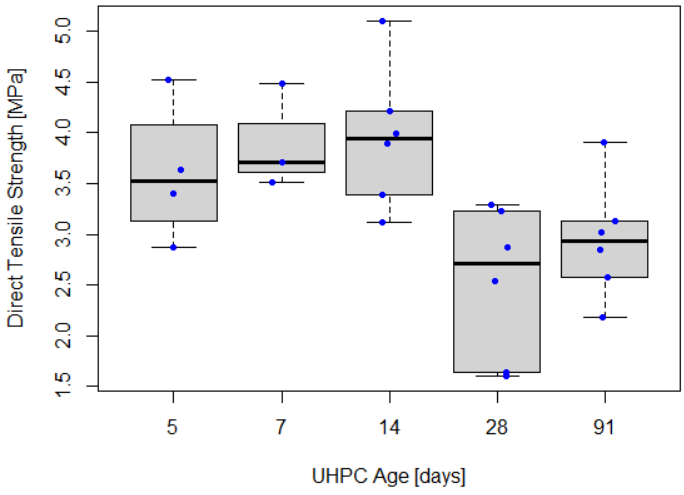

Figure 4-4 Direct tensile strength at the time of test

The typical modes of failure observed in the direct tension tests are shown in Figure 4-5. In the direct tension tests, the O-ring that was placed on the interface between the two materials and forced the location of failure to occur around the interface. As can be seen in Figure 4-5(a), the failure plane of the specimen showed obvious aggregates fracture and the darker colour of the HSC concrete can be seen in both surfaces. In contrast, Figure 4-5 (b) shows lighter colour UHPC on the left and more obvious sign of the pulling out of the fibers, which indicated the PIF.

(a) (b)

Figure 4-5 Modes of failure: (a) HSC failure; (b) PIF

In general, the direct tensile strength of the specimens was higher when the specimens failed in the HSC, compared to the PIF as shown in Figure 4-6. The strength variability was higher in the PIF specimens. The specimens tested at the earlier age (i.e., day 5, 7 and 14) failed at a higher strength, compared to those tested on day 28 and 91 with similar mode of failure. 83 % of the day 28 specimens failed partially at the interface, which also has the lowest average tensile strength among the tests and led to larger variability of test results.

As seen in Figure 4-6, the average direct tensile strength for PIF and HSC failure specimens were 3.00 MPa and 3.64 MPa, respectively. The HSC direct tensile strength in the current test was

lower compared to the average splitting tensile strength of HSC of 4.79 MPa. The observation came as no surprise; as explained by Liao et al. (2020), the loading of concrete in compression overestimates the tensile strength of the material in splitting tensile test. Whereas for the direct tension test used here, the entire cross-section is subjected to uniform tension stress leading to smaller strength values and more conservative results. Because the location of the median in the PIF group is within the box zone of the HSC failure group, there is no significant difference in the strength between these two groups. The whiskers in the PIF group are longer compared to those in the HSC failure group indicating that there is a larger spread of values in the PIF group.

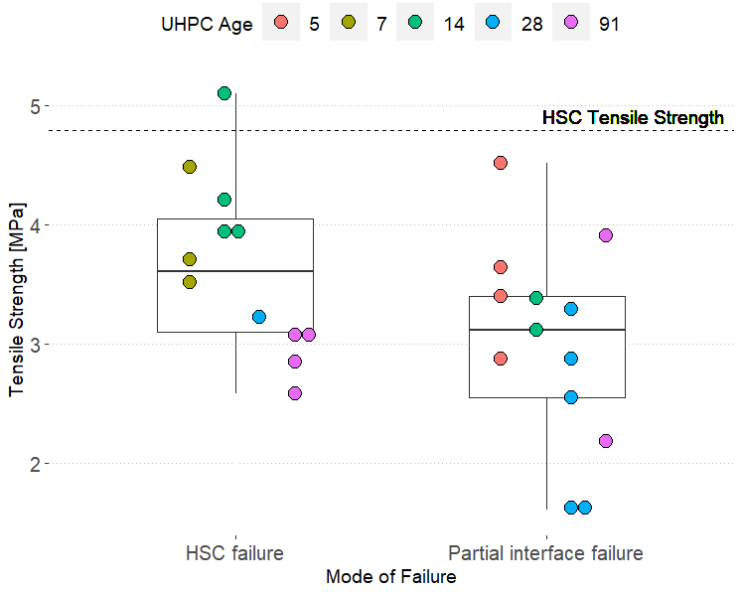

Figure 4-6 Relationship between the direct tensile strength and the modes of failure

4.4.1.2. Surface Profile Analysis – Direct Tension Specimens

The relationships between the surface profile and the direct tensile strength, as well as the modes of failure of the early age direct tension test specimens are presented in this section. As provided in the previous section, the relationship between the direct tensile strength and the

UHPC age was not conclusive. Therefore, it is necessary to investigate the relationship between the strength data and the interface parameters. Table 4-4 shows the summary of the interface parameters considered in this study, while a complete list of parameters for all the specimens can be found in Appendix 15. The parameters that were considered are: R_a, mean texture depth (MTD), mean profile depth (MPD), true surface area and interfacial area ratio. The average value from all direct tension tests is included in the second column, while the values for specimens that failed in HSC and in PIF modes of failure are separated in the last two columns of the table. On average, the surface parameters of the PIF specimens were 2 to 8 % larger compared to the specimens that experienced HSC failure.

Table 4-4 Summary of interface parameters of UHPC early age direct tensile bond specimens

Parameters	Average Values for UHPC Early Age Direct Tension Test Specimens		
	All Specimens	Specimens that Experienced HSC Failure	Specimens that Experienced PIF
Ra (mm)	1.61	1.57	1.66
MTD (mm)	3.03	2.90	3.14
MPD (mm)	2.00	1.95	2.04
True Surface Area (mm^2)	8151.07	8087.92	8209.37
Interfacial Area Ratio	1.33	1.31	1.34

Correlation between the parameters and direct tensile strength is shown in Figure 4-7. When analysing the complete set of data, the least correlation with direct tensile strength was found to be 20 % for the MTD parameter. The highest correlation for all specimens was found to be the correlation of true surface area with a value of 48 %. However, as explained in Section 3.3.2.6, the individual plane surface area used to analyze the true surface area was different due to data processing. For example, the plane surface area detected for the direct tension bond interface

ranged between 3293 mm^2 and 3619 mm^2, while theoretically the plane surface area of a circle with 76 mm diameter should be equaled to 4536 mm^2. Because the true surface area calculated was based on the plane surface area detected, the uncertainty of the plane surface area processed might have resulted in inaccurate correlation between the surface parameter and the direct tensile strength. All of the interface parameters did not show significant correlation with the direct tensile strength when the modes of failure were disregarded.

When taking the modes of failure into consideration, the PIF specimens showed stronger correlation of the interface parameters with the direct tensile strength. This has indicated that the interface roughness and direct tensile strength was not mutually dependent in the HSC failure. For those specimens Ra, MTD and MPD have only weak correlations of 12 % to 22 % with the direct tensile strength. Interestingly, stronger correlation of 62 % was observed between the true surface area and the direct tensile strength in both modes of failure, while R_a, MPD and interfacial area ratio have moderate correlation of 55 %, 54 % and 50 %, respectively in the PIF specimens.

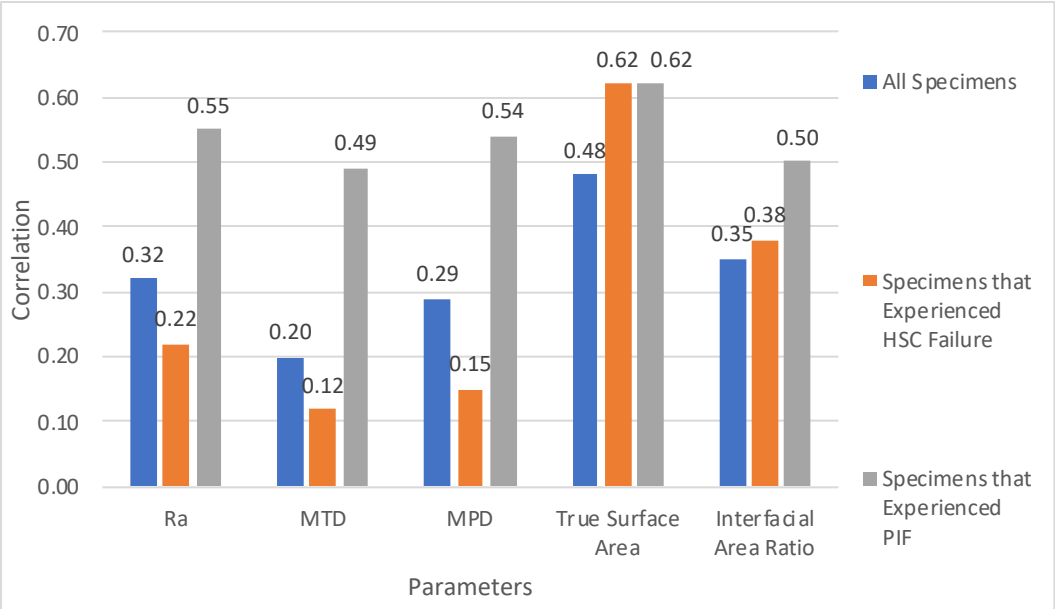

Figure 4-7 Correlation between the interface parameters and the UHPC early age direct tensile strength

The age of UHPC, bond strength and mode of failure are all considered in Figure 4-8 for each roughness parameter. The figure shows that the modes of failure were not influenced by any of the interface parameters, nor UHPC age at the day of testing. Another observation was that the distribution of the points was not consistent among the parameters. For example, the specimen may have a low interfacial area ratio but high MTD or MPD. The findings indicate that the texture indices (such as MTD and MPD) are not good indicators of evaluating the degree of aggregate exposure on a surface (Liu 2015, Li et al. 2016), because only limited information is captured from the surfaces. The box plots interfacial area ratio showed that their interface parameters were likely to be different between the modes of failure as the median lines lay outside of the interquartile range. Review of the data clearly shows that for the PIF mode, the bond strength is only related to the true surface area parameter in Figure 4-8(d). That is the only relationship where lower values of strength were associated with lower values of the parameter.

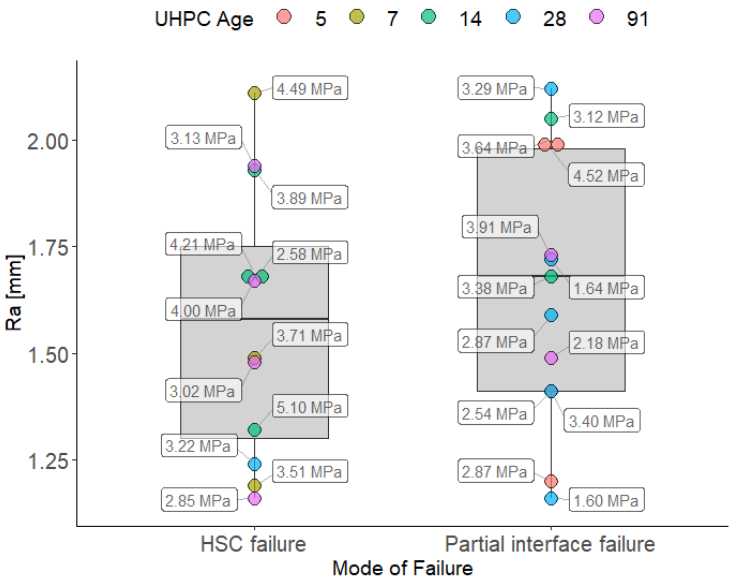
UHPC Age 5 7 14 28 91
Ra [mm]
2.00
1.75
1.50
1.25
4.49 MPa
3.13 MPa
3.89 MPa
4.21 MPa
2.58 MPa
4.00 MPa
3.71 MPa
3.02 MPa
5.10 MPa
3.22 MPa
3.51 MPa
2.85 MPa
3.29 MPa
3.12 MPa
3.64 MPa
4.52 MPa
3.91 MPa
3.38 MPa
1.64 MPa
2.87 MPa
2.18 MPa
2.54 MPa
3.40 MPa
2.87 MPa
1.60 MPa
HSC failure
Partial interface failure
Mode of Failure

(a)

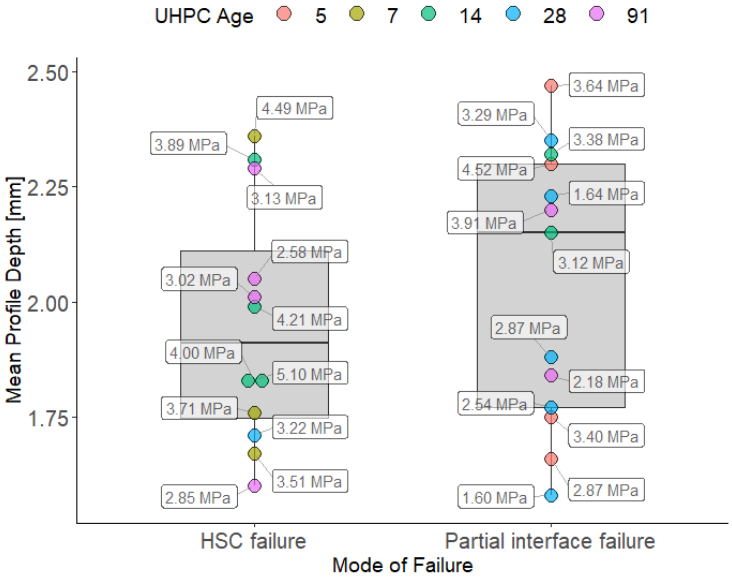
UHPC Age 5 7 14 28 91
Mean Profile Depth [mm]
2.50
2.25
2.00
1.75
4.49 MPa
3.89 MPa
3.13 MPa
2.58 MPa
3.02 MPa
4.21 MPa
4.00 MPa
5.10 MPa
3.71 MPa
3.22 MPa
3.51 MPa
2.85 MPa
3.64 MPa
3.29 MPa
3.38 MPa
4.52 MPa
1.64 MPa
3.91 MPa
3.12 MPa
2.87 MPa
2.18 MPa
2.54 MPa
3.40 MPa
1.60 MPa
2.87 MPa
HSC failure
Partial interface failure
Mode of Failure

(b)

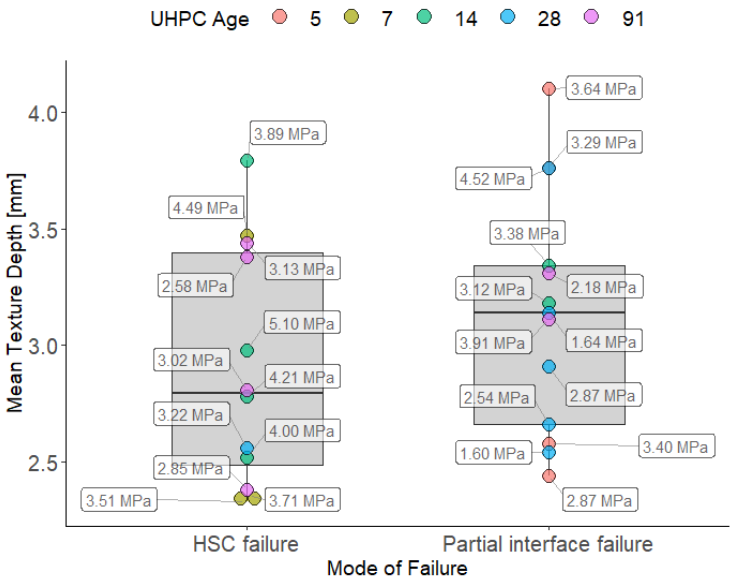
UHPC Age 5 7 14 28 91
Mean Texture Depth [mm]
4.0
3.5
3.0
2.5
3.89 MPa
4.49 MPa
2.58 MPa
3.13 MPa
5.10 MPa
3.02 MPa
4.21 MPa
3.22 MPa
4.00 MPa
2.85 MPa
3.51 MPa
3.71 MPa
3.64 MPa
3.29 MPa
4.52 MPa
3.38 MPa
3.12 MPa
2.18 MPa
3.91 MPa
1.64 MPa
2.54 MPa
2.87 MPa
1.60 MPa
3.40 MPa
2.87 MPa
HSC failure
Partial interface failure
Mode of Failure

(c)

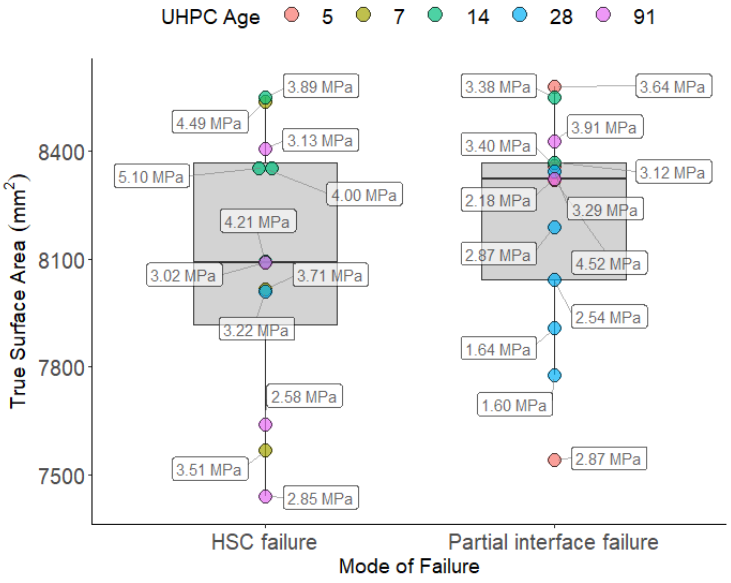
UHPC Age 5 7 14 28 91
True Surface Area (mm^2)
8400
8100
7800
7500
3.89 MPa
4.49 MPa
3.13 MPa
5.10 MPa
4.00 MPa
4.21 MPa
3.02 MPa
3.71 MPa
3.22 MPa
2.58 MPa
3.51 MPa
2.85 MPa
3.38 MPa
3.64 MPa
3.91 MPa
3.40 MPa
3.12 MPa
2.18 MPa
3.29 MPa
2.87 MPa
4.52 MPa
2.54 MPa
1.64 MPa
1.60 MPa
2.87 MPa
HSC failure
Partial interface failure
Mode of Failure

(d)

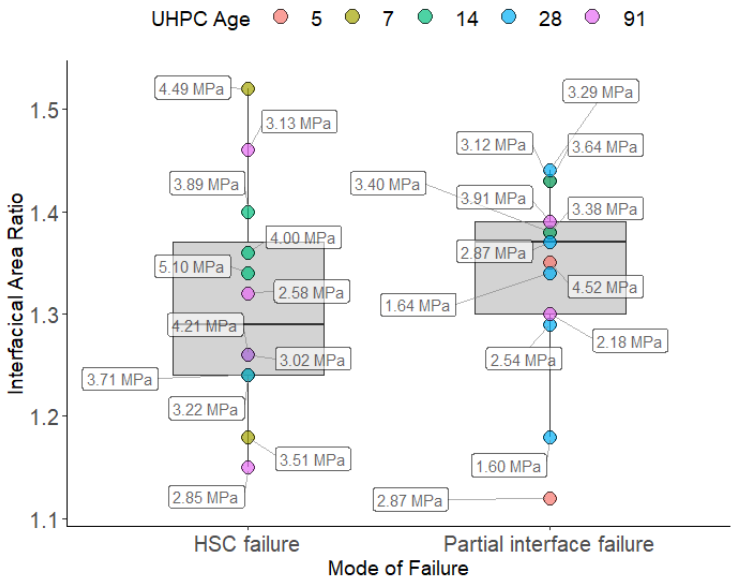

(e)

Figure 4-8 Modes of failure distribution of the UHPC early age specimens according to interface parameters: (a) R_a; (b) MPD; (c) MTD; (d) true surface area and (e) interface area ratio

4.4.1.3. Pull Off

Table 4-5 provides a summary of the pull off tests performed throughout the program. A total of 16 specimens with three partially cored prisms were cast for the pull off test. Like the direct tension test, tensile strength of the specimen was calculated by dividing the ultimate load by the surface area of the cylinder perpendicular to the applied load. Comparing to the modes of failure observed in the direct tension tests, the pull off test specimens showed a more distinctive mode of failure compared to the direct tension tests as depicted in Figure 4-9.

Table 4-5 Summary of the pull off tests

UHPC Age (days)	Number of Specimens	Average Tensile Strength (MPa)	STD (MPa)	COV
5	1	3.87	-	-
7	6	5.20	0.30	6%
14	6	4.33	0.57	13%
28	5	3.88	0.48	12%
91	7	3.80	0.44	12%

STD – Standard Deviation
COV – Coefficient of Variation

(a) (b) (c)

Figure 4-9 Modes of failure: (a) epoxy failure; (b) HSC failure; (c) PIF

The test results from the specimens that have failed in the epoxy were not considered in the analysis that follows. This mode of failure does not provide useful information regarding the performance of the two materials, and it represents neither the bond strength nor the tensile strength of the specimens. The STD and COV acquired from the test are relatively low when compared to the other tests in this program – averaging from 6 % to 13 %, revealing high consistency in the pull off tensile test performance.

There was no test performed on day 1 because it was not possible to drill the UHPC one day after casting without causing damage to the specimen. On top of that, the epoxy was not properly

cured for the specimens on day 5 due to poorly mixed resin, hence only one test result was successfully obtained on day 5.

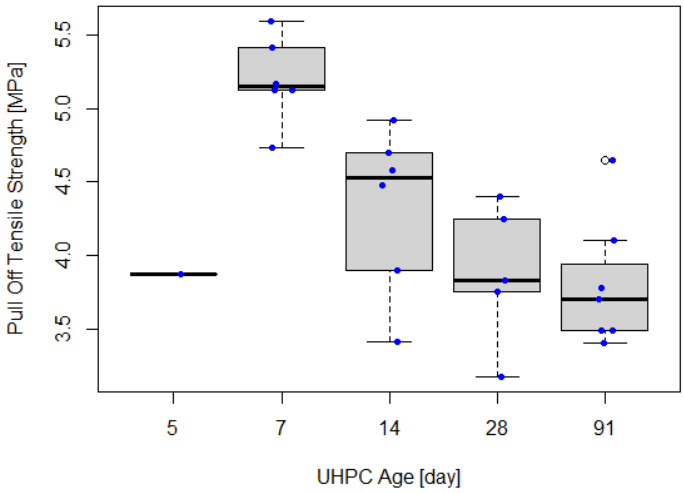

Figure 4-10 Pull off tensile strength at the day of test

The test results showed high tensile strength between the two concretes. The highest tensile strength – 5.42 MPa, was recorded on day 7, and a decreasing trend was observed throughout the program. Even with the lowest pull off tensile strength – 3.17 MPa, the test result has well exceeded the “excellent” bond strength as classified by Sprinkel and Ozyildirim (2000), which also exceeded the minimum tensile bond strength suggested by ACI 546 (2006). The outlier detected on day 91 may be due to specimen variability and it was included in the mean, STD and COV calculation. Considering the modes of failure in the day 91 test, there was no justifiable reason for excluding outlier presented in Figure 4-10 in the mean, STD and COV analysis.

Figure 4-11 shows that HSC failure was found primarily in specimens aged up to 7 days. There is one point that shows relatively low tensile strength that failed in HSC failure mode at 91 days,

but majority of the specimens tested that day failed in PIF mode. According to the box plot diagram, the 91-day test point in this group is an outlier. It was shown in the direct tension test results that the strength has decreased after day 14 which is also reflected in the pull off tests results. The average pull off strength of PIF and HSC failure specimens were calculated to be 4.01 MPa and 5.03 MPa, respectively. Figure 4-11 also shows that the pull off tensile strength of specimens that have failed in the HSC on day 7 and 14 was close to or higher than the HSC splitting tensile strength – 4.79 MPa. Along with the decrease in the tensile strength, the mode of failure also shifted from failure at the HSC on day 7 to PIF later, on days 14 to 91. As shown in the figure, the median lines of both box plots lay outside of the other group's box zone, indicating that the groups were significantly different. Also, PIF mode have a taller box plot, which imply wider variability of data.

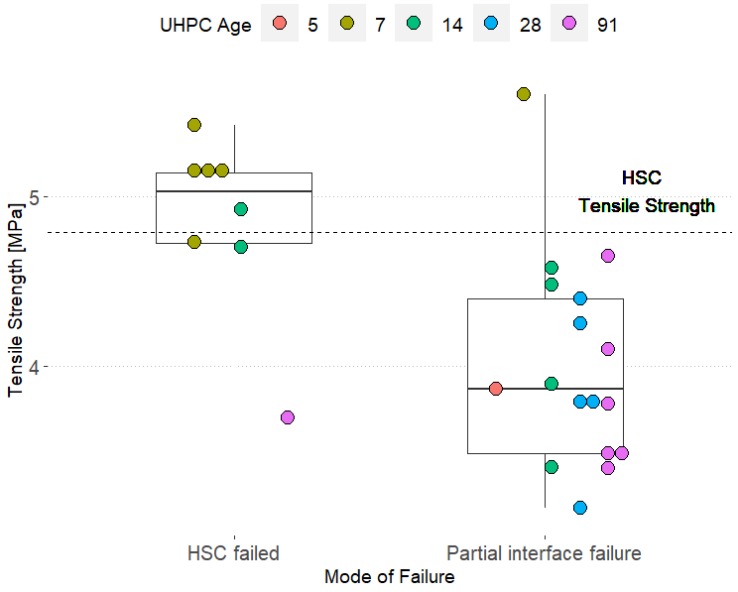

Figure 4-11 Relationship between the pull off tensile strength and the modes of failure

4.4.2. Slant Shear Test

The shear keys on bridges are subjected to complex loading conditions because of its geometry. The slant shear tests were performed to evaluate the interface bond performance under combination of shear and compression loading. A total of 34 tests were conducted; six specimens were tested for day 1 to day 28, while four specimens were available for day 91 test. The average slant shear strength, shear stress and normal stress calculated are listed in Table 4-6, along with their respective STDs and COVs.

Table 4-6 Summary of the slant shear tests

UHPC Age (days)	Average Slant Shear Strength (MPa)	Average σ (MPa)	Average τ (MPa)	STD σ (MPa)	STD τ (MPa)	COV σ and τ
1	20.0	10.1	17.4	2.4	4.2	24 %
5	24.0	12.2	21.1	2.2	3.8	18 %
7	30.6	15.6	27.0	3.1	5.4	20 %
14	27.4	13.8	23.9	2.1	3.6	15 %
28	31.4	16.4	28.4	3.2	5.5	19 %
91	25.9	13.3	23.0	2.0	3.5	15 %

σ – normal stress
τ – shear stress
STD – Standard Deviation
COV – Coefficient of Variation

As mentioned in Section 3.3.2.3, the first specimen of each set of slant shear test was loaded under load control of 66 kN/min, in accordance with the ASTM standards. The loading rate for the rest of the specimens were back calculated after acquiring the rate from one specimen under load control in each test. Loading rate used on day 1, 5 and 7 was 0.75 mm/min, 0.6 mm/min on day 14, 0.9 mm/min on day 28 and 0.45 mm/min on day 91. The trend of the strength can be related to the loading rate applied during the tests; the highest loading rate was used on day 28,

resulting in a higher average slant shear strength of 31.4 MPa, while lowest loading rate used on day 91 yields lower slant shear strength of 25.9 MPa. Normally, higher loading rate results in an increase in compressive strength of the concrete because of lower energy dispersion (Fu et al. 1991). The high COVs ranging from 15 % to 24 % reported were in the range of similar research done previously (Harris et al. 2014, Carbonell Muñoz 2012).

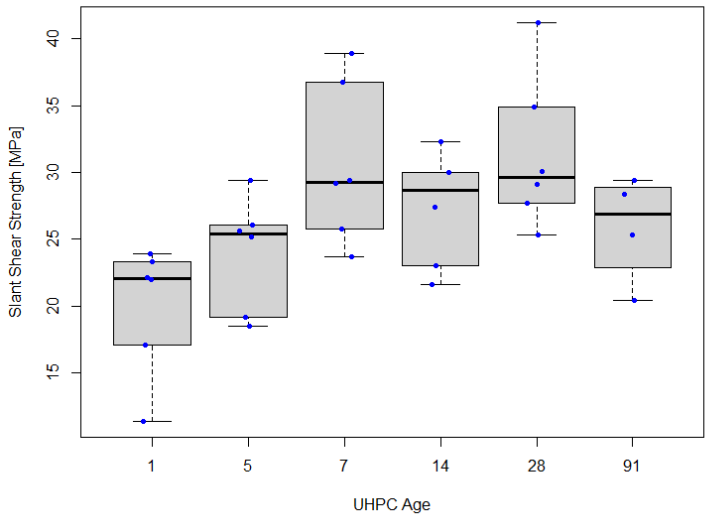

Figure 4-12 Slant shear strength at the day of test

The change in slant shear strength with the age of UHPC is presented in a box plot in Figure 4-12. The box plot shows that the strength has increased substantially on days 7 to 91, when the data is compared to day 1. There was a larger spread of data on days 1, day 7 and day 28. Except for the two slant shear tests on day 1 with values of 17.2 MPa and 11.5 MPa, the rest of the test results showed high values of slant shear strength: exceeding the ACI 546 (2006) slant shear minimum requirement strength on day 28 even after only one day of casting.

The two modes of failure are shown in Figure 4-13: HSC and interface failure; HSC failure with the bond interface still intact to the UHPC material. The modes of failure can be seen shifting from the HSC and interface failure to the HSC failure starting from day 14 in Figure 4-14. All specimens from day 28 and day 91 except for one failed at the HSC. The change in the modes of failure revealed an improvement in the bond performance as the material strength of UHPC increased. The box plot also shows that there are two outlier values in the HSC failure group, one at the bottom and the other at the top of the strength distribution. Excluding the outliers, the average slant shear strength for HSC failure and PIF specimens was 26.4 MPa and 27.0 MPa, respectively.

(a) (b)

Figure 4-13 Modes of failure: (a) HSC and interface failure; (b) HSC failure

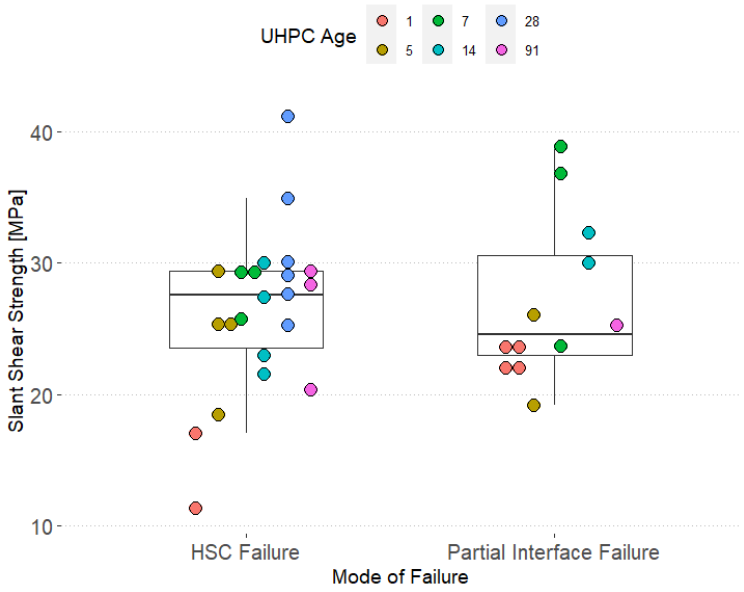

Figure 4-14 Relationship between the slant shear strength and the modes of failure

4.4.3. Bi-Shear

The summary of the test results for the bi-shear tests was tabulated in Table 4-7. A total of 42 specimens were tested, with an average of six specimens tested at the same day. The shear strength was expressed by only using the first peak load in Equation 3-5. The loading rates of the tests were the same as the ones applied on the slant shear strength specimens.

Table 4-7 Summary of bi-shear tests

UHPC Age (days)	Number of Specimens	Average Shear Strength (MPa)	STD (MPa)	COV
1	6	3.45	1.53	44%
5	6	3.75	1.10	29%
7	6	4.42	1.22	28%
14	6	4.71	1.66	35%
28	6	5.53	3.02	55%
91	4	6.63	2.12	32%

STD – Standard Deviation
COV – Coefficient of Variation

A wide range of standard deviation was observed, ranging from 1.10 MPa to 3.02 MPa, with a COV ranging from 28 % to 55 %. The mean shear strength showed a gradual increase of 36 % from day 1 to day 14 test, then 17 % and 19 % increase on day 28 and 91, respectively. The speculated loading rate effect on the slant shear strength was not detected in the bi-shear tests. An exceptionally high shear strength of 10.74 MPa was recorded on day 28, resulting in a high STD and COV. High COV was frequently recorded due to the nature of the test set-up also shown by other researchers (Semendary and Svecova 2020a, Valikhani et al. 2020). The box plots in Figure 4-15 show that the strength distribution on day 28 was skewed in comparison to the data for other test days.

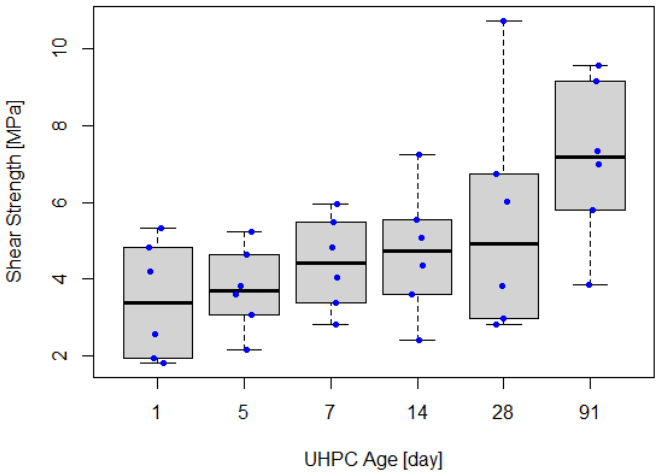

Figure 4-15 Bi-shear strength at the day of test

(a) (b) (c)

Figure 4-16 Bi-shear mode of failure: (a) A shape failure; (b) shear on both sides; (c) bond interface

It is important to note that the shear stress calculated does not necessarily represent the bond strength, as the load P, used to calculate this stress was taken from the first sudden drop in the load-stroke graph obtained from the testing machine. The sudden drop in the load has indicated that there was a sudden drop in the load capacity. Even though it is usually not clear what caused the drop in the load, it is assumed that it was a crack at the interface between the HSC and UHPC. Unlike in conventional concrete, the steel fibers in the UHPC were designed to help mitigate internal cracks and transfer load to avoid brittle failure mode. The fibers bridge the cracks and allow the UHPC to carry additional load post crack initiation. Hence, it is common that the specimen does not fail directly at the bond interface between the UHPC and HSC but instead in the weaker material, in this case – the HSC. As illustrated in Figure 4-16, the modes of failure for the bi-shear specimens can be complex and difficult to be identified during the tests. Nevertheless, the bi-shear test provides an indication of the minimum bond strength due to direct shear.

4.4.4. Cohesion and Friction

With the limited number of data and large COVs detected in the current study, the 5th percentile of the test results was used for a more conservative prediction of the cohesion and friction coefficients. Table 4-8 and Table 4-9 summarize the cohesion and internal friction angles obtained from Mohr-Coulomb's and Carol's approaches. The tensile strength used in the analysis included test results from both direct tension and pull off tests.

Table 4-8 Friction coefficient and cohesion values using Mohr-Coulomb's approach

UHPC Age	Slant Shear Test		Tensile Strength, f_t (Cohesion)	Friction Coeff., μ	Internal Friction Angle, ∅
	τ_n (MPa)	σ_n (MPa)	c (MPa)		
1	11.2	-6.47	-	-	-
5	16.38	-9.46	2.98	1.42	54.84
7	21.29	-12.29	3.59	1.44	55.22
14	19.35	-11.17	3.26	1.44	55.22
28	23.21	-13.4	1.62	1.61	58.15
91	18.98	-10.96	2.42	1.51	56.49

Table 4-9 Friction coefficient and cohesion values using Carol's approach

UHPC Age	Slant shear		Direct Shear (MPa)	Friction Coeff., μ	Internal Friction Angle, ∅	Tensile Strength, f_t (MPa)	$c = \frac{2-\sin \emptyset}{\cos \emptyset} \cdot f_t$ (MPa)	$\frac{c}{Direct\ Shear}$	$\frac{c}{f_t}$
	τ_n (MPa)	σ_n (MPa)							
1	11.20	-6.47	1.84	1.45	55.41	0.82[1]	1.69	-	2.06
5	16.38	-9.46	2.38	1.48	55.95	2.98	5.68	2.39	1.91
7	21.29	-12.29	2.96	1.49	56.13	3.59	6.92	2.34	1.93
14	19.35	-11.17	2.71	1.49	56.13	3.26	5.57	2.05	1.71
28	23.21	-13.40	2.86	1.52	56.66	1.62	2.63	0.92	1.62
91	18.98	-10.96	4.34	1.34	53.27	2.42	4.85	1.12	2.00

[1]back calculated values using the c to direct shear ratio of 0.92

Due to the lack of tensile strength data from day 1, the cohesion value was calculated by multiplying the minimum 0.92 cohesion to direct shear ratio by the direct shear of 1.84 MPa. Then, the tensile bond strength was back calculated from the cohesion value in column eight of Table 4-9. The interface internal friction angle obtained ranges from 55.22° to 58.15° and 53.27° to 56.66° for Mohr-Coulomb's and Carol's approach, respectively. Since the internal friction angles were greater than 30°, Equation 2-8 was used in calculating the Carol's approach cohesion value.

The values obtained agree with previous work presented by Espeche and Leon (2011), where the range of cohesion and tensile strength ratio was between 1.75 and 2.0. While on the other hand, the cohesion to direct shear ratio showed by Zanotti and Randl (2019) ranged between 0.84 and 0.96, which was much lower than the ratio from the current study, and the one by Espeche and Leon (2011).

All friction coefficients calculated using both approaches, except for day 91 friction coefficient using Carol's approach, were higher than the friction coefficients specified in CSA S6 (2019) and AASHTO (2017) of 1.4 for concrete placed monolithically. The cohesion on day 28 and day 91 using the Mohr-Coulomb's approach, and day 1 and day 28 using the Carol's approach on the other hand, were less than the 2.76 MPa, specified in AASHTO (2017). However, all cohesion and friction coefficients calculated using both approaches exceeded the specified values in CSA S6 (2019) and AASHTO (2017), except day 28 cohesion using the Mohr-Coulomb's approach for normal weight concrete placed on intentionally roughened surface.

4.5. Durability Test – Freeze-Thaw Cycles

The test results obtained from the direct tension, pull off, slant shear and bi-shear tests after FT cycles, and their respective modes of failure were recorded and discussed in the following sections. The detailed results for each test can be found in the Appendix 9 to 12.

4.5.1. Tensile Test

4.5.1.1. Direct Tension

On average, four specimens were tested for each test. The summary of the test results can be found in Table 4-10. Based on the test results collected, it was observed that the overall range of the COV was from 12 % to 32 %. The boxplots of the bond strength under tensile stresses for different FT cycles is depicted in Figure 4-17. There was no clear trend in the bond strength demonstrated for specimens conditioned in different FT cycles. Only the FT-60 median line was outside of the interquartile range of the rest of the box plots, which indicated that the FT-60 was likely to be different group than the rest. There was a large spread in strength values for specimens that were subjected to 180 FT cycles.

Table 4-10 Summary of the direct tension tests

Specimens	Number of Specimens	Average Tensile Strength (MPa)	STD (MPa)	COV
FT-60	4	4.0	0.9	22%
FT-120	4	3.8	0.6	15%
FT-180	4	3.5	1.1	32%
Control	4	3.7	0.4	12%

STD – Standard Deviation
COV – Coefficient of Variation

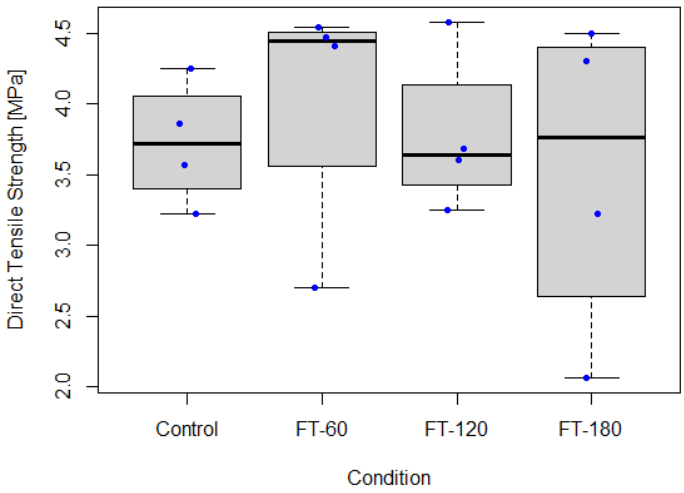

Figure 4-17 Direct tensile strength after FT cycles

The modes of failure observed in these tests were similar to the ones observed in UHPC early age tests. Seven out of 16 specimens failed in the HSC. As shown in Figure 4-18, there was no conclusive evidence that the number of FT cycles has caused a shift in mode of failure in the direct tension test. One specimen from the group FT-180 that experienced HSC failure mode was shown as an outlier. The tensile strength from the direct tension tests did not differ much between the two modes of failure, but the specimens that failed in the HSC showed a higher consistency in the tensile strength values. Also, although the average tensile strength for specimens that failed in the HSC (4.21 MPa) was somewhat higher than those with the PIF (3.66 MPa), the average direct tensile strength of HSC failure specimens was 12 % lower than the HSC splitting tensile strength. The median line of the PIF did not overlap with the interquartile range of the HSC failure box plot, indicating that the two groups were likely to be different.

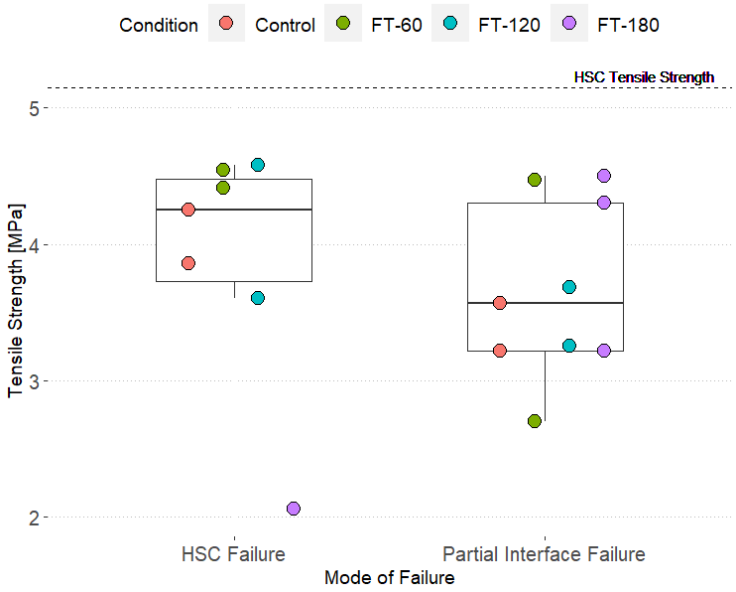

Figure 4-18 Relationship between the direct tensile strength and the mode of failure

4.5.1.2. Surface Profile Analysis – Direct Tension Specimens Subjected to Freeze-Thaw Cycles

A summary of the interface parameters for durability test specimens used in the current test is provided in Table 4-11 and a complete list of interface parameters for all the specimens can be found in Appendix 16. As presented in the previous section, since the tensile strength attained did not vary with the FT cycles, it is in general justifiable to compare all the interface parameters with the direct tensile strength and the specimens' modes of failure. The outlier from FT-180 observed in Figure 4-18 was removed in the following analysis.

Unlike the UHPC early age direct tension tests, the PIF specimens have higher magnitudes of the interface parameters compared to the HSC failure specimens, except for MPD. The Ra, MTD, true surface area and interfacial area ratio of the PIF specimens were 1 % to 7 % larger than the HSC failure group, while MPD in the HSC failure group was 1 % higher compared to the PIF specimens.

Table 4-11 Summary of the interface parameters for tensile bond specimens subjected to FT cycling

Parameters	Average Values for Tensile Bond Specimens Subjected to FT Cycling		
	All Specimens	Specimens that Experienced HSC Failure	Specimens that Experienced PIF
Ra (mm)	0.93	0.89	0.95
MTD (mm)	1.96	1.94	1.98
MPD (mm)	1.37	1.38	1.37
True Surface Area (mm^2)	7254.16	7198.92	7290.99
Interfacial Area Ratio	1.07	1.04	1.10

The correlations between the tensile strength and the interface parameters are shown in Figure 4-19. One of the specimens from the control set lost its identifier, hence its interface parameters were not included in the analysis. All the interface parameters, regardless of the modes of failure, showed negative correlations with the direct tensile strength and the R_a was practically not correlated to the direct tensile strength. Some of strongest negative correlations with the tensile strength were the MTD in HSC failure and interfacial area ratio in the PIF in the specimens that failed in PIF mode. The rest of the interface parameters, ranging from 15 % to 44 %, were considered to have weak correlations with the direct tensile strength.

The negative correlations obtained did not agree with any of the literature review, additional research must be carried out. With a total of only 16 specimens, the sample size is too small to draw meaningful conclusions.

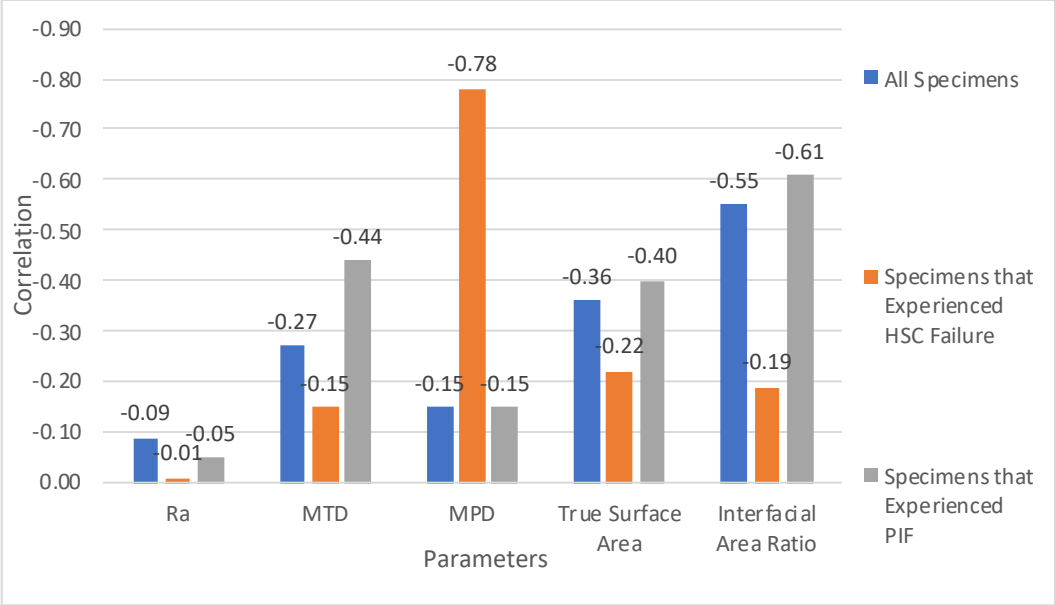

Figure 4-19 Summary of the interface parameters for tensile bond specimens subjected to FT cycling

Figure 4-20 shows the distribution of the interface parameters in relation to the modes of failure. Similar to the UHPC early age bond test specimens, the data points are not consistent when they were compared among the interface parameters. That means that, low R_a corresponds to high MPD or high MTD corresponds to low interfacial area ratio. The MPD box plot median line of the specimens with HSC failure lay outside of the interquartile range of the PIF box plot – which indicates that the groups of MPD were likely to be different. The figures also showed that the average MPD of the PIF specimens was lower than that of the specimens that failed in the HSC. Again, the reliability of the current study can be improved with larger sample size and extensive experimental testing.

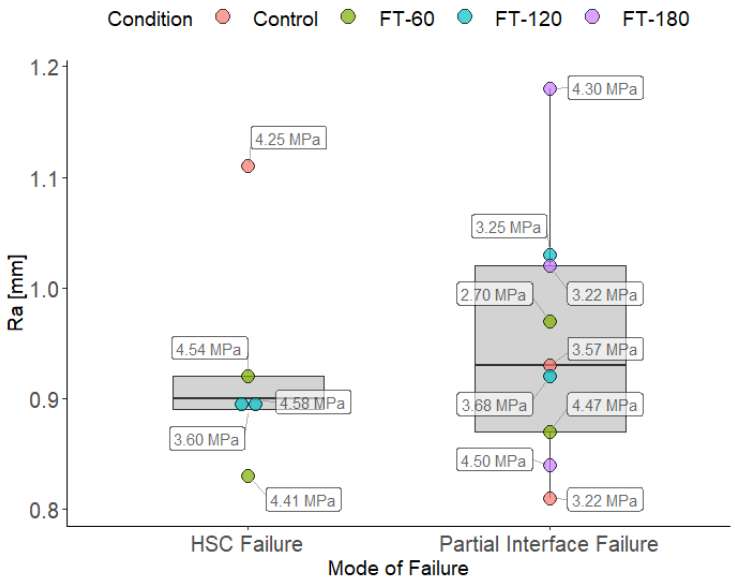
Condition
Control
FT-60
FT-120
FT-180
Ra [mm]
1.2
1.1
1.0
0.9
0.8
4.25 MPa
4.30 MPa
3.25 MPa
2.70 MPa
3.22 MPa
4.54 MPa
3.57 MPa
4.58 MPa
3.68 MPa
4.47 MPa
3.60 MPa
4.50 MPa
4.41 MPa
3.22 MPa
HSC Failure
Partial Interface Failure
Mode of Failure

(a)

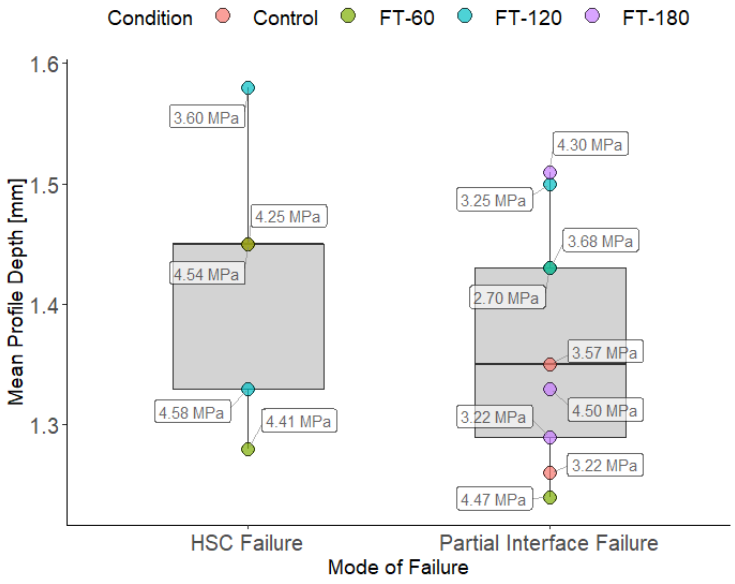
Condition
Control
FT-60
FT-120
FT-180
Mean Profile Depth [mm]
1.6
1.5
1.4
1.3
3.60 MPa
4.30 MPa
4.25 MPa
3.25 MPa
3.68 MPa
4.54 MPa
2.70 MPa
3.57 MPa
4.58 MPa
4.41 MPa
3.22 MPa
4.50 MPa
3.22 MPa
4.47 MPa
HSC Failure
Partial Interface Failure
Mode of Failure

(b)

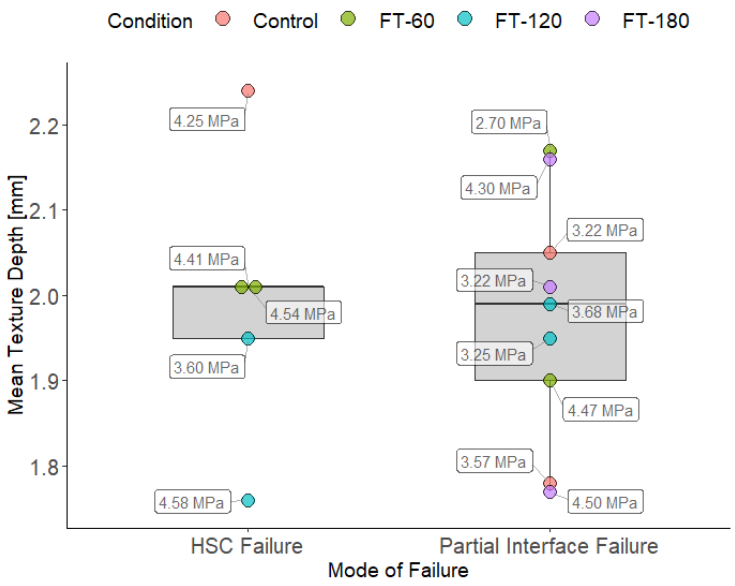
Condition
Control
FT-60
FT-120
FT-180
Mean Texture Depth [mm]
2.2
2.1
2.0
1.9
1.8
4.25 MPa
4.41 MPa
4.54 MPa
3.60 MPa
4.58 MPa
2.70 MPa
4.30 MPa
3.22 MPa
3.22 MPa
3.68 MPa
3.25 MPa
4.47 MPa
3.57 MPa
4.50 MPa
HSC Failure
Partial Interface Failure
Mode of Failure

(c)

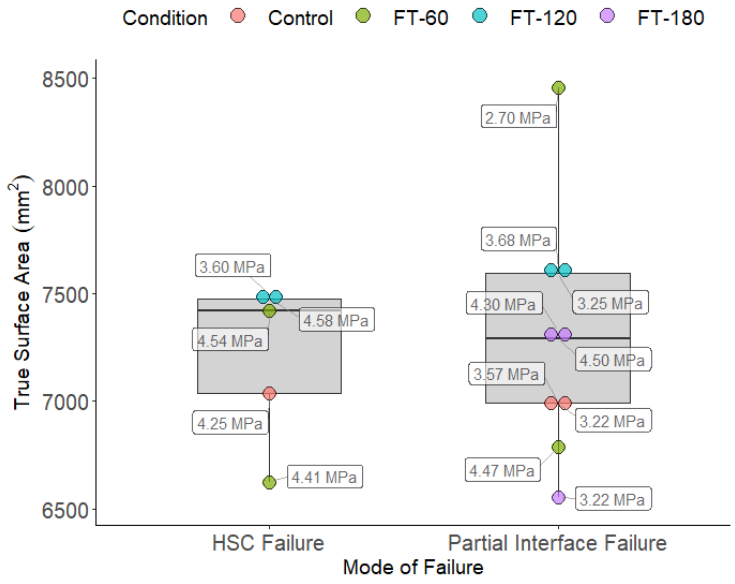
Condition
Control
FT-60
FT-120
FT-180
True Surface Area (mm²)
8500
8000
7500
7000
6500
3.60 MPa
4.58 MPa
4.54 MPa
4.25 MPa
4.41 MPa
2.70 MPa
3.68 MPa
4.30 MPa
3.25 MPa
4.50 MPa
3.57 MPa
3.22 MPa
4.47 MPa
3.22 MPa
HSC Failure
Partial Interface Failure
Mode of Failure

(d)

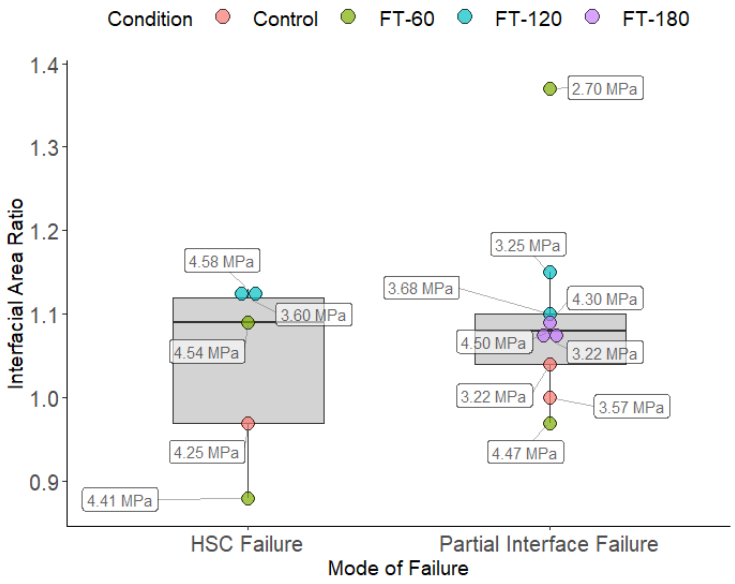

(e)

Figure 4-20 Modes of failure distribution of the durability specimens according to interface parameters: (a) R_a; (b) MPD; (c) MTD; (d) true surface area and (e) interface area ratio

4.5.1.3. Pull Off Testing after Freeze-Thaw Cycling

Table 4-12 presents the summary of the 17 pull off tensile bond tests performed after FT cycling. The tests were conducted after undergoing 60, 120 and 180 FT cycles. The FT cycles did not affect the pull off tensile strength as depicted in Figure 4-21, with the average tensile strength recorded between 4.05 MPa and 4.58 MPa. Low COVs of 14 % to 22 % observed throughout the tests showed conformity and consistency of the test results. All the specimens satisfied the ACI 546 (2006) 28-day tensile bond strength, and exceeded the “excellent” classification as stated by Sprinkel and Ozyildirim (2000). The results are comparable to the other research available in literature (Carbonell Muñoz 2012, Haber et al. 2018, De la Varga et al. 2018, Semendary and Svecova 2020a, Semendary and Svecova 2020b).

Table 4-12 Summary of the pull off tests

Specimens	Number of Specimens	Average Tensile Strength (MPa)	STD (MPa)	COV
FT-60	4	4.44	0.98	22%
FT-120	5	4.05	0.65	16%
FT-180	4	4.58	0.61	13%
Control	4	4.58	0.63	14%

STD – Standard Deviation
COV – Coefficient of Variation

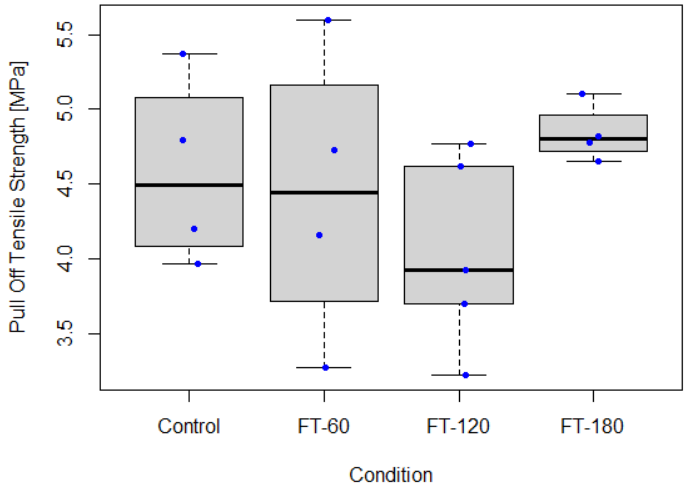

Figure 4-21 Pull off tensile strength after FT cycles

As shown in Figure 4-22, 10 out of 16 specimens failed in the HSC after FT cycles, compared to only 6 out of 16 specimens failing in HSC in the direct tension test when no thermal cycling was introduced. This means that the thermal cycles negatively affected the HSC. The interface bond strength was greater than the HSC strength after freeze-thaw cycling. All the specimens, except one control specimen and one FT-60 specimen, recorded tensile strength lower than the HSC splitting tensile strength. The average pull off tensile strength of PIF (4.59 MPa) was 5 % higher than HSC failure (4.37 MPa) specimens.

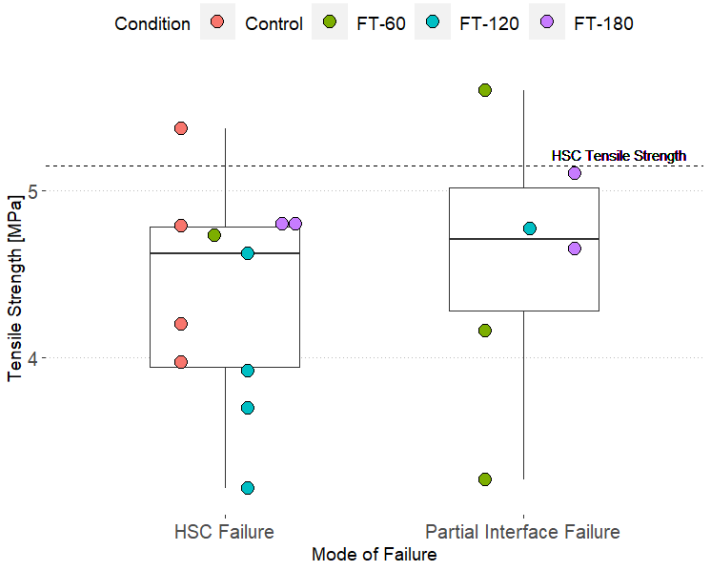

Figure 4-22 Relationship between the pull off tensile strength and the modes of failure of FT specimens

4.5.2. Slant Shear Test after Freeze-Thaw Cycling

There were total of 28 specimens tested to evaluate the bond strength of the two materials under combination of compression and shear stress. One of the specimens from FT-60 group was loaded by mistake, hence only three test data are available. Table 4-13 provides the summary of the average slant shear strength, shear and normal stresses, as well as the STDs and COVs for these stresses when tested at room temperature and at -20°C. The first specimens in the control, FT-60 and FT-120 sets were loaded under load control to determine the loading rate that was used to find displacement control rate for remaining specimens. The calculated loading rates for the control, FT-60 and FT-120 were 0.33 mm/min, 0.42 mm/min and 0.34 mm/min, respectively. The decision to maintain 0.33 mm/min loading rate for the rest of the tests was made with the purpose of reducing variables throughout the experiments.

Table 4-13 Summary of the slant shear test results

Specimen	Number of Specimens	Average Slant Shear Strength (MPa)	Average σ (MPa)	Average τ (MPa)	STD σ (MPa)	STD τ (MPa)	COV σ and τ
FT-60	3	31.7	16.6	28.7	4.0	6.9	24%
FT-120	4	29.3	15.1	26.2	3.8	6.5	25%
FT-180	4	32.1	16.5	28.5	2.5	4.4	15%
Control	4	30.8	15.8	27.3	2.4	4.2	15%
FT-60-C	4	38.5	19.6	34.0	3.7	6.4	19%
FT-120-C	4	41.9	21.6	37.5	2.4	4.1	11%
FT-180-C	4	40.7	20.6	35.7	2.0	3.4	10%

STD – Standard Deviation
COV – Coefficient of Variation

As shown in Figure 4-23, the slant shear strength was not influenced by the number of FT cycles applied. However, there was a difference in strength based on whether the test was performed at the room temperature or in the chamber. All the tests conducted in the chamber resulted in a higher slant shear strength and lower COVs compared to their counterparts tested at room temperature. The average slant shear strength of FT-60-C, FT-120-C and FT-180-C was 21 %, 43 %, and 27 % higher than their respective counterparts tested at room temperature. The highest slant shear strength of 46.5 MPa was obtained in the FT-120-C specimens and the lowest slant shear strength of 19.5 MPa was obtained in the FT-120 specimens. Overall, the COV for all FT-120, including FT-120-C specimens was 25 %. The number of FT cycles did not affect the slant shear strength.

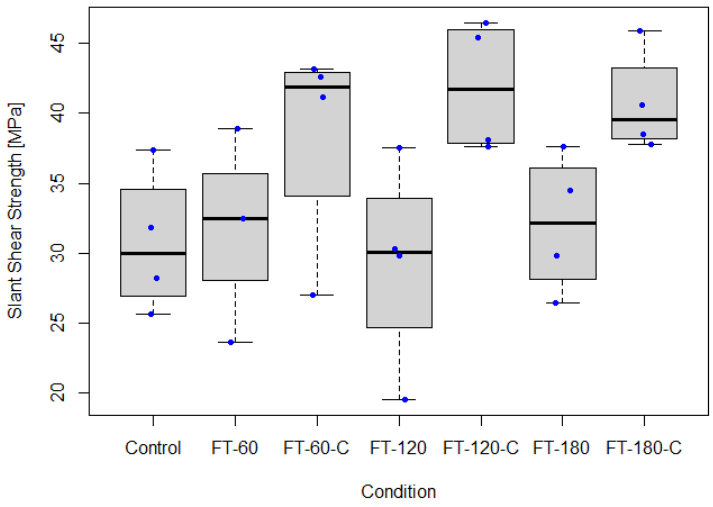

Figure 4-23 Slant shear strength after FT cycles

There were only five out of the 27 specimens that have a combination of HSC and bond interface failure as indicated in Figure 4-24. The average slant shear strength of PIF and HSC failure specimens were 36.3 MPa and 34.8 MPa, respectively. The plots do not imply causation of the slant shear strength with both modes of failure. However, test results showed satisfactory bond behaviour between the two cementitious materials with the HSC material properties being the limiting factor of the overall bond performance. Furthermore, the slant shear load-stroke graph shows that the specimens tested in the chamber failed in a brittle and explosive manner with no sign of decrease in load capacity before failure (see Figure 4-25). The load-stroke diagrams for the rest of the tests can be found in Appendix 11

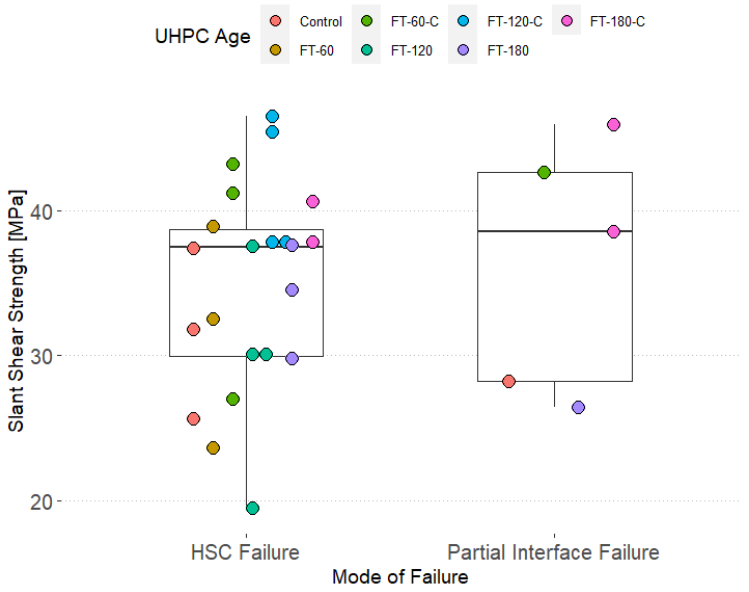

Figure 4-24 Relationship between the slant shear strength and modes of failure

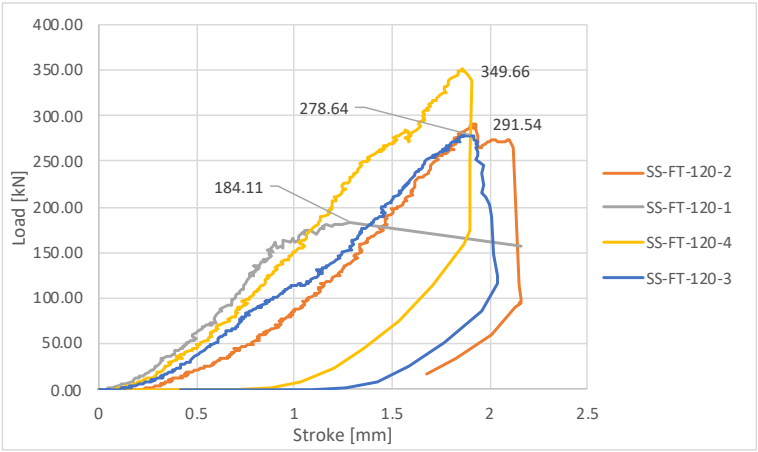

(a)

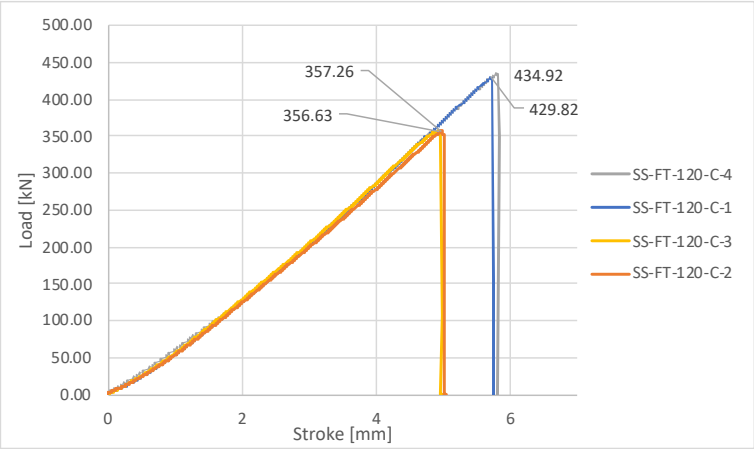

(b)

Figure 4-25 Example of slant shear load-stroke diagram: (a) 120 FT cycles specimens tested at room temperature; (b) 120 FT cycles specimens tested in the chamber

4.5.3. Bi-Shear

The summary of the 28 specimens assessed under direct shear loading is presented in Table 4-14. High COVs in the range of 20 % and 29 % were reported from the tests performed at room temperature, and 17 % to 38 % from the tests conducted in the chamber -20°C. The loading rates used were identical to those used for the other slant shear tests. The average shear strength of FT-60-C, FT-120-C and FT-180-C was 4 %, 18 % and 41 % higher than that of their respective counterparts tested at room temperature.

Table 4-14 Summary of bi-shear test results

Specimen	Number of Specimens	Average shear (MPa)	STD (MPa)	COV
FT-60	4	6.64	1.89	29%
FT-120	4	8.79	2.09	24%
FT-180	4	6.44	1.31	20%
Control	4	7.68	1.77	23%
FT-60-C	4	6.91	1.36	20%
FT-120-C	4	10.33	1.80	17%
FT-180-C	4	9.05	3.43	38%

STD – Standard Deviation
COV – Coefficient of Variation

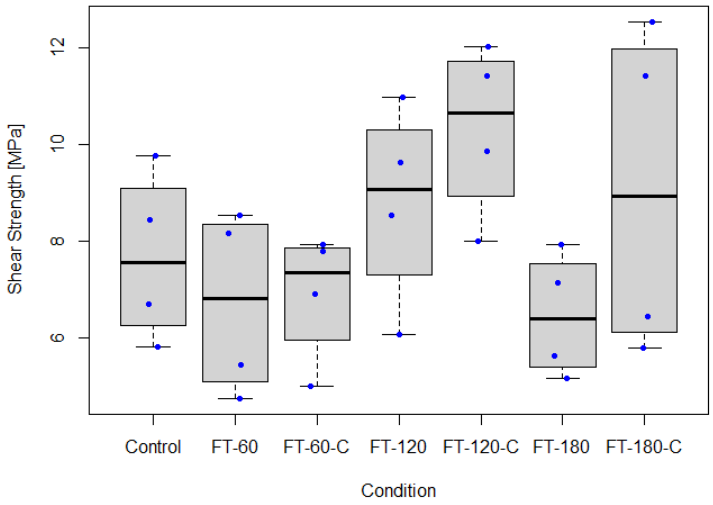

Figure 4-26 Shear strength after FT cycles

In terms of shear strength, the FT-120 showed higher median shear strength compared to the remaining FT specimens tested at room temperature. The median strength of specimens in groups FT-180 and FT-60 remained nearly constant. Therefore, the FT cycling did not have negative effect of the bi-shear strength of the specimens. The modes of failure in the bi-shear tests were complicated to characterize. The specimens usually failed at the HSC on one side and/or with fragmented pieces of HSC along the bond line. Another difference between the

specimens tested at room temperature and those tested in the environmental chamber subjected to -20°C is shown in Figure 4-27. The specimens tested at -20°C show a more brittle behaviour compared to those tested at room temperature. In an example shown in Figure 4-27, the load-stroke diagrams indicated brittle failure with no warning of impending failure for specimens tested in the chamber, compared to the tests performed at room temperature. The load-stroke diagrams of the other bi-shear tests are attached in Appendix 12.

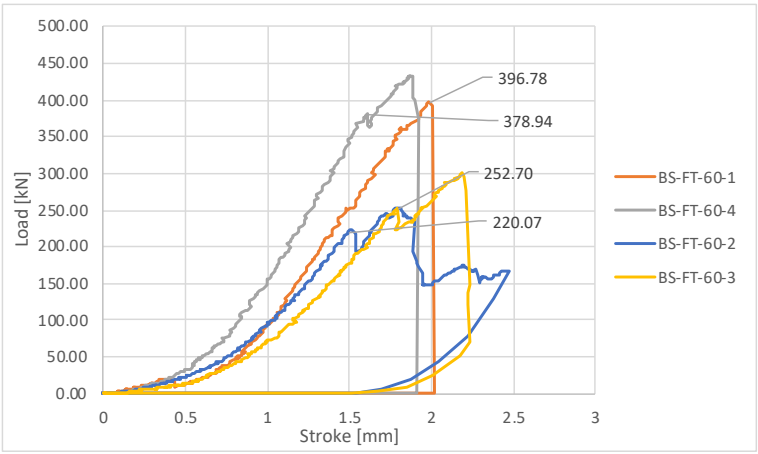

(a)

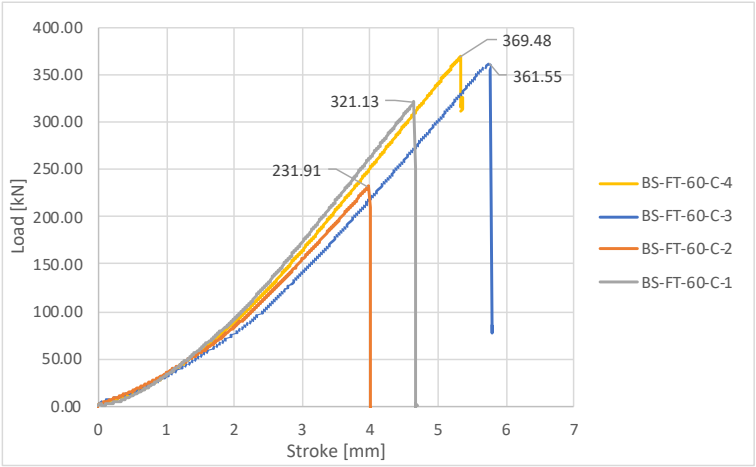

(b)

Figure 4-27 Example of bi- shear load-stroke diagram: (a) 60 FT cycles specimens tested at room temperature; (b) 60 FT cycles specimens tested in the chamber

4.5.4. Cohesion and Friction

For the cohesion and friction coefficient evaluation of the FT cycles tests – 5th percentile values of the overall test results were used in the analysis. The tensile strength in Table 4-15 and Table 4-16 comprises direct tension and pull off test data.

Table 4-15 Friction coefficient and cohesion values for specimens FT using Mohr-Coulomb's approach

Condition	Slant Shear Test		Tensile Strength, f_t (Cohesion)	Friction Coeff., μ	Internal Friction Angle, $\emptyset$
	τ_n (MPa)	σ_n (MPa)	c (MPa)		
FT-60	22.02	-12.71	2.9	1.49	56.13
FT-120	18.82	-10.87	3.23	1.46	55.59
FT-180	23.84	-13.77	2.47	1.55	57.17
Control	23.17	-13.38	3.35	1.48	55.95
FT-60-C	26.28	-15.17	-	-	-
FT-120-C	33.9	-19.57	-	-	-
FT-180-C	33.04	-19.07	-	-	-

Table 4-16 Friction coefficient and cohesion values for specimens FT using Carol's approach

Condition	Slant Shear		Direct Shear (MPa)	Friction Coeff., μ	Internal Friction Angle, Ø	Tensile Strength, f_t (MPa)	$c = \frac{2-\sin \emptyset}{\cos \emptyset} \cdot f_t$ (MPa)	$\frac{c}{Direct\ Shear}$	$\frac{c}{f_t}$
	τ_n (MPa)	σ_n (MPa)							
FT-60	22.02	-12.71	4.84	1.35	53.47	2.9	5.83	1.20	2.01
FT-120	18.82	-10.87	6.44	1.14	48.74	3.23	6.11	0.95	1.89
FT-180	23.84	-13.77	5.23	1.35	53.47	2.47	4.96	0.95	2.01
Control	23.17	-13.38	5.94	1.29	52.22	3.35	6.61	1.11	1.97
FT-60-C	26.28	-15.17	5.28	1.38	54.07	2.47[1]	5.02	0.95	2.03
FT-120-C	33.9	-19.57	8.29	1.31	52.64	3.97[1]	7.88	0.95	1.99
FT-180-C	33.04	-19.07	5.89	1.42	54.85	2.72[1]	5.60	0.95	2.05

[1]back calculated values using the c to direct shear ratio of 0.95

Due to the limited data available, FT-60-C, FT-120-C and FT-180-C cohesion and friction coefficients were not calculated using the Mohr-Coulomb's approach. Caution should be taken when using the FT-60-C, FT-120-C and FT-180-C cohesion and friction coefficients acquired from the Carol's approach because the tensile bond strength does not represent the real data and was back calculated from minimum cohesion to direct shear ratio of 0.95.

The cohesion to tensile strength ratios obtained were a few points higher than the ones presented by Espeche and Leon (2011) – the range of cohesion and tensile strength ratio reported was between 1.75 and 2.0. While the cohesion to direct shear ratios were slightly higher than the 0.84 – 0.96 showed by Zanotti and Randl (2019). The higher cohesion and lower friction coefficients obtained using Carol's approach in comparison to the Mohr-Coulomb's approach agreed with the Zanotti and Randl (2019) findings.

Other than the cohesion value estimated using the Mohr-Coulomb's approach for FT-180 specimens, the rest of the cohesion values calculated were larger than the specified values of 1.0 MPa and 2.76 MPa in the CSA S6 (2019) and AASHTO (2017), respectively for concrete placed monolithically. Both AASHTO (2017) and CSA S6 (2019) underestimated all but FT-180-C friction coefficient calculated from Carol's approach. Nonetheless, all cohesion and friction coefficients calculated using both approaches exceeded the specified values for normal weight concrete placed on intentionally roughened surface.

4.6. Discussion of the Effect of the UHPC Early Age and the Freeze-Thaw Testing on Bond Strength

The summary of individual test data from UHPC early age tests and the durability tests, including the strength, modes of failure and interface parameters are discussed in the following sections.

4.6.1. Tensile Test Results Discussion

Figure 4-28 shows the overall tensile bond behaviour under direct tension and pull off tests. As can be seen in the figure, higher tensile strength was recorded from pull off tests compared to the direct tension tests. On average, the percent difference between the pull off and direct tension strength were between 8 % to 55 % and 7 % to 30 % for UHPC early age and durability test specimens, respectively.

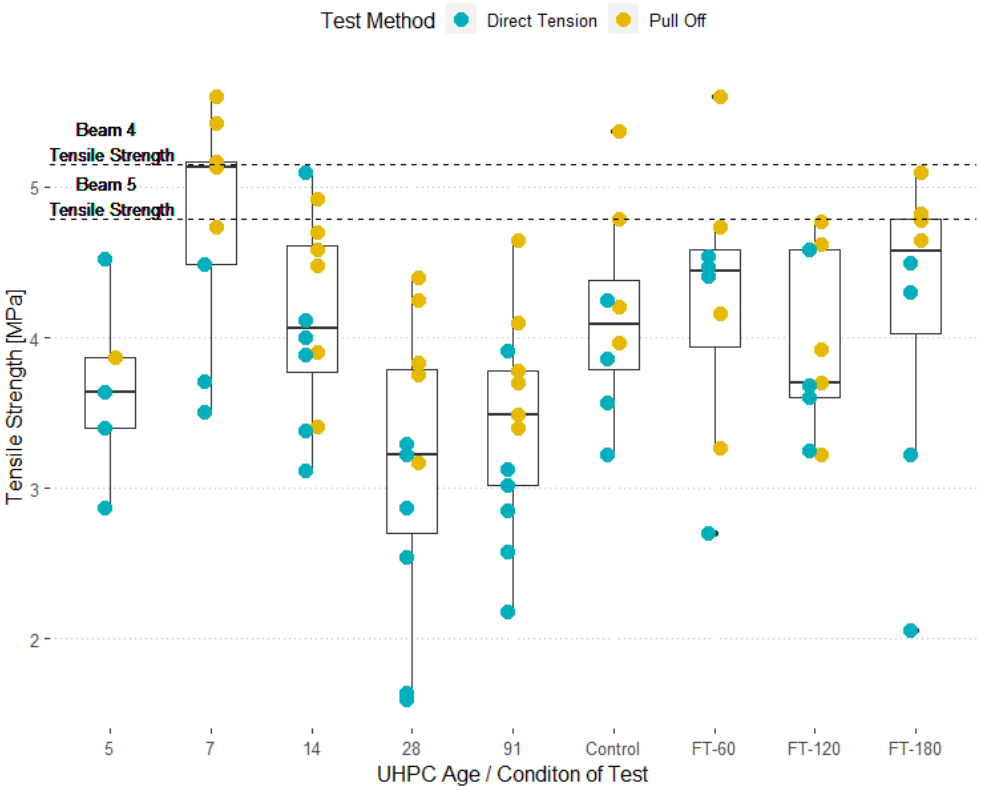

Figure 4-28 Summary of tensile strength from all direct tension and pull off tests

As provided in Table 4-17, the average tensile strength increased by 30 % from day 5 to 7 in the UHPC early age direct tension and pull off tests, but the tensile strength was seen to be tapering off after day 7, to 3.41 MPa on day 91. Zhang et al. (2020) also noticed a slight decrease in the bond strength obtained from splitting tensile, slant shear and direct tensile tests after a peak tensile strength observed on day 28 in NSC and UHPC bond interface. The negative effect of long-term shrinkage on the bond strength was speculated according to the authors.

Table 4-17 Summary of all pull off and direct tensile strengths

Assessment method	Test specimen group	Number of Specimens	Average Tensile Strength (MPa)	STD (MPa)	COV
UHPC Early Age	5 days	5	3.66	0.61	17 %
	7 days	9	4.77	0.74	15 %
	14 days	12	4.14	0.64	15 %
	28 days	11	3.14	0.93	30 %
	91 days	13	3.41	0.66	19 %
Durability	Control	8	3.98	0.51	13 %
	FT-60	8	4.26	0.52	12 %
	FT-120	9	3.93	0.59	15 %
	FT-180	8	4.48	0.61	14 %

STD – Standard Deviation
COV – Coefficient of Variation

In terms of tensile strength, the FT cycles did not affect the performance in both direct tension and pull off tests in the current study. By omitting the outlier shown in Figure 4-28, the average tensile strength of the control, FT-60, FT-120 and FT-180 calculated were 3.98 MPa, 4.26 MPa, 3.93 MPa and 4.48 MPa, respectively, with COV between 12 % and 15 %. The effect of FT cycles on the tensile strength showed improvement with respect to 28- and 91-days tests, and the tensile strength from the durability specimens was comparable to the day 14 test. The 6.2 % to 7 % of air were entrained in the HSC as provided by Lafarge may have given rise to the satisfactory durability performance of the concrete. As indicated by Carbonell Muñoz (2012), splitting tensile tests after 300 FT cycles performed in accordance with ASTM C666 Procedure A have slightly increase the bond strength, and extended FT cycles have little to no effect on the bond capacity.

Although the early age bond strength and durability test specimens were cast from different batches of HSC and varied interface parameters were quantitated (see Table 4-18), the test

results from the control set in the durability tests were very close to the test results obtained from day 14 in the early UHPC age bond specimens. This has demonstrated that the HSC material properties were likely to be the same and inter-batch variability has little effect on the tensile bond performance in the study.

4.6.1.1. UHPC Early Age Bond Test

As shown in Figure 4-29, approximately 59 % of the direct tension and pull off test specimens experienced PIF. A higher tensile strength of 4.13 MPa was recorded when specimens failed at HSC as opposed to the 3.63 MPa (outlier is excluded) when they failed in the PIF mode. All specimens from day 5 and all except one specimen from day 28 failed at the interface. On the other hand, only one out of nine specimens failed in the interface when the highest average tensile strength was observed on day 7. This one test was identified as outlier by the box plot analysis in Figure 4-29. This has indicated that the developed tensile bond strength was the strongest on day 7, and then the tensile bond strength suddenly decreased significantly after day 7 along with the shift in mode of failure. Further examination with more experimental testing will be required to understand the connection between the mode of failure and the tensile strength of the system.

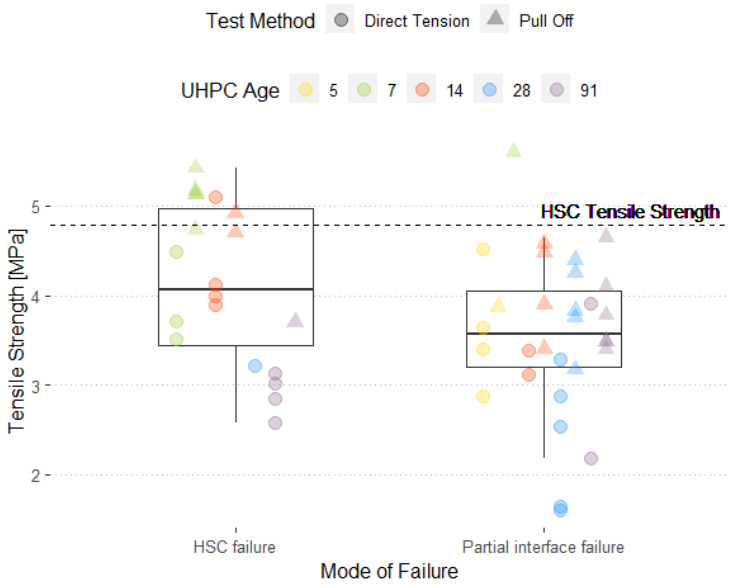

Figure 4-29 Bond age tensile tests and their respective modes of failure

4.6.1.2. Durability Test

Box plot analysis was performed on all specimens tested in tension. Figure 4-30 shows the box plot analysing the effect of test type – direct tension and pull off test, and the test exposure on specimen failure mode. As shown in Figure 4-30, approximately 55 % of the direct tension and pull off test specimens failed in the HSC. The HSC failure mode specimens have an average tensile strength of 4.32 MPa, excluding the detected outlier. The average tensile bond strength of the PIF specimens was calculated to be 4.03 MPa. The tensile bond strength for PIF specimens appeared to have higher COV of 21 % compared to 13 % of the HSC failure mode. Unlike the findings of research done by Carbonell Muñoz (2012), the FT cycles in the current study did not affect the mode of failure of the specimens.

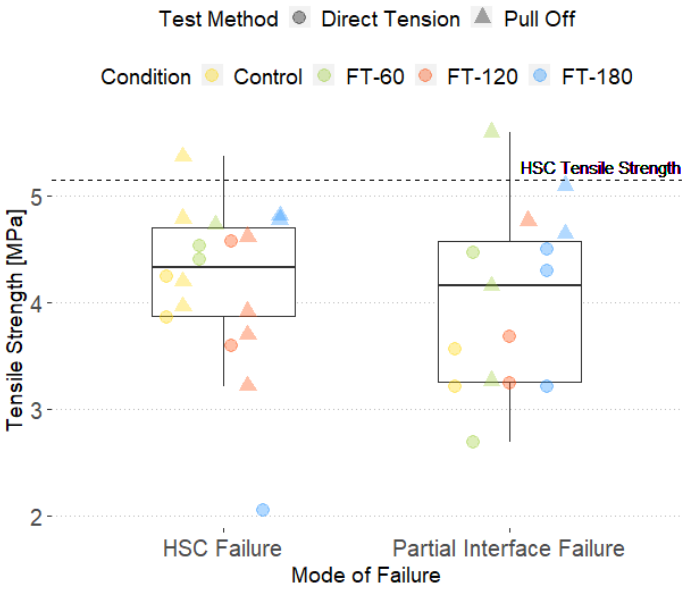

Figure 4-30 Durability tensile tests and their respective modes of failure

4.6.1.3. Surface Profile Analysis Summary

The interface parameters from all the direct tension test specimens were summarized in Table 4-18. The UHPC early age bond test specimens have a higher average for all interface parameters – which is explained by the rougher surface as depicted in Figure 4-31. Among the parameters, the R_a of the UHPC early age direct tension test specimens have the largest difference of 73 % when compared to the durability test specimens. The average direct tensile strength of the control specimens from the durability test group was in fact 28 % higher than that of the day 91 specimens of the UHPC early age test group despite the larger values of the interface parameters observed.

As presented in Table 4-18, each interface parameter provides different measurements of the surface roughness amplitudes. Although AASHTO (2017) and CSA S6 (2019) have specified the required minimum amplitude of the interface surface roughness, there is no clear indication on

the quantification method used to characterize the amplitude of the exposed aggregates surfaces. The lack of additional information in the code and standard can be confusing for engineers. According to Sprinkel (1997), minimum 250 psi (1.72 MPa) tensile bond strength was enough to achieve good long term bond performance. Bond interface with 1.5 mm amplitude macrotexture measured using the Sand Patch Method (ASTM E 965) was considered adequate to achieve good bond strength (250 psi). Carbonell Muñoz (2012) has demonstrated that the MTD of 0.6 mm to 1.06 mm was enough to achieve ACI 546 (2006) requirements for slant shear and pull off strength. In spite the fact that the Ra and MPD of the durability test specimens were lower compared to the UHPC early age test specimens, the tensile strength recorded satisfied ACI 546 (2006) 28 days direct tensile strength of 2.1 MPa.

Table 4-18 Summary of the interface parameters for both batches of specimens

Parameters (Average Values)	UHPC Early Age Test Specimens	Durability Test Specimens
Ra (mm)	1.61	0.93
Sand Patch Method (mm)	3.03	1.96
Mean Profile Depth (mm)	2.00	1.37
True Surface Area (mm^2)	8151.07	7254.16
Interfacial Area Ratio	1.33	1.07

(a) (b)

Figure 4-31 HSC exposed aggregate surfaces: (a) early age bond specimen; (b) durability direct tension test specimen

The correlations between the interface parameters of the UHPC early age specimens and durability bond tensile strength specimens are provided in Table 4-19 and Table 4-20, respectively. Overall, the interface parameters showed high correlation with each other in the UHPC early age bond tensile test specimens. The commonly used R_a has 86 %, 83 % and 92 % correlation with the interfacial area ratio, MTD and MPD, respectively. The MTD and MPD were strongly correlated with each other, which was in lieu of Liu (2015) findings. Compared to correlation of all parameters with direct tensile strength, the highest correlation was found with the true surface area parameter.

Conversely, among the correlations between the interface parameters, R_a has 69 % and 65 % correlation with MTD and MPD respectively in the durability bond tensile test specimens, while all other parameters were weakly correlated. The correlation with direct tensile strength of the

durability specimens was the highest with the interfacial area ratio. The correlation was found to be negative, meaning that the higher parameter values correspond to lower strength.

Table 4-19 Correlation between the interface parameters of UHPC early age bond direct tension test data

Parameters		Correlation					
		DT Strength	R_a	MTD	MPD	True Surface Area	Interfacial Area Ratio
Correlation	DT Strength	1.00	0.32	0.20	0.29	0.48	0.35
	R_a	0.32	1.00	0.83	0.92	0.70	0.86
	MTD	0.20	0.83	1.00	0.90	0.65	0.74
	MPD	0.29	0.92	0.90	1.00	0.69	0.81
	True Surface Area	0.48	0.70	0.65	0.69	1.00	0.85
	Interfacial Area Ratio	0.35	0.86	0.74	0.81	0.85	1.00

DT – Direct Tensile

Table 4-20 Correlation between the interface parameters of durability direct tension test data

Parameters		Correlation					
		DT Strength	R_a	MTD	MPD	True Surface Area	Interfacial Area Ratio
Correlation	DT Strength	1.00	-0.09	-0.27	-0.15	-0.36	-0.55
	R_a	-0.09	1.00	0.69	0.65	0.15	0.18
	MTD	-0.27	0.69	1.00	0.50	0.17	0.14
	MPD	-0.15	0.65	0.50	1.00	0.55	0.41
	True Surface Area	-0.36	0.15	0.17	0.55	1.00	0.89
	Interfacial Area Ratio	-0.55	0.18	0.14	0.41	0.89	1.00

DT – Direct Tensile

Table 4-21 summarizes of correlation between the interface parameters of all the direct tension test data from both test methods. The interface parameters showed strong correlations among each other; whereas evidently, the weak correlations with the direct tensile strength

demonstrated that the interface parameters did not significantly affect the direct tensile strength. The findings from the current study refuted the hypothesis of the tensile bond strength reliance on the vertical anchorage of surface irregularities in the mechanical interlock mechanism, which can be quantified by the effective surface contact area between the two concretes (Bissonnette et al. 2012).

Bissonnette et al. (2012) have pointed out that the interface roughness affects the tensile bond strength only to a certain degree, and other variables such as the material strength and curing condition also contribute to the interface bond performance. The authors also explained that the interface roughness does not affect tensile pull off strength as much as shear bond strength (Valikhani et al. 2020). Nonetheless, if the hypothesis of interlocking mechanism depends on the effective surface contact area remains valid, then theoretically the true surface area or the interfacial area ratio would be the most suitable quantification methods to relate the bond tensile strength to the interface preparation condition.

Table 4-21 Correlation between the interface parameters of all tensile test data

Parameters	DT Strength	R_a	MTD	MPD	True Surface Area	Interfacial Area Ratio
DT Strength	1.00	-0.04	-0.10	-0.06	-0.09	-0.16
R_a	-0.04	1.00	0.93	0.96	0.79	0.87
MTD	-0.10	0.93	1.00	0.95	0.78	0.83
MPD	-0.06	0.96	0.95	1.00	0.82	0.87
True Surface Area	-0.09	0.79	0.78	0.82	1.00	0.94
Interfacial Area Ratio	-0.16	0.87	0.83	0.87	0.94	1.00

4.6.2. Slant Shear Test Results Discussion

A box plot analysis of the slant shear strength from both test methods is shown in Figure 4-32. The average slant shear strength has increased 53 % after seven days of casting and the COVs were consistently between 16 % and 20 %. Since the slant shear bond strength is largely dependent on the material compressive strength in the NSC – UHPC interface (Zhang et al. 2020), the high rate of slant shear strength development may be due to the rapid strength gain of UHPC at early age. The UHPC compressive strength reached 135 MPa on day 7 (see Section 4.3), which was also 80 % of the highest UHPC compressive strength obtained throughout the experiment. All the specimens have satisfied the ACI 546 (2006) minimum bond strength requirement (see Table 2-4).

Again, the comparable average slant shear strength of 30.8 MPa, 31.7 MPa, 29.3 MPa and 32.1 MPa from the control, FT-60, FT-120 and FT-180, respectively showed that the FT cycles did not impact the slant shear performance. According to Graybeal (2006) and Hasnat and Ghafoori (2021), FT cycles have improved UHPC compressive strength due to the high rate of hydration of the excessive pozzolanic materials during the thawing period. The slant shear strength obtained from specimens tested at -20 °C was higher than the ones tested at room temperature, with the same number of FT cycles applied.

The speculations for the unchanged control and FT-60 slant shear strength could be that the 60 FT cycles selected was the actual representation of the number of FT cycles in an outdoor environment or the number of FT cycles simulated were too small to significantly affect the slant shear performance.

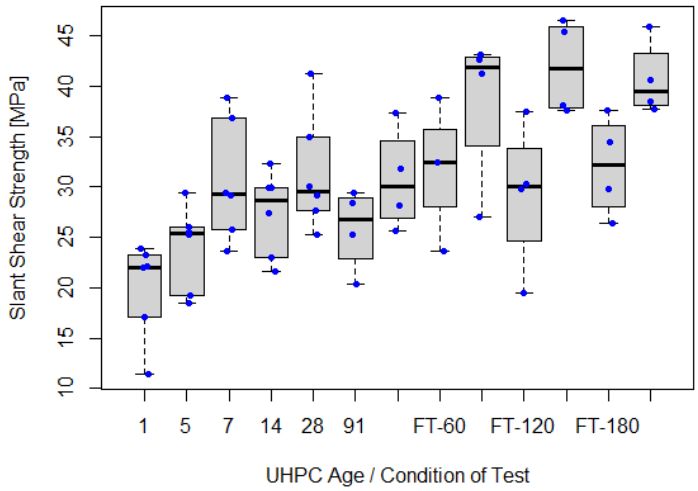

Figure 4-32 Summary of the slant shear test results

Figure 4-33 shows the box plot analysis of the effect of early age, and FT cycling of the slant shear specimens on the type of failure. Approximately 72 % of the slant shear test specimens failed in the HSC with the bond interface still intact, as presented in the figure, suggesting that the HSC material properties were the limiting factor for the interface bond performance. The box plot also shows that most of the interface failures occurred in the early age specimens. The average slant shear strength of the specimens with bond interface failure was 29.7 MPa with 27 % COV, while the average slant shear strength of the specimens with HSC failure mode was 30.6 MPa with 26 % of COV. However, there were 87 % of the specimens that were subjected to FT cycles tested in the room temperature that failed in the HSC, compared to 65 % of the UHPC early age bond test specimens – suggesting a shift in the mode of failure to a more brittle manner after undergoing FT cycles.

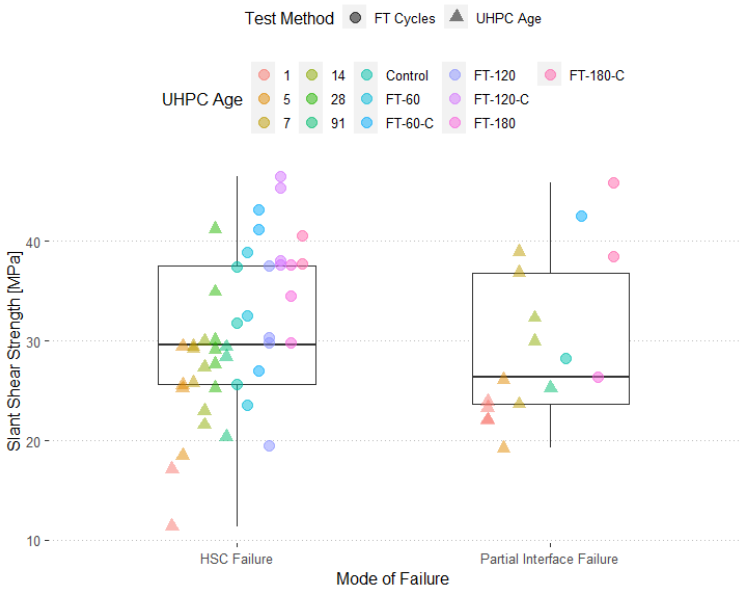

Figure 4-33 Summary of slant shear strength and modes of failure

4.6.3. Bi-Shear Test Results Discussion

The box plot analysis of the direct shear strength specimens for both early age and FT test is provided in Figure 4-34. The direct shear strength in the UHPC early age bond tests increases as UHPC matures. The ultimate average shear strength gained on day 91 was 6.63 MPa, which was 92 % increase of the initial shear strength on day 1. Valikhani et al. (2020) reported similar shear strength of 6.3 MPa for sandblasted, NSC to UHPC interface. Semendary and Svecova (2020b) has recorded an average shear strength of 6.5 MPa on day 7 after UHPC casting, while later saw a 45 % plunge in shear strength on day 28. The authors also noticed a shift in modes of failure from HSC to interface bond failure.

The average shear strength drew parallels between the day 91 of the UHPC early age bond tests, the control and FT-60 cycles of the durability tests. It implied that: (1) the bi-shear strength of the durability test specimens did not vary from the UHPC early age test specimens and (2) 60 FT

cycles selected represented the number of FT cycles in an outdoor environment well. The strengths of 91-day test and durability test specimens are higher than the strength of the specimens tested between day 1 and 14. The box plots for those days are all below the box plots for the remainder of the test days. It should be noted that the tests on day 28 and FT-180-C show a very large spread. This is denoted by the large whisker in the box plot for day 28, and the long box for the test FT-180-C. Overall there was no negative effect of the FT cycling on the specimens bi-shear strength.

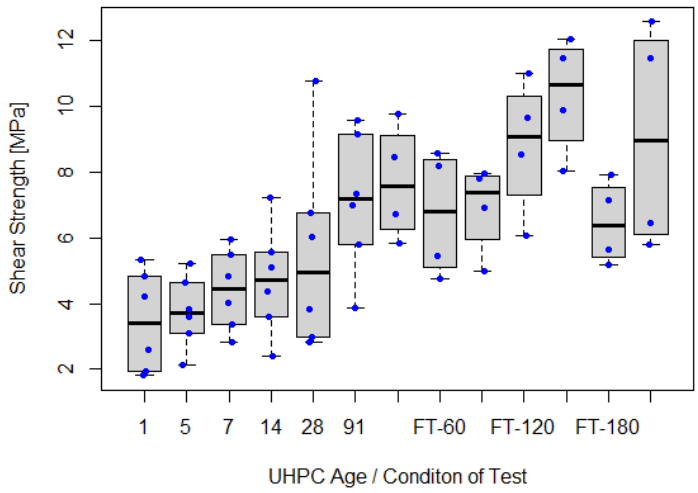

Figure 4-34 Summary of the shear test results

4.7. Fatigue Test of the Direct Tension Specimens

After being subjected to 180 freeze-thaw (FT) cycles, total of nine direct tension specimens were tested for their fatigue and direct tension performance. There were three groups of specimens tested in this portion of the experimental program, including three specimens that were tested for only the direct tensile strength.

Three specimens were tested for their direct tensile strength using the set up as mentioned in Section 3.3.2.6. These tests were conducted to compare the direct tensile strength between the specimens with and without undergoing cyclic loading, as well as the influence of the direct tensile strength using different test set up. Table 4-22 presents the direct tension test results. The direct tensile strength of specimen 3 exceeded the MTS machine maximum capacity of 25 kN. Therefore, it was not tested to failure and the direct tensile strength was recorded to be 5.48 MPa. The average direct tensile strength recorded was 5 MPa, which was 43 % increase compared to the durability FT-180 specimens. Both PIF and HSC failure were observed from the tests, and the direct tensile strength of the HSC failure specimen was 11 % higher than the PIF specimens.

Table 4-22 Summary of the direct tension tests

Specimen	Load Rate (mm/min)	Direct Tensile Strength (MPa)	Modes of Failure
1	1	4.12	PIF
2	1	5.40	HSC failure
3	1	5.48	Exceeded machine maximum load limit

The fatigue test specimens were cycled between 13 kN in compression and 14 kN in tension under 1 Hz loading rate. These loads were selected as they corresponded to 60 % of the maximum strains that were measured in the UHPC shear key in Little Morris Bridge. The results of the test program are shown in Table 4-23. Specimens that underwent 1,000,000 without failure were subjected to direct tension test following the fatigue loading. All modes of failure observed in these tests are depicted in Figure 4-35.

Table 4-23 Summary of group 2 fatigue tests

Specimen	Fatigue test			Direct tension test	
	Applied Load (kN)	Number of Cycles	Modes of Failure	Direct Tensile Strength (MPa)	Modes of Failure
F-2-1	-13; +14	23,604	HSC	-	-
F-2-2	-13; +14	26,514	UHPC	-	-
F-2-3	-13; +14	1,000,000	-	4.87	HSC
F-2-4	-13; +14	558	HSC	-	-
F-2-5	-13; +14	49,104	HSC	-	-
F-2-6	-13; +14	19,111	HSC	-	
F-2-7	-13; +14	1,000,000	-	5.34	PIF

Seven specimens were tested in the fatigue tests. There were two specimens that have successfully completed one million tension-compression loading cycles, and the rest of the specimens failed within 558 and 49,104 load cycles. Three modes of failure observed during the cyclic loading were HSC, UHPC and PIF. The average direct tensile strength obtained after a million load cycles was 5.11 MPa – which was 46 % higher than the average direct tensile strength of the FT-180 specimens tested without undergoing cyclic loading. The test results from both groups indicated that the cyclic loading did not diminish the direct tensile strength of the specimens. Comparing F-2-3 to F-2-7, the direct tensile strength of the PIF specimen was 10 % higher than the HSC failure specimen.

(a) (b)

(c)

Figure 4-35 Modes of failure: (a) UHPC; (b); partial interface and; (c) HSC failure

5. Conclusions and Recommendations

The objective of this research project was to investigate the interface bond performance between the HSC and UHPC. This work was completed along with the implementation of UHPC in the shear key of a precast box girder bridge over the Little Morris River in Manitoba. The following sections provide recommendations based on the results of this experimental program and their analysis.

5.1. Conclusions

The conclusions for the tensile, slant shear and bi-direct tests are as follows:

- Most of the UHPC early age direct tension tests achieved the minimum ACI 546 (2006) 28-day direct tensile strength of 1.7 MPa to 2.1 MPa. There were two of the tests on day 28 that achieved lower strength – 1.6 MPa and 1.64 MPa. With the direct tension test results alone, the tensile strength decreased from day 14 to day 28 and remained unchanged even on day 91 test. The average direct tensile strength of specimens that experienced the HSC failure mode was 3.64 MPa. This was slightly higher than the strength of specimens that have failed at the interface, while it was lower than the HSC splitting tensile strength.
- The average values of the interface parameters: R_a, MTD, MPD, true surface area and interfacial area ratio for the UHPC early age bond tensile tests were 1.61 mm, 3.03 mm, 2.00 mm, 8151.07 mm^2 and 1.33, respectively. The specimens that failed partially at the interface (PIF mode) had 2 to 8 % larger interface parameters than the HSC failure

specimens. The strongest correlation was identified between the interfacial area ratio and the direct tensile strength, and it was 35 %. The interface parameters were deemed to influence the direct tensile strength more in PIF specimens compared to the HSC mode of failure.

- The tensile strength of the UHPC early age pull off tests showed a declining trend from day 7 to day 91. All tensile strengths exceeded the ACI 546 minimum 28- day required direct tensile strength. A shift in the mode of failure from HSC failure to PIF was observed initiating from day 7.
- The direct tensile strength and modes of failure have no association to the number of FT cycles. The tensile strength of the specimens that failed in HSC was higher than that of specimens that failed in PIF, while it was 12 % lower than the HSC tensile splitting strength.
- The average values of the interface parameters such as R_a, MTD, MPD, true surface area and interfacial area ratio in the durability tensile tests were 0.93 mm, 1.96 mm, 1.37 mm, 7254.16 mm^2 and 1.07, respectively. There was no correlation observed between R_a and the direct tensile strength, while the interfacial area ratio was 55 % negatively correlated to the direct tensile strength. When comparing both failure modes to the influence of the interface parameters on direct tensile strength, MPD showed strongest negative correlation with direct tensile strength of 78 % in HSC failure specimens, while the interfacial area ratio was 61 % negatively correlated with the direct tensile strength for

specimens that failed partially at the interface. No relationship was found between the modes of failure and the interface parameters.

- The average pull off tensile strength ranged between 4.05 MPa and 4.58 MPa. The pull off tensile strength and modes of failure were not affected by FT cycles.
- By combining all the tensile tests performed, pull off tests generally resulted in a higher tensile strength compared to the direct tension tests. The peak average tensile strength diminished from 4.77 MPa on day 7 to 3.41 MPa on day 91; while performance in both direct tension and pull off tests was not affected by the number of FT cycles.
- The interface parameters considered in this study were not correlated with the direct tensile strength, when test data from both UHPC early age and durability test was compiled. That means that their values are not indicative of bond performance.
- The average slant shear strength reached its peak of 30.6 MPa seven days after UHPC casting, then it fluctuated between 25.9 MPa and 31.4 MPa from day 14 to day 91. All UHPC early age bond test specimens satisfied the ACI 546 minimum slant shear bond strength requirements. Regardless of the number of FT cycles applied, the average slant shear strength tested at room temperature ranged between 29.3 MPa and 32.1 MPa. 87 % of the durability specimens tested at room temperature experienced HSC failure mode in comparison to 65 % of the UHPC early age test specimens. This means that the HSC was negatively affected by the FT cycles.

- The average bi-shear strength increased from 3.45 MPa on day 1 to 6.63 MPa on day 91. There was no conclusive evidence that show relationship between the number of FT cycles and the shear strength.
- A good comparison was found between test results from the control group that was exposed to outdoor environment for 1 year and FT-60 specimens. This indicates that the FT cycles applications were comparable to actual climate simulation.
- Slant shear and bi-shear strengths were not affected by the number of FT cycles as much as the age of the UHPC and the testing conditions. Evident strength development was observed at UHPC early age, particularly from day 1 to day 7. Emphasis should be given to the early age bond performance, instead of the durability performance when designing the application of UHPC.
- Both slant shear and bi-shear specimens failed at a higher load when tested at -20 °C compared to room temperature testing. This means that bond performance during winter months will be better.
- The 5^{th} percentile of the test results was used in the cohesion and friction coefficient calculation. In the UHPC early age bond tests, the range of cohesion and friction coefficient calculated using Mohr-Coulomb's approach were 1.62 MPa to 3.59 MPa and 1.42 to 1.61, respectively; the range of cohesion and friction coefficient calculated using Carol's approach were 1.69 MPa to 6.92 MPa and 1.34 to 1.52, respectively. In the durability tests, the range of cohesion and friction coefficient calculated using Mohr-Coulomb's approach were 2.47 MPa to 3.35 MPa and 1.46 to 1.55, respectively; the range

of cohesion and friction coefficient calculated using Carol's approach were 4.96 MPa to 7.88 MPa and 1.29 to 1.42, respectively. All the cohesion and friction coefficients obtained were more conservative compared to the values specified in CSA S6 and AASHTO LRFD for normal weight concrete placed against intentionally roughened surface.

- The average direct tensile strength of the specimens using the fatigue test set up, without undergoing cyclic loading was at least 5 MPa, which was 43 % higher than the direct tensile strength of the samples that were forced to fail around the bond interface using the metal sleeve.
- The minimum and maximum load cycles achieved were 558 and 1,000,000, respectively, when the applied load cycled between 14 kN in tension and 13 kN in compression. The average direct tensile strength obtained after 1,000,000 load cycles was 5.11 MPa.
- Fatigue testing of specimens previously subjected to 180 FT to up to 1,000,000 cycles did not decrease the bond strength achieved at the interface.

5.2. Shortcomings and Recommendations

Based on the results of this experimental work, the following recommendations were formulated to improve future work:

- The early age shrinkage of UHPC is one of the important factors affecting early age bond performance of UHPC and needs to be studied further.
- The interface parameters affect the shear bond performance more than the tensile bond performance; it is therefore recommended to perform the interface profile analysis on the specimens used for shear test methods to relate the variables.

- Future work is recommended to evaluate the bond tension-compression fatigue performance at different frequency levels, as well as the fatigue performance under shear loading.

References

American Association of State Highway and Transportation Officials (AASHTO). (2017). AASHTO LRFD Bridge Design Specifications (8th Edition). American Association of State Highway and Transportation Officials (AASHTO). Retrieved from https://app.knovel.com/hotlink/toc/id:kpAASHTO94/aashto-lrfd-bridge-design/aashto-lrfd-bridge-design

ACI 318. 2014. *Building Code Requirements for Structural Concrete (ACI 318-14); and Commentary (ACI 318R-14).* Farmington Hills, MI: American Concrete Institute.

ACI 546. 2006. *Guide for the Selection of Materials for the Repair of Concrete: ACI 546.3R-06.* Farmington Hills, MI: American Concrete Institute (ACI).

Acosta, David, Olmer García, and Jorge Aponte. 2006. "Laser Triangulation for Shape Acquisition in a 3D Scanner Plus Scanner." *Proceedings - Electronics, Robotics and Automotive Mechanics Conference, CERMA 2006* 2: 14–19. https://doi.org/10.1109/CERMA.2006.54.

ASTM International. 1998 (Reapproved 2003). *C1404/C1404M - 98 Standard Test Method for Bond Strength of Adhesive Systems Used with Concrete as Measured by Direct Tension (Withdrawn 2010, No Replacement).* West Conshohocken, PA: ASTM International.

—. 2004. *C1583/C1583M-04e1 Standard Test Method for Tensile Strength of Concrete Surfaces and the Bond Strength or Tensile Strength of Concrete Repair and Overlay Materials by Direct Tension (Pull-off Method) (Withdrawn 2013).* West Conshohocken, PA: ASTM International.

—. 2012. *C882/C882M-12 Standard Test Method for Bond Strength of Epoxy-Resin Systems Used with Concrete By Slant Shear.* West Conshohocken, PA: ASTM International.

—. 2013. *C882/C882M-13a Standard Test Method for Bond Strength of Epoxy-Resin Systems Used with Concrete By Slant Shear.* West Conshohocken, PA: ASTM International.

—. 2014. *C469/C469M-14e1 Standard Test Method for Static Modulus of Elasticity and Poisson's Ratio of Concrete in Compression.* West Conshohocken, PA: ASTM International.

—. 2014. *C230/C230M-14 Standard Specification for Flow Table for Use in Tests of Hydraulic Cement.* West Conshohocken, PA: ASTM International.

—. 2015. *C666/C666M-15 Standard Test Method for Resistance of Concrete to Rapid Freezing and Thawing.* West Conshohocken, PA: ASTM International.

—. 2015. *E1845-15 Standard Practice for Calculating Pavement Macrotexture Mean Profile Depth.* West Conshohocken, PA: ASTM International.

—. 2017. *C496/C496M-17 Standard Test Method for Splitting Tensile Strength of Cylindrical Concrete Specimens.* West Conshohocken, PA: ASTM International.

—. 2017. *C1856/C1856M-17 Standard Practice for Fabricating and Testing Specimens of Ultra-High Performance Concrete.* West Conshohocken, PA: ASTM International.

—. 2018. *C39/C39M-18 Standard Test Method for Compressive Strength of Cylindrical Concrete Specimens.* West Conshohocken, PA: ASTM International.

—. 2019. *E965-15(2019) Standard Test Method for Measuring Pavement Macrotexture Depth Using a Volumetric Technique.* West Conshohocken, PA: ASTM International.

Bissonnette, Benoît, Alexander M. Vaysburd, and Kurt F. von Fay. 2012. "Best Practices for Preparing Concrete Surfaces Prior to Repairs and Overlays." Denver, Colorado: U.S. Department of the Interior Bureau of Reclamation Technical Service Center.

Carbonell Muñoz, Miguel Ángel. 2012. "Compatibility of Ultra High Performance Concrete as Repair Material : Bond Characterization with Concrete under Different Loading Scenarios," Master's Thesis, Michigan Technological University, 2012. http://digitalcommons.mtu.edu/etds/225

Carbonell, M. A., Harris, D. K., Ahlborn, T. M., and Froster, D. C. 2013. "Bond Performance Between Ultrahigh-Performance Concrete And Normal-Strength Concrete." *J. Mater. Civ. Eng.*, https://doi.org /10.1061/(ASCE)MT.1943- 5533.0000890, 04014031.

Carbonell Muñoz, Miguel A., Devin K. Harris, Theresa M. Ahlborn, and David C. Froster. 2014. "Bond Performance between Ultrahigh-Performance Concrete and Normal-Strength Concrete." *Journal of Materials in Civil Engineering* 26 (8): 1–9. https://doi.org/10.1061/(ASCE)MT.1943-5533.0000890.

CSA. 2019. CAN/CSA-S6-19, Canadian Highway Bridge Design Code. Canadian Standards Association (CSA), Mississauga, ON, Canada.

Hanna, Kromel E., George Morcous, and Maher K. Tadros. 2009. "Transverse Post-Tenioning Design and Detailing of Precast, Prestressed Concrete Adjacent Box Girder Bridges." *PCI Journal* 160-174.

El-Remaily, A., M. K. Tadros, T. Yamane, and G. Krause. 1996. "Transverse design of adjacent precast prestressed concrete box girder bridges." *Precast Prestressed Concr. Inst. J*. 41 (4): 96–113. https://doi.org /10.15554/pcij.07011996.96.113.

Espeche, Ariel D., and Javier León. 2011. "Estimation of Bond Strength Envelopes for Old-to-New Concrete Interfaces Based on a Cylinder Splitting Test." *Construction and Building Materials* 25 (3): 1222–35. https://doi.org/10.1016/j.conbuildmat.2010.09.032.

Federal Highway Administration. 2014. *Design and Construction of Field-Cast UHPC Connections, FHWA-HRT-14-084*.

Federal Highway Administration. 2019. U.S. Department of Transportation. December 2. Accessed March 25, 2021. https://highways.dot.gov/research/structures/ultra-high-performance-concrete/deployments.

Fu, H.C., M.A. Erki, and M. Seckin. 1991. "Review of Effects of Loading Rate on Concrete in Compression." *Journal of Structural Engineering* 3645-3659.

Grace, Nabil F., Elin A. Jensen, and Mena R. Bebawy. 2012. "Transverse Post-Tensioning Arrangement for Side-by-Side Box-Beam Bridges." *PCI Journal* 57 (2): 48–63. https://doi.org/10.15554/pcij.03012012.48.63.

Graybeal, Benjamin A. 2006. "Material Property Characterization of Ultra-High Performance Concrete." FHWA-HRT-06-103: 186. https://doi.org/10.1063/1.456828.

Gulyas, Robert J., Gregory J. Wirthlin, and Jeffrey T. Champa. 1995. "Evaluation of Keyway Grout Test Methods for Precast Concrete Bridges." *PCI Journal* 40 (1): 44–57. https://doi.org/10.15554/pcij.01011995.44.57.

Haber, Zachary B., Igor De La Varga, and Benjamin A. Graybeal. 2018. "Properties and Behavior of UHPC-Class Materials," FHWA-HRT-18-036: 153.

Haber, Zachary B, and Benjamin A Graybeal. 2018. "Performance of Grouted Connections for Prefabricated Bridge Deck Elements," FHWA-HIF-19-003: 156

Harris, Devin K., Miguel A. Carbonell Muñoz, Amir Gheitasi, Theresa M. Ahlborn, and Sarah V. Rush. 2014. "The Challenges Related to Interface Bond Characterization of Ultra-High-Performance Concrete With Implications for Bridge Rehabilitation Practices." *Advances in Civil Engineering Materials* 4: 20140034. https://doi.org/10.1520/acem20140034.

Hasnat, Ariful, and Nader Ghafoori. 2021. "Freeze–Thaw Resistance of Nonproprietary Ultrahigh-Performance Concrete." *Journal of Cold Regions Engineering* 35 (3): 1–9. https://doi.org/10.1061/(asce)cr.1943-5495.0000255.

Huckelbridge, Arthur A., Hassan El-Esnawi, and Fred Moses. 1995. "Shear Key Performance in Multibeam Box Girder Bridges." *Journal of Performance of Constructed Facilities* 9 (4): 271–85. https://doi.org/10.1061/(asce)0887-3828(1995)9:4(271).

Hussein, Husam H., Shad M. Sargand, and Eric P. Steinberg. 2018. "Shape Optimization of UHPC Shear Keys for Precast, Prestressed, Adjacent Box-Girder Bridges." *Journal of Bridge Engineering* 23 (4): 1–16. https://doi.org/10.1061/(ASCE)BE.1943-5592.0001220.

Hussein, Husam H., Kenneth K. Walsh, Shad M. Sargand, and Eric P. Steinberg. 2016. "Interfacial Properties of Ultrahigh-Performance Concrete and High-Strength Concrete Bridge Connections." *Journal of Materials in Civil Engineering* 28 (5): 1–10. https://doi.org/10.1061/(ASCE)MT.1943-5533.0001456.

HyMIT. 2013. *LS-40 Pavement Surface Analyzer, Operation Manual.*

Jiqiu, Yuan, Benjamin A. Graybeal, and Kevin Zmetra. 2018. "Adjacent Box Beam Connections:

Performance and Optimization," FHWA-HRT-17-093: 129.

JSCE. 2007. *Standard Specifications for Concrete Structures-2007 by Japan Society of Civil Engineers*. JSCE; 2007.

Krzywinski, Martin, and Naomi Altman. 2014. "Visualizing Samples with Box Plots." *Nature Methods* 11 (2): 119–20. https://doi.org/10.1038/nmeth.2813.

De la Varga, I., Z. B. Haber, and B. A. Graybeal. 2018. "Enhancing Shrinkage Properties and Bond Performance of Prefabricated Bridge Deck Connection Grouts: Material and Component Testing." *Journal of Materials in Civil Engineering* 30 (4): 04018053. https://doi.org/10.1061/(asce)mt.1943-5533.0002235.

Lall, Jyotirmay, Sreenivas Alampalli, and Eugene F. DiCocco. 1998. "Performance of Full-Depth Shear Keys in Adjacent Prestressed Box Beam Bridges." *PCI Journal* 43 (2): 72–79. https://doi.org/10.15554/pcij.03011998.72.79.

Lee, Ming Gin, Chui Te Chiu, and Yung Chih Wang. 2005. "The Study of Bond Strength and Bond Durability of Reactive Powder Concrete." *ASTM Special Technical Publication* 2 (1463): 104–13. https://doi.org/10.1520/stp11662s.

Li, Lin, Kelvin C.P. Wang, and Qiang Joshua Li. 2016. "Geometric Texture Indicators for Safety on AC Pavements with 1 Mm 3D Laser Texture Data." *International Journal of Pavement Research and Technology* 9 (1): 49–62. https://doi.org/10.1016/j.ijprt.2016.01.004.

Liao, Wen Cheng, Po Shao Chen, Chung Wen Hung, and Suyash Kishor Wagh. 2020. "An Innovative Test Method for Tensile Strength of Concrete by Applying the Strut-and-Tie Methodology." *Materials* 13 (12): 1–20. https://doi.org/10.3390/ma13122776.

Liu, Q. 2015. "Three-Dimensional Pavement Surface Texture Measurement and Statistical Analysis." PhD Thesis, University of Manitoba. https://mspace.lib.umanitoba.ca/handle/1993/30996.

Miller, Richard A., George M. Hlavacs, Todd Long, and Andreas Greuel. 1999. "Full-Scale Testing of Shear Keys for Adjacent Box Girder Bridges." *PCI Journal* 44 (6): 80–90. https://doi.org/10.15554/pcij.11011999.80.90.

Momayez, A., M. R. Ehsani, A. A. Ramezanianpour, and H. Rajaie. 2005. "Comparison of Methods for Evaluating Bond Strength between Concrete Substrate and Repair Materials." *Cement and Concrete Research* 35 (4): 748–57. https://doi.org/10.1016/j.cemconres.2004.05.027.

Perez, Fabien, Benoît Bissonnette, and Richard Gagné. 2009. "Parameters Affecting the Debonding Risk of Bonded Overlays Used on Reinforced Concrete Slab Subjected to Flexural Loading." *Materials and Structures/Materiaux et Constructions* 42 (5): 645–62. https://doi.org/10.1617/s11527-008-9410-x.

Prairie Climate Centre. 2019. Climate Atlas of Canada. July 10. Accessed November 2019. https://climateatlas.ca

Russell, Henry G. 2011. “Adjacent Precast Concrete Box-Beam Bridges: State of the Practice.” *PCI Journal* 56 (1): 75–91. https://doi.org/10.15554/pcij.01012011.75.91.

Santos, Dinis S., Pedro M.D. Santos, and Daniel Dias-Da-Costa. 2012. “Effect of Surface Preparation and Bonding Agent on the Concrete-to-Concrete Interface Strength.” *Construction and Building Materials* 37: 102–10. https://doi.org/10.1016/j.conbuildmat.2012.07.028.

Santos, Pedro M.D., and Júlio, Eduardo N.B.S. 2012. “A State-of-the-Art Review on Shear-Friction.” *Engineering Structures* 45: 435–48. https://doi.org/10.1016/j.engstruct.2012.06.036.

—. 2013. “A State-of-the-Art Review on Roughness Quantification Methods for Concrete Surfaces.” *Construction and Building Materials* 38: 912–23. https://doi.org/10.1016/j.conbuildmat.2012.09.045.

Semendary, Ali A., Waleed Hamid, Issam Khoury, Eric P. Steinberg, and Kenneth K. Walsh. 2019. “Experimental Investigation of Direct Tension Bond Performance of High-Strength Concrete and Ultrahigh-Performance Concrete Connections.” *Journal of Materials in Civil Engineering* 31 (9): 1–13. https://doi.org/10.1061/(ASCE)MT.1943-5533.0002800.

Semendary, Ali A., and Dagmar Svecova. 2020a. “Factors Affecting Bond between Precast Concrete and Cast in Place Ultra High Performance Concrete (UHPC).” *Engineering Structures* 216 (May): 110746. https://doi.org/10.1016/j.engstruct.2020.110746.

—. 2020b. “Interfacial Parameters for Bridge Connections at High-Strength Concrete-Ultrahigh-Performance Concrete Interface.” *Journal of Materials in Civil Engineering* 32 (4): 1–14. https://doi.org/10.1061/(ASCE)MT.1943-5533.0003107.

Sprinkel, Michael M., 1997. “Preparing Bridge Decks for Overlays”. *Aberdeen’s Concrete Repair Digest* 8(5): 242 – 247

Sprinkel, Michael M., and Celik Ozyildirim. 2000. “Evaluation of High Performance Concrete Overlays Placed on Route 60 over Lynnhaven Inlet in Virginia.” Rep. No. VTRC 01-R1, Virginia Transportation Research Council, Charlottesville, VA.

Tayeh, B. A., Abu Bakar, B. H., Megat Johari, M. A., and Zeyad, A. M. (2014). “Microstructural Analysis of the Adhesion Mechanism between Old Concrete Substrate and UHPFC*.” J. Adhes. Sci. Technol.*, 28(18), 1846–1864.

Valikhani, Alireza, Azadeh Jaberi Jahromi, Islam M. Mantawy, and Atorod Azizinamini. 2020. “Experimental Evaluation of Concrete-to-UHPC Bond Strength with Correlation to Surface Roughness for Repair Application.” *Construction and Building Materials* 238: 117753. https://doi.org/10.1016/j.conbuildmat.2019.117753.

Yoo, Doo Yeol, Jung Jun Park, Sung Wook Kim, and Young Soo Yoon. 2013. “Early Age Setting, Shrinkage and Tensile Characteristics of Ultra High Performance Fiber Reinforced Concrete.” *Construction and Building Materials* 41: 427–38. https://doi.org/10.1016/j.conbuildmat.2012.12.015.

Yuan, Jiqiu, and Benjamin Graybeal. 2016. “Full-Scale Testing of Shear Key Details for Precast Concrete Box-Beam Bridges.” *Journal of Bridge Engineering* 21 (9). https://doi.org/10.1061/(ASCE)BE.1943-5592.0000906.

Zanotti, Cristina, and Norbert Randl. 2019. “Are Concrete-Concrete Bond Tests Comparable?” *Cement and Concrete Composites* 99 (November 2018): 80–88. https://doi.org/10.1016/j.cemconcomp.2019.02.012.

Zhang, Yang, Ping Zhu, Zhaoqian Liao, and Lianhua Wang. 2020. “Interfacial Bond Properties between Normal Strength Concrete Substrate and Ultra-High Performance Concrete as a Repair Material.” *Construction and Building Materials* 235: 117431. https://doi.org/10.1016/j.conbuildmat.2019.117431.

Zhou, Zhidong, and Pizhong Qiao. 2018. “Durability of Ultra-High Performance Concrete in Tension under Cold Weather Conditions.” *Cement and Concrete Composites* 94 (August): 94–106. https://doi.org/10.1016/j.cemconcomp.2018.08.019.

Appendix

1. Precast Box Beam Material Properties from Lafarge

Table A1.1 Precast box beam material properties

Girder No.	Air %	Slump (mm)	Average Day 28 Strength (MPa)	Average (MPa)	Standard Deviation	Coefficient of Variation
1	7.2 %	220	79.0	74.5	5.4	7%
1	7.2 %	250	76.0			
1	7.5 %	250	68.6			
2	5.1 %	230	86.7	88.1	7.9	9%
2	5.8 %	210	80.9			
2	5.8 %	210	96.6			
3	6.8 %	230	87.8	86.2	1.4	2%
3	6.6 %	230	85.2			
3	6.8 %	230	85.6			
4	6.2 %	240	83.5	77.2	7.2	9%
4	7.4 %	250	69.4			
4	7.0 %	230	78.7			
5	6.7 %	220	82.7	80.2	2.8	3%
5	7.6 %	230	80.8			
5	6.4 %	230	77.2			
6	6.3 %	230	85.8	81.4	5.3	7%
6	7.5 %	250	75.5			
6	5.3 %	240	82.8			
7	7.8 %	240	80.6	77.4	3.9	5%
7	7.4 %	250	73.1			
7	6.8 %	230	78.6			
8	7.8 %	240	85.8	84.0	4.5	5%
8	5.8 %	250	78.8			
8	5.1 %	240	87.3			
Average				81.1	6.3	8%

2. On-Site UHPC Material Properties

LAFARGE
DUCTAL®

QUALITY CONTROL TESTING RESULTS

Project: PR 422 Little Morris
Client: M.D. Steele
Weather:

Date: 8/1/2019
Tech Rep: JT
Mix Type: JS1000

Total Amount Batched - 4.8 m3

Batch #	Mixer ID	Time		Mix Temp	Ambient	Flow		Lot #	Comments
		Start	Finish	Finish	Temp	Static	Dynamic		
1	R	7:08	7:28	26	20	210	220		
2	L	7:17	7:36	27	20	210	220		
3	R	7:36	7:57	28	20	225	235		
4	L	7:46	8:07	27	20	225	235		
5	R	8:05	8:22	28	20	225	235		
6	L	8:15	8:39	29	20	225	235		
7	R	8:35	8:56	31	20	225	235		
8	L	8:54	9:13	30	20	220	230		
9	R	9:12	9:27	31	20	220	230		
10	L	9:28	9:43	31	25	210	220		
11	R	9:37	9:58	31	25	220	230		
12	L	9:52	10:19	33	25	205	215		
13	R	10:18	10:37	34	25	205	215		
14	L	10:32	10:50	34	25	210	220		
15	R	10:45	11:06	34	25	210	220		
16	L	11:06	11:20	34	25	220	230		
17	R	11:20	11:54	34	25	220	230		
18	L	11:49	12:06	34	25	220	230		
19	R	12:06	12:22	34	28	210	220		
20	L	12:18	12:39	34	28	210	220		
21	R	12:30	12:45	34	28	210	220		
22	L	12:43	1:02	34	28	210	220		
23	R	12:56	1:19	34	28	210	220		
24	L	1:13	1:38	34	28	210	220		
25	R	1:34	1:52	35	28	210	220		
26	L	1:49	2:13	36	28	210	220		
27	R	2:00	2:19	36	28	210	220		
28	L	2:14	2:33	36	28	210	220		
29	R	2:35	2:52	36	30	220	230		
30	L	2:47	3:05	36	30	220	230		
31	R	3:00	3:17	35	30	220	230		
32	L	3:12	3:28	36	30	220	230		

Casting Location:	
Mixer ID(s) #:	
Batch Size and Bag Format:	
Comments:	

Figure A2.1 Fresh UHPC material properties

3. HSC Material Properties Tested in the Lab

Table A3.1 HSC compressive strength tested in the lab

Test Dates (2019)	Girder	Load (LB)	Strength (Psi)	Strength (MPa)	Average (MPa)	Comment
03-Oct	1	93780	7462.8	51.5[1]		
03-Oct	1	77340	6154.5	42.4[1]		
03-Oct	1	122070	9714.0	67.0		
04-Oct	1	133990	10662.6	73.5	75.7	retested after modulus test
04-Oct	1	130940	10419.9	71.8		retested after modulus test
04-Oct	1	143340	11406.6	78.6		retested after modulus test
13-Nov	1	142970	11377.2	78.4		
13-Nov	1	154390	12286.0	84.7		
03-Oct	2	160390	12763.4	88.0		retested after modulus test
03-Oct	2	133810	10648.3	73.4		
03-Oct	2	140470	11178.2	77.1	86.9	retested after modulus test
04-Oct	2	161010	12812.8	88.3		retested after modulus test
13-Nov	2	168010	13369.8	92.2		
13-Nov	2	186300	14825.3	102.2		
04-Oct	3	144400	11491.0	79.2		
04-Oct	3	101140	8048.5	55.5		
04-Oct	3	102770	8178.2	56.4	71.9	
13-Nov	3	148880	11847.5	81.7		
13-Nov	3	157910	12566.1	86.6		
04-Oct	4	127470	10143.7	69.9		
04-Oct	4	84450	6720.3	46.3[1]		
04-Oct	4	120740	9608.2	66.2		
04-Oct	4	124420	9901.0	68.3	70.8	retested after modulus test
04-Oct	4	136750	10882.2	75.0		retested after modulus test
04-Oct	4	111100	8841.1	61.0		retested after modulus test
13-Nov	4	140430	11175.1	77.0		
13-Nov	4	142890	11370.8	78.4		
6-Aug	5	139470	11098.7	76.5		
6-Aug	5	128140	10197.1	70.3	73.9	
6-Aug	5	136680	10876.6	75.0		
03-Oct	6	130190	10360.2	71.4		retested after modulus test
03-Oct	6	116710	9287.5	64.0	75.6	retested after modulus test
03-Oct	6	134570	10708.7	73.8		retested after modulus test

03-Oct	6	134910	10735.8	74.0		
13-Nov	6	157730	12551.8	86.5		
13-Nov	6	153010	12176.1	84.0		
04-Oct	7	89290	7105.5	49.0[1]		
04-Oct	7	143330	11405.8	78.6		
04-Oct	7	146890	11689.1	80.6	86.3	
13-Nov	7	163640	13022.1	89.8		
13-Nov	7	168160	13381.7	92.3		
13-Nov	7	164650	13102.4	90.3		
04-Oct	8	101940	8112.1	55.9		
04-Oct	8	133360	10612.5	73.2		
04-Oct	8	84630	6734.6	46.4		
13-Nov	8	125520	9988.6	68.9	73.6	
13-Nov	8	166160	13222.6	91.2		
14-Nov	8	158810	12637.7	87.1		
14-Nov	8	168370	13398.5	92.4		

[1] outlier(s): excluded from average compressive strength calculation

Table A3.2 HSC modulus of elasticity

Date of Testing (2019)	Girder	40% of f'_c (MPa)	Nearest 40% f'_c (MPa)	Stress @ ε_1 (MPa)	Strain at 40% f'_c (MPa)	Modulus of Elasticity (MPa)	Average E (MPa)
04-Oct	1	30.2	30.22	2.35	0.00081	36590	
04-Oct	1		30.27	1.69	0.00084	35934	36744
04-Oct	1		30.08	2.24	0.00079	37708	
03-Oct	2		35.69	3.01	0.00084	41374	
03-Oct	2	35.8	35.82	2.91	0.00090	38655	40000
04-Oct	2		35.88	2.75	0.00088	39989	
04-Oct	4		30.61	2.29	0.00083	36364	
04-Oct	4	30.7	30.84	2.53	0.00082	37121	36743
04-Oct	4		30.67	2.33	0.00083	36742	
03-Oct	6		29.17	2.04	0.00079	36434	
03-Oct	6	29.2	29.22	1.85	0.00077	37714	37418
03-Oct	6		29.20	2.55	0.00075	38108	

Table A3.3 HSC Poisson's ratio

Date of Testing (2019)	Girder	ε_{t1}	ε_{t2}	Poisson's Ratio	Average

04-Oct	1	0.0000244	0.0002408	0.28	0.28
04-Oct	1	0.0000203	0.0002259	0.26	
04-Oct	1	0.0000243	0.0002409	0.29	
03-Oct	2	0.0000203	0.0002331	0.27	0.26
03-Oct	2	0.0000236	0.0002369	0.25	
04-Oct	2	0.0000271	0.0002544	0.27	
04-Oct	4	0.0000100	0.0002078	0.25	0.26
04-Oct	4	0.0000217	0.0002226	0.26	
04-Oct	4	0.0000260	0.0002364	0.27	
03-Oct	6	0.0000214	0.0002184	0.26	0.27
03-Oct	6	0.0000265	0.0002102	0.25	
03-Oct	6	0.0000306	0.0002274	0.28	

Table A3.4 HSC splitting tensile strength

Date of Testing (2019)	Girder	Splitting Tensile Strength (MPa)	Average (MPa)
04-Oct	1	5.38	5.52
04-Oct		5.41	
04-Oct		5.78	
03-Oct	2	6.10	5.52
03-Oct		4.91	
04-Oct		5.55	
04-Oct	4	4.91	5.15
04-Oct		5.70	
04-Oct		4.84	
7-Aug	5	5.61	4.79
7-Aug		4.11	
7-Aug		4.64	
03-Oct	6	4.94	5.66
03-Oct		6.13	
03-Oct		5.92	

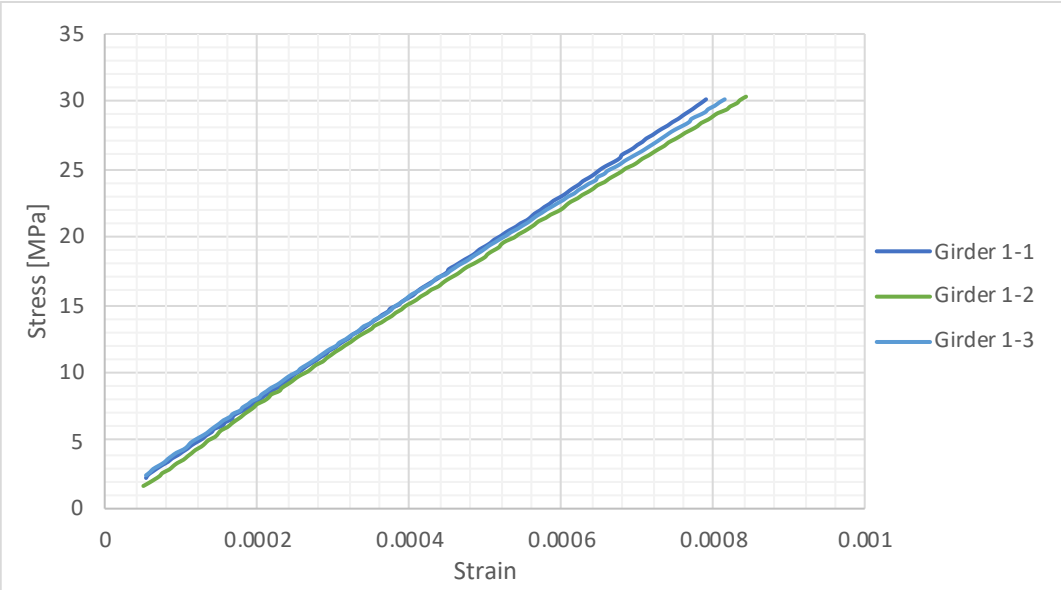

Figure A3.1 Stress-strain graph for Beam 1 HSC loaded to 40 % of the compressive strength

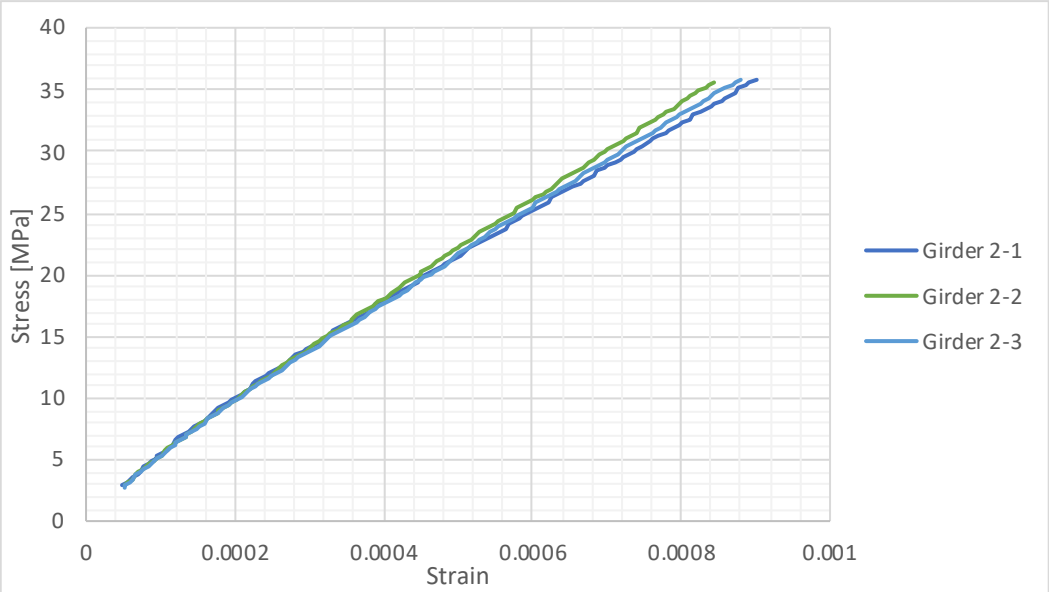

Figure A3.2 Stress-strain graph for Beam 2 HSC loaded to 40 % of the compressive strength

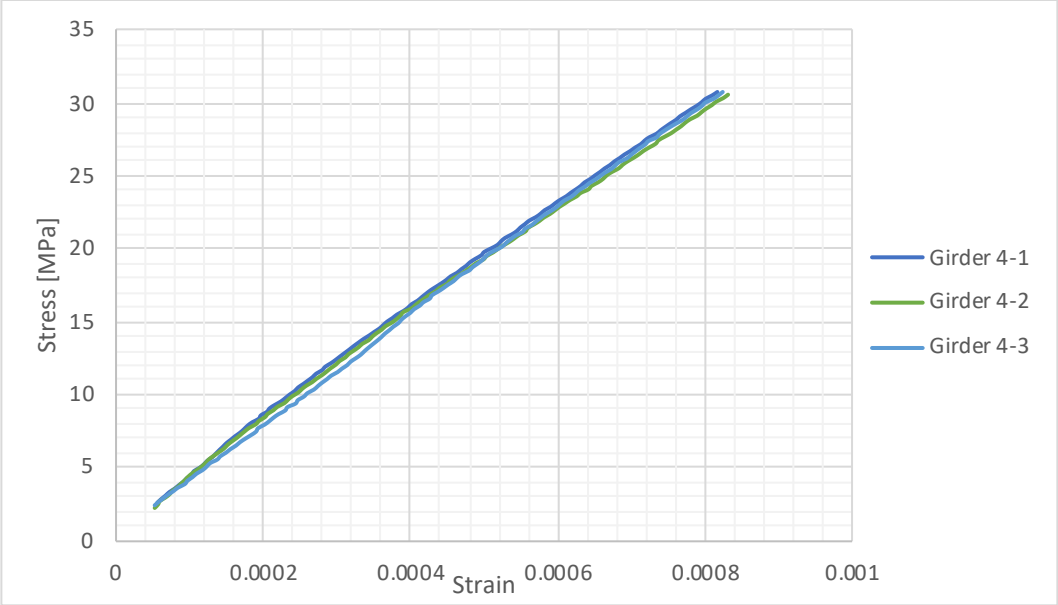

Figure A3.3 Stress-strain graph for Beam 4 HSC loaded to 40 % of the compressive strength

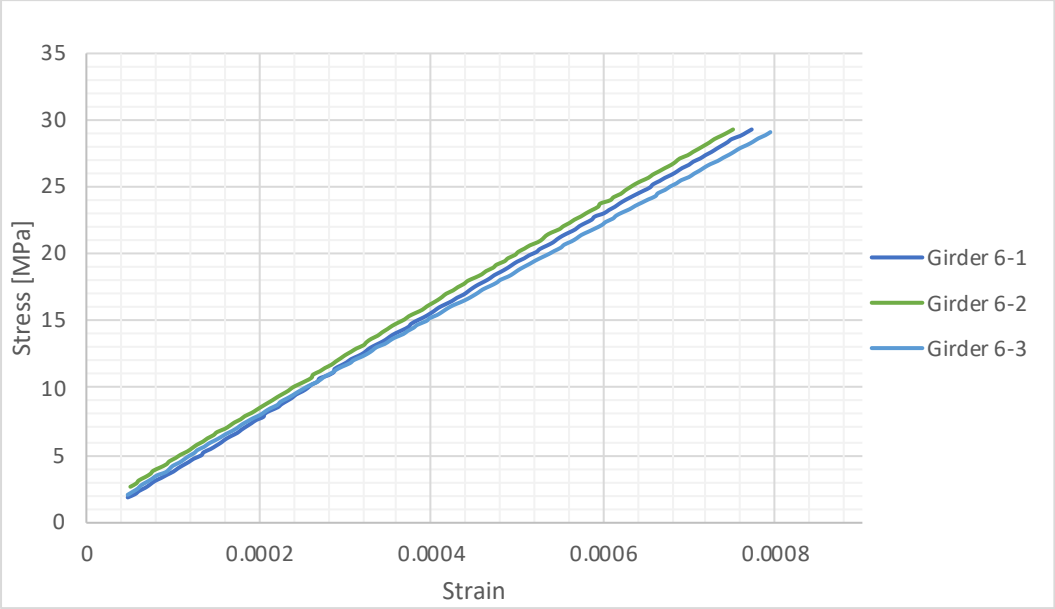

Figure A3.4 Stress-strain graph for Beam 6 HSC loaded to 40 % of the compressive strength

4. UHPC Material Properties Tested in the Lab

Table A4.1 UHPC compressive strength

Date of Casting	UHPC Age (days)	Strength (MPa)	Average (MPa)	Comment
30-Jul	1	16.9	14.7	
30-Jul	1	16.8		
30-Jul	1	10.3		
30-Jul	3	113.2	106.3	
30-Jul	3	103.9		
30-Jul	3	101.8		
30-Jul	7	152.5	138.2	
30-Jul	7	126.9		
30-Jul	7	135.2		
30-Jul	14	146.5	146.4	
30-Jul	14	139.1		
30-Jul	14	153.4		
30-Jul	28	172.1	164.4	
30-Jul	28	162.9		
30-Jul	28	158.1		
01-Aug	1	40.8	43.5	
01-Aug	1	40.9		
01-Aug	1	48.7		
01-Aug	5	103.3	125.1	
01-Aug	5	137.4		
01-Aug	5	127.1		
01-Aug	5	125.7		
01-Aug	5	131.8		
01-Aug	7	98.9	135.0	
01-Aug	7	148.1		
01-Aug	7	148.7		
01-Aug	7	144.2		
01-Aug	14	171.9	167.9	
01-Aug	14	163.7		
01-Aug	14	168.3		
01-Aug	28	136.1	152.7	
01-Aug	28	168.4		
01-Aug	28	153.7		
01-Aug	91	148.5	164.2	
01-Aug	91	184.0		

01-Aug	91	160.1		

Table A4.2 UHPC modulus of elasticity

Date of Casting	UHPC Age (days)	40% f'c (MPa)	Modulus of Elasticity (MPa)	Average (MPa)
30-Jul	1	5.87	11797	16388
30-Jul			12395	
30-Jul			24973	
30-Jul	3	42.52	42123	42257
30-Jul			42392	
30-Jul			55660	
01-Aug	1	17.38	33159	28264
01-Aug			24850	
01-Aug			26784	
01-Aug	5	52.20	46137	43421
01-Aug			42988	
01-Aug			41137	
01-Aug	7	58.80	41612	45597
01-Aug			44795	
01-Aug			50383	
01-Aug	14	67.18	50588	51039
01-Aug			52377	
01-Aug			50152	
01-Aug	28	61.10	50444	50392
01-Aug			48889	
01-Aug			51842	
01-Aug	91	65.67	61371	58721
01-Aug			57162	
01-Aug			57630	
01-Aug	106	65.67	55573	53894
01-Aug			54277	
01-Aug			53510	

5. Direct Tension Test Results

Table A5.1 Summary of direct tension test results at UHPC early age

UHPC Age (days)	Tensile Strength (MPa)	Average Tensile Strength (MPa)	Mode of Failure	STD (MPa)	COV
5	Exp. error	3.6	-	0.7	19 %
	3.46		C		
	4.52		A		
	3.64		A		
	2.87		A		
	3.40		A		
7	3.71	3.9	B	0.5	13 %
	3.51		B		
	3.75		C		
	3.58		C		
	4.49		B		
	Exp. error		-		
14	4.00	3.9	B	0.7	18 %
	4.21		B		
	3.12		A		
	3.89		B		
	3.38		A		
	5.10		B		
28	1.64	2.5	A	0.8	30 %
	2.87		A		
	2.54		A		
	1.60		A		
	3.29		A		
	3.22		A		
91	2.85	2.9	B	0.6	20 %
	2.18		A		
	3.02		B		
	3.13		B		
	2.58		B		
	3.91		A		

Note: A: PIF, B: HSC failure, C: Epoxy failure

6. Pull Off Test Results

Table A6.1 Summary of pull off test results at UHPC early age

UHPC Age (days)	Tensile Strength (MPa)	Average Tensile Strength (MPa)	Mode of Failure	STD (MPa)	COV
5	3.87	3.87	A	-	-
	-		C		
	4.92		C		
	3.27		C		
7	5.13	5.20	B	0.30	6 %
	5.17		B		
	4.73		B		
	5.13		B		
	5.60		A		
	5.42		B		
14	3.41	4.33	A	0.57	13 %
	3.90		A		
	4.70		B		
	4.48		A		
	4.58		A		
	4.92		B		
28	4.40	3.88	A	0.48	12 %
	5.27		C		
	3.17		A		
	3.83		A		
	4.25		A		
	3.75		A		
91	3.40	3.80	A	0.44	12 %
	3.49		A		
	2.94		C		
	3.78		A		
	2.29		C		
	4.06		C		
	4.65		A		
	3.49		A		
	4.10		A		
	3.70		B		
	0.45		C		

	4.58		C		

Note: A: PIF, B: HSC failure, C: Epoxy failure

7. Slant Shear Test Results

Table A7.1 Summary of slant shear test results at UHPC early age

UHPC Age (days)	Specimen ID	Slant Shear Strength (MPa)	Average (MPa)	Mode of Failure	Normal stress (MPa) σ	Shear (MPa) τ	Average σ	Average τ	STD σ	STD τ	σ and τ COV
1	1	17.1	20.0	B	8.6	14.9	10.1	17.4	2.4	4.2	24 %
	2	23.3		A	11.5	19.9					
	3	22.0		A	11.2	19.4					
	4	22.1		A	11.2	19.5					
	5	11.4		B	5.8	10.0					
	6	23.9		A	12.0	20.8					
5	1	29.4	24.0	B	15.0	25.9	12.2	21.1	2.2	3.8	18 %
	2	18.5		B	9.4	16.2					
	3	25.6		B	12.9	22.4					
	4	25.2		B	13.0	22.5					
	5	19.2		A	9.7	16.8					
	6	26.1		A	13.2	22.8					
7	1	23.7	30.6	A	12.0	20.8	15.6	27.0	3.1	5.4	20 %
	2	36.8		A	18.8	32.6					
	3	29.2		B	14.7	25.5					
	4	29.4		B	15.0	26.0					
	5	38.9		A	19.8	34.3					
	6	25.8		B	13.2	22.8					
14	1	30.0	27.4	B	14.7	25.5	13.8	23.9	2.1	3.6	15 %
	2	32.3		A	16.4	28.5					
	3	23.0		B	11.6	20.1					
	4	21.6		B	11.0	19.1					
	5	30.0		A	15.1	26.1					
	6	27.4		B	14.0	24.2					
28	1	30.1	31.4	B	16.1	27.9	16.4	28.4	3.2	5.5	19 %
	2	25.3		B	13.1	22.7					
	3	34.9		B	17.4	30.2					
	4	27.7		B	14.3	24.7					
	5	41.2		B	22.1	38.4					
	6	29.1		B	15.4	26.7					

91	1	28.4	25.9	B	14.6	25.4	13.3	23.0	2.0	3.5	15 %
	2	20.4		B	10.6	18.4					
	3	25.3		A	12.8	22.1					
	4	29.4		B	15.1	26.2					

Note: σ = normal stress; τ = shear stress; A: HSC and bond interface failed; B: HSC failed

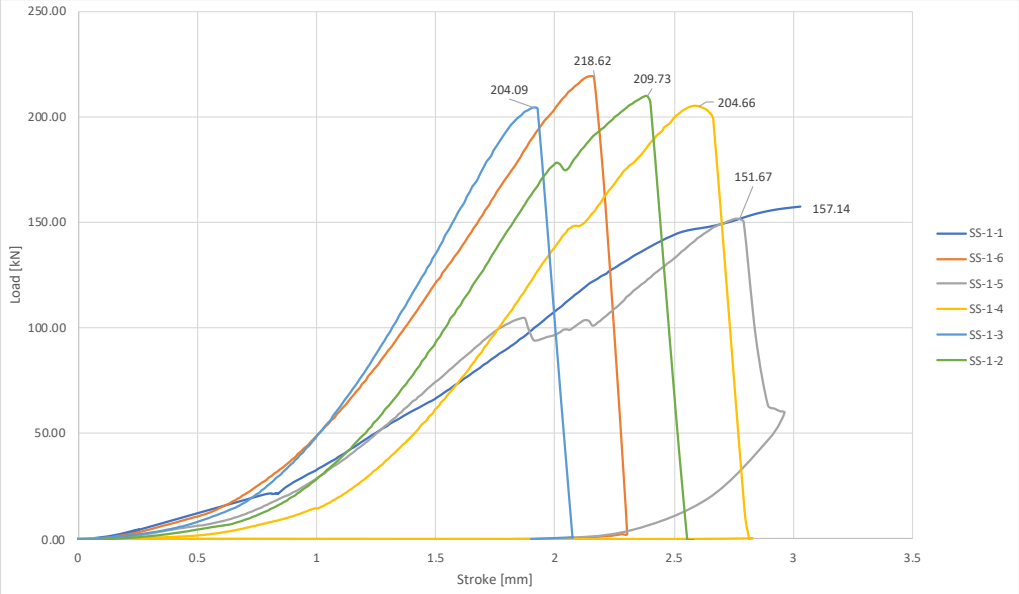

Figure A7.1 Load-stroke diagram for slant shear test on day 1 after UHPC casting

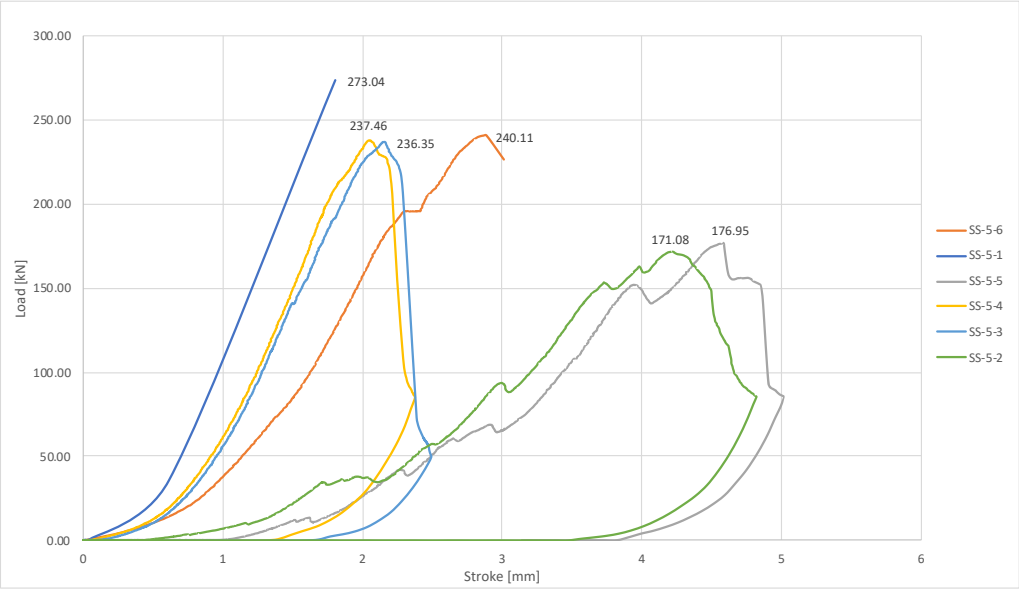

Figure A7.2 Load-stroke diagram for slant shear test on day 5 after UHPC casting

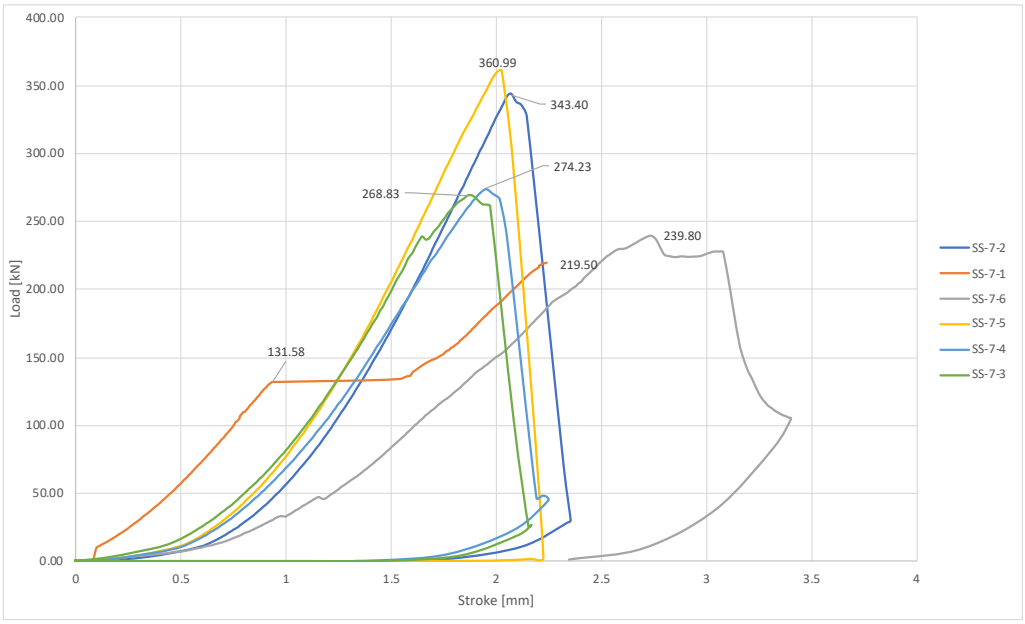

Figure A7.3 Load-stroke diagram for slant shear test on day 7 after UHPC casting

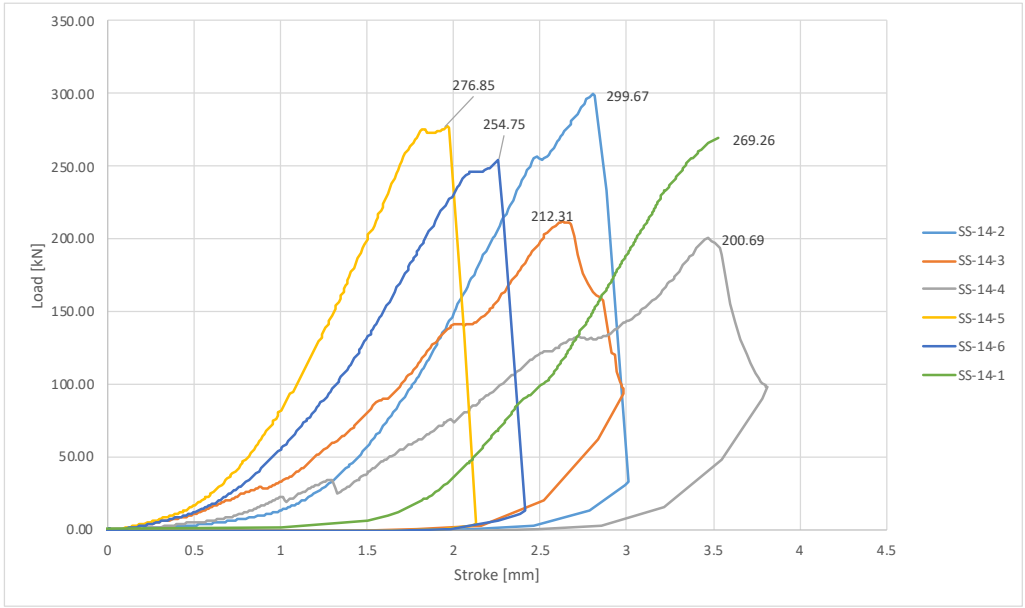

Figure A7.4 Load-stroke diagram for slant shear test on day 14 after UHPC casting

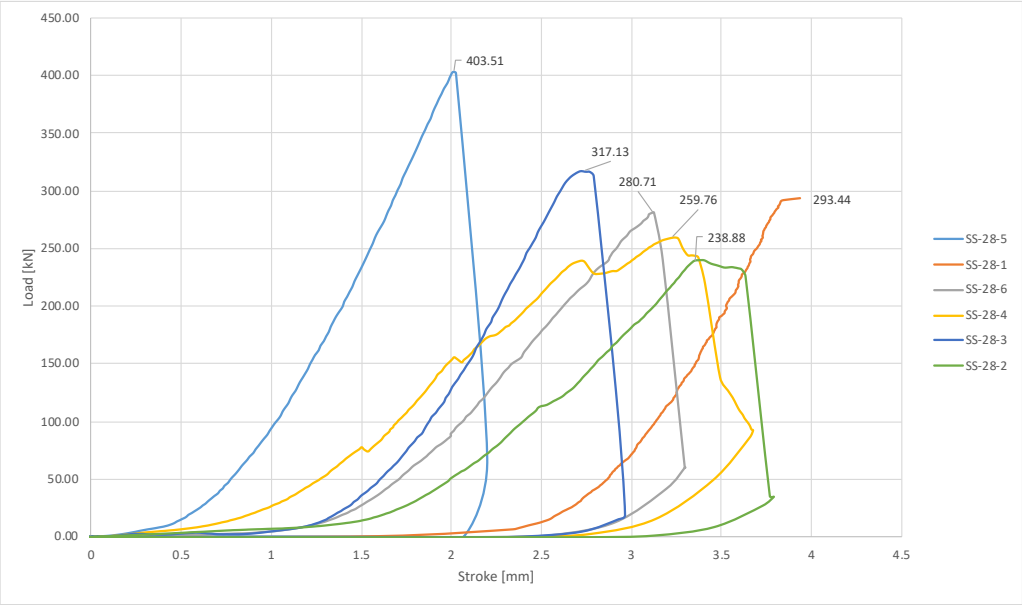

Figure A7.5 Load-stroke diagram for slant shear test on day 28 after UHPC casting

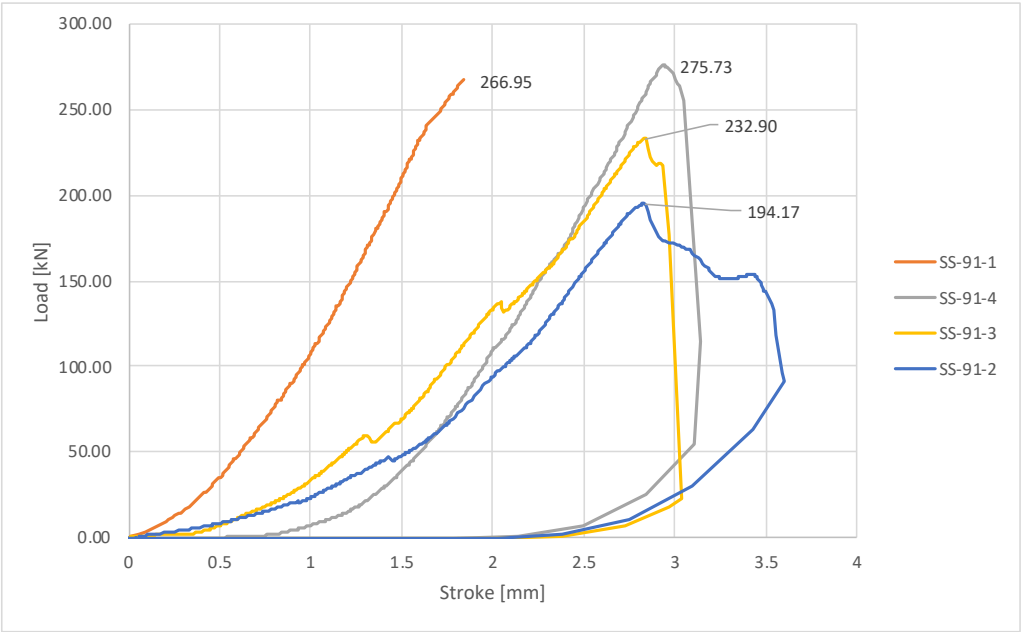

Figure A7.6 Load-stroke diagram for slant shear test on day 91 after UHPC casting

8. Bi-Shear Test Results

Table A8.1 Summary of bi-shear test results at UHPC early age

UHPC Age (days)	Specimen ID	Shear Strength (MPa)	Average Shear (MPa)	STD (MPa)	COV
1	11	4.82	3.45	1.53	44 %
	12	2.58			
	13	5.34			
	14	1.81			
	17	1.94			
	18	4.20			
5	3	3.08	3.75	1.10	29 %
	4	4.63			
	5	2.15			
	6	5.23			
	25	3.60			
	26	3.81			
7	1	4.03	4.42	1.22	28 %
	2	4.84			
	23	2.82			
	24	5.49			
	41	3.38			
	42	5.96			
14	8	7.23	4.71	1.66	35 %
	7	5.55			
	22	3.60			
	9	5.08			
	21	2.41			
	10	4.37			
28	19	2.99	5.53	3.02	55 %
	20	3.83			
	33	6.74			
	34	10.74			
	39	2.82			
	40	6.03			
91	15	5.79	6.63	2.12	32 %
	16	7.00			
	27	9.15			

	29	9.56			
	31	7.34			
	32	3.85			

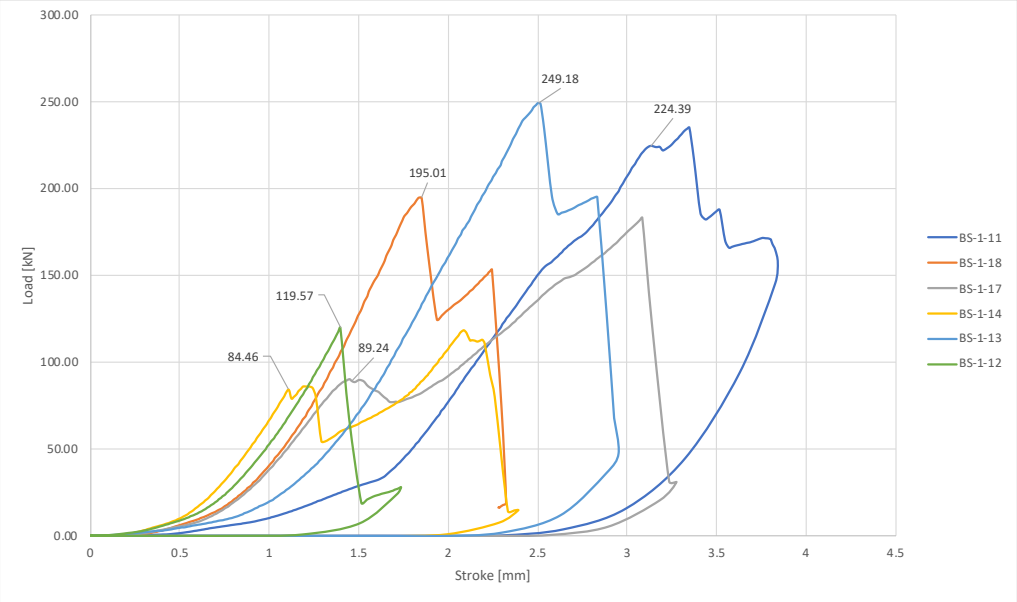

Figure A8.1 Load-stroke diagram for bi-shear test on day 1 after UHPC casting

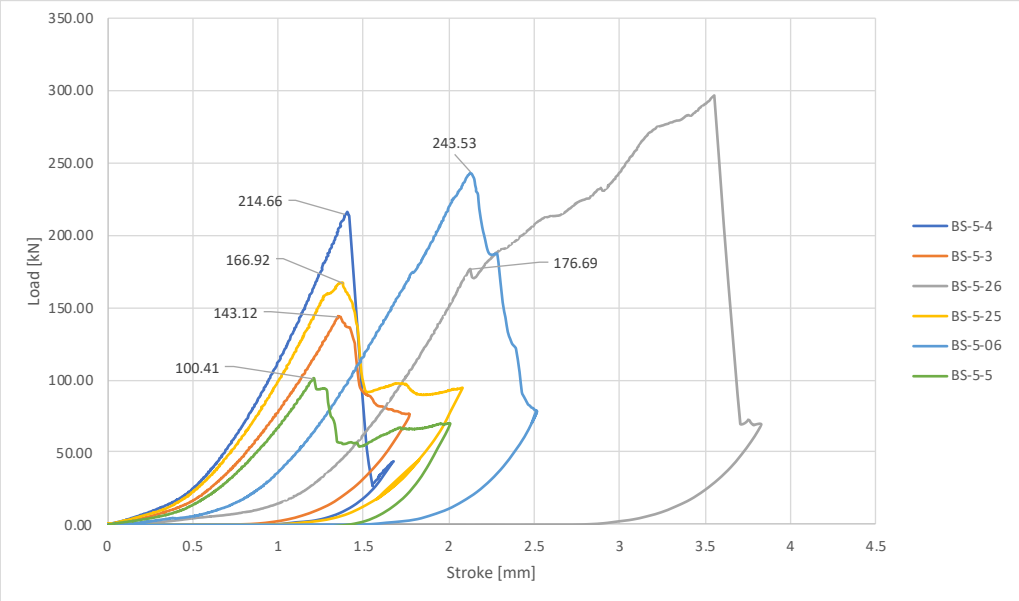

Figure A8.2 Load-stroke diagram for bi-shear test on day 5 after UHPC casting

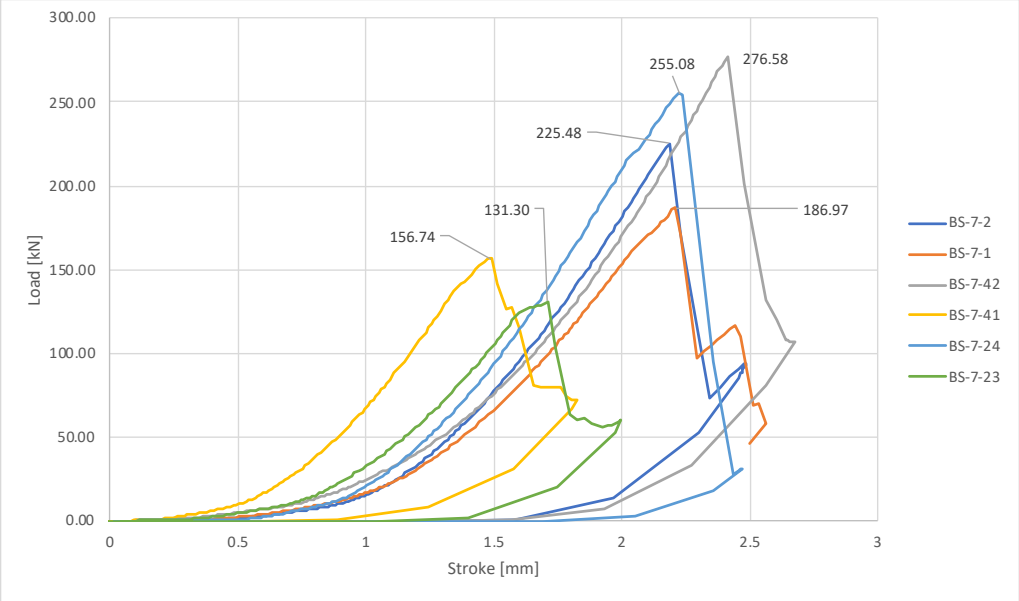

Figure A8.3 Load-stroke diagram for bi-shear test on day 7 after UHPC casting

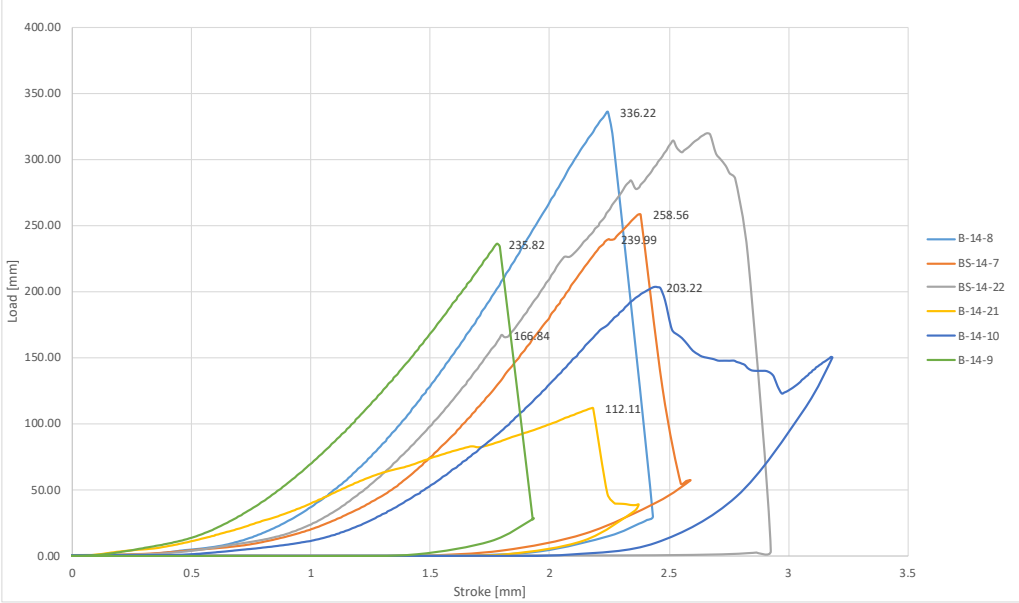

Figure A8.4 Load-stroke diagram for bi-shear test on day 14 after UHPC casting

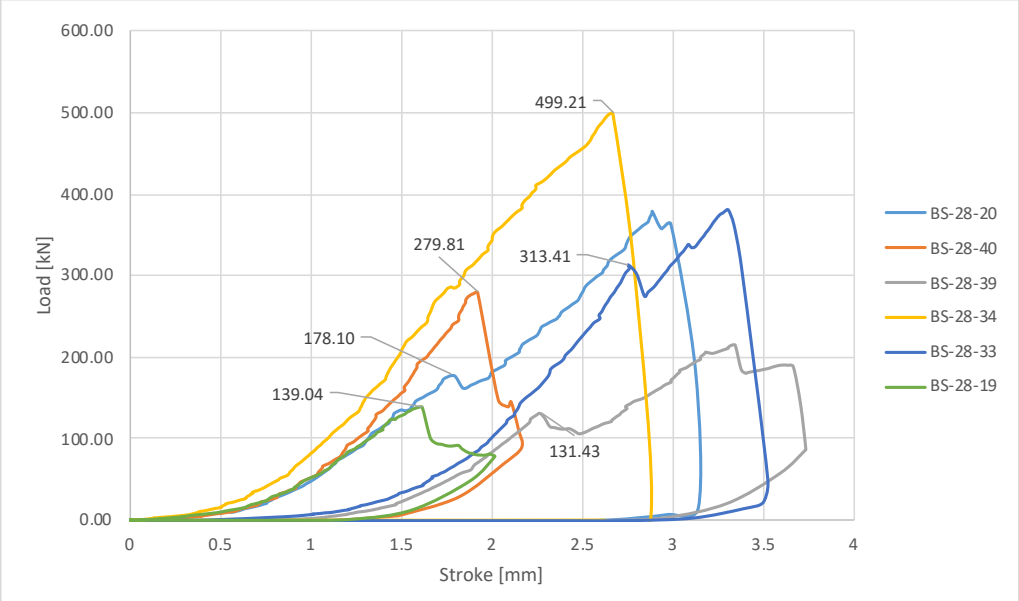

Figure A8.5 Load-stroke diagram for bi-shear test on day 28 after UHPC casting

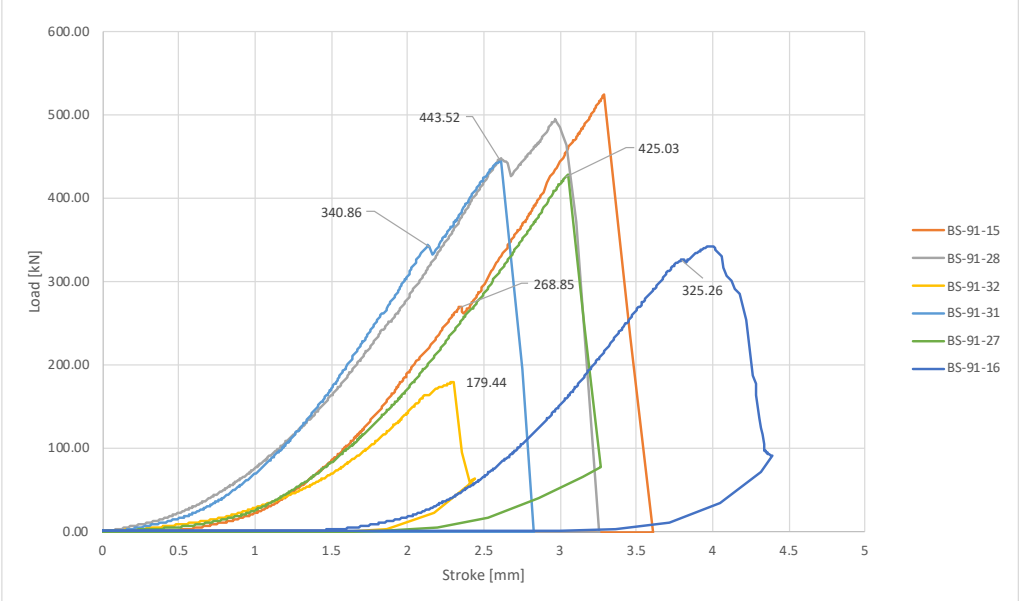

Figure A8.6 Load-stroke diagram for bi-shear test on day 91 after UHPC casting

9. Durability Direct Tension and Pull Off Test Results

Table A9.1 Summary of direct tension test results after FT cycles

Specimen	Tensile Strength (MPa)	Average Tensile Strength (MPa)	Mode of Failure	STD (MPa)	COV
FT-60	2.70	4.0	A	0.9	22 %
	4.41		B		
	4.54		B		
	4.47		A		
FT-120	3.60	3.8	B	0.6	15 %
	4.58		B		
	3.25		A		
	3.68		A		
FT-180	4.30	3.5	A	1.1	32 %
	3.22		A		
	4.50		A		
	Exp. error		C		
	2.06		B		
Control	3.57	3.7	A	0.4	12 %
	3.86		B		
	4.25		B		
	3.22		A		

Note: A: PIF, B: HSC failure, C: Epoxy failure

10. Durability Pull Off Test Results

Table A10.1 Summary of pull off test results after FT cycles

Specimen	Tensile Strength (MPa)	Average Tensile Strength (MPa)	Mode of Failure	STD (MPa)	COV
FT-60	3.27	4.44	A	0.98	22 %
	5.6		A		
	4.73		B		
	4.16		A		
FT-120	3.22	4.05	B	0.65	16 %
	4.62		B		
	3.92		B		
	3.7		B		
	4.77		A		
FT-180	4.82	4.58	B	0.61	13 %
	4.78		B		
	5.1		A		
	4.65		A		
Control	5.37	4.58	B	0.63	14 %
	3.97		B		
	4.79		B		
	4.2		B		

Note: A: PIF, B: HSC failure

11. Durability Slant Shear Tests Results

Table A11.1 Summary of slant shear test results after FT cycles

Specimen	Slant Shear Strength (MPa)	Average (MPa)	Mode of Failure	Normal stress σ (MPa)	Shear stress τ (MPa)	Average σ	Average τ	STD σ	STD τ	σ and τ COV
FT-60	23.6	31.7	B	12.2	21.1	16.6	28.7	4.0	6.9	24 %
	38.9		B	20.0	34.6					
	Exp. error		-	-	-					
	32.5		B	17.6	30.5					
FT-120	19.5	29.3	B	10.1	17.5	15.1	26.2	3.8	6.5	25 %
	30.3		B	16.0	27.7					
	29.8		B	15.3	26.5					
	37.5		B	19.2	33.2					
FT-180	34.5	32.1	B	17.8	30.9	16.5	28.5	2.5	4.4	15 %
	26.4		A	13.5	23.4					
	29.8		B	15.3	26.6					
	37.6		B	19.2	33.2					
Control	37.4	30.8	B	18.7	32.4	15.8	27.3	2.4	4.2	15 %
	25.6		B	13.2	22.8					
	28.2		A	14.6	25.4					
	31.8		B	16.7	28.9					
FT-60-C	41.2	38.5	B	21.3	36.9	19.6	34.0	3.7	6.4	19 %
	27.0		B	14.1	24.4					
	42.6		A	21.3	36.9					
	43.2		B	21.7	37.6					
FT-120-C	45.4	41.9	B	23.6	40.8	21.6	37.5	2.4	4.1	11 %
	38.1		B	19.6	33.9					
	37.6		B	19.6	33.9					
	46.5		B	23.8	41.3					
FT-180-C	45.9	40.7	A	23.4	40.5	20.6	35.7	2.0	3.4	10 %
	40.6		B	20.3	35.1					
	38.5		A	19.7	34.1					
	37.8		B	19.0	32.9					

Note: σ = normal stress; τ = shear stress; A: HSC and bond interface failed; B: HSC failed

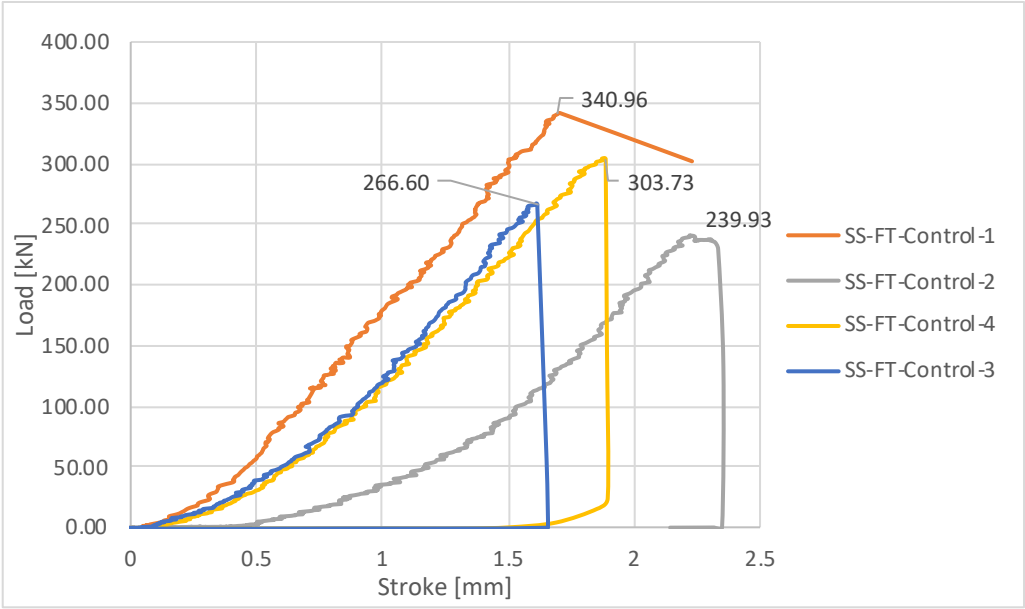

Figure A11.1 Load-stroke diagram for control slant shear test

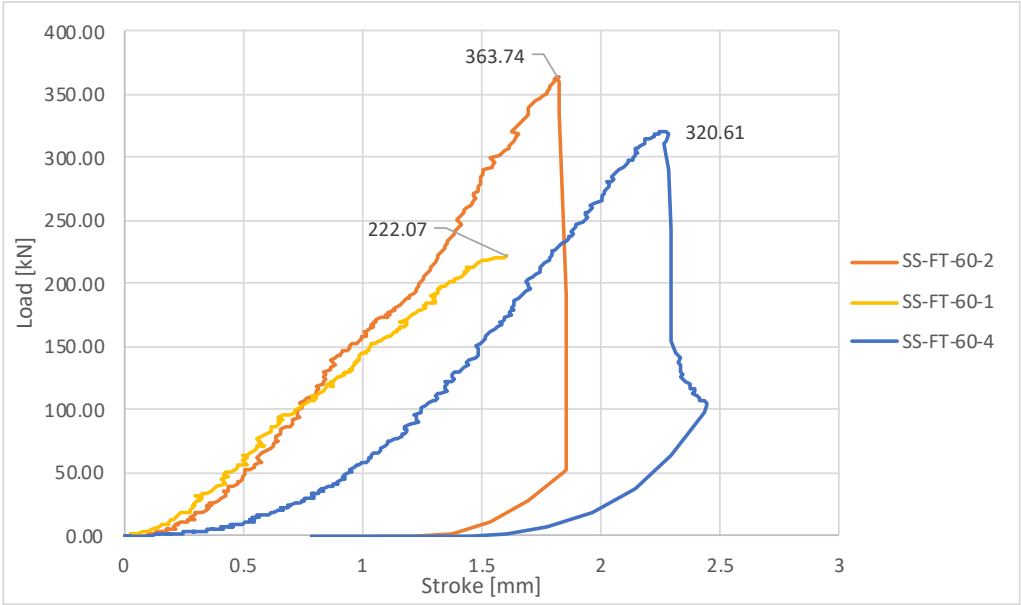

Figure A11.2 Load-stroke diagram for slant shear test after 60 FT cycles

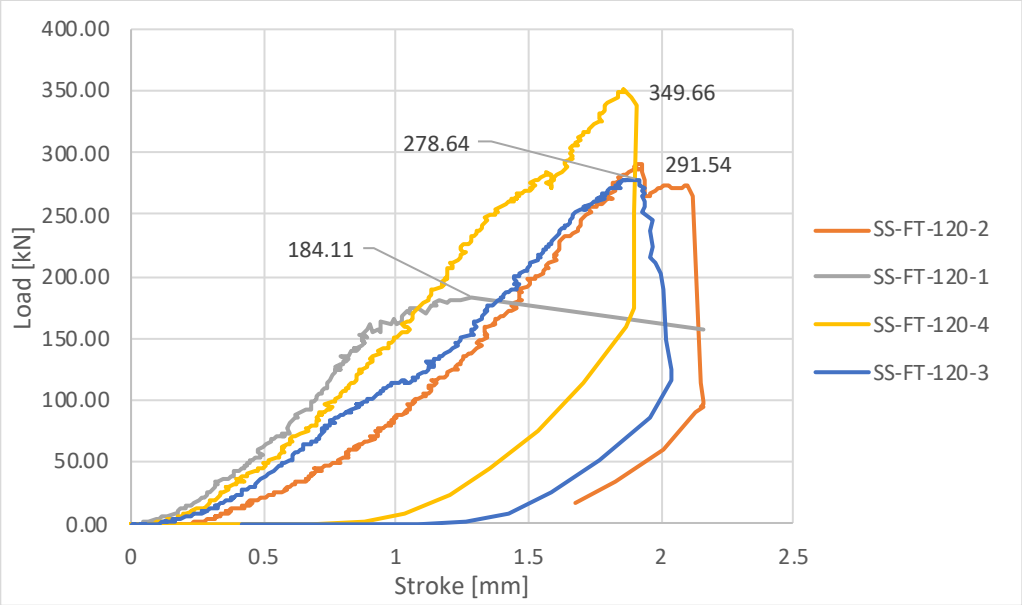

Figure A11.3 Load-stroke diagram for slant shear test after 120 FT cycles

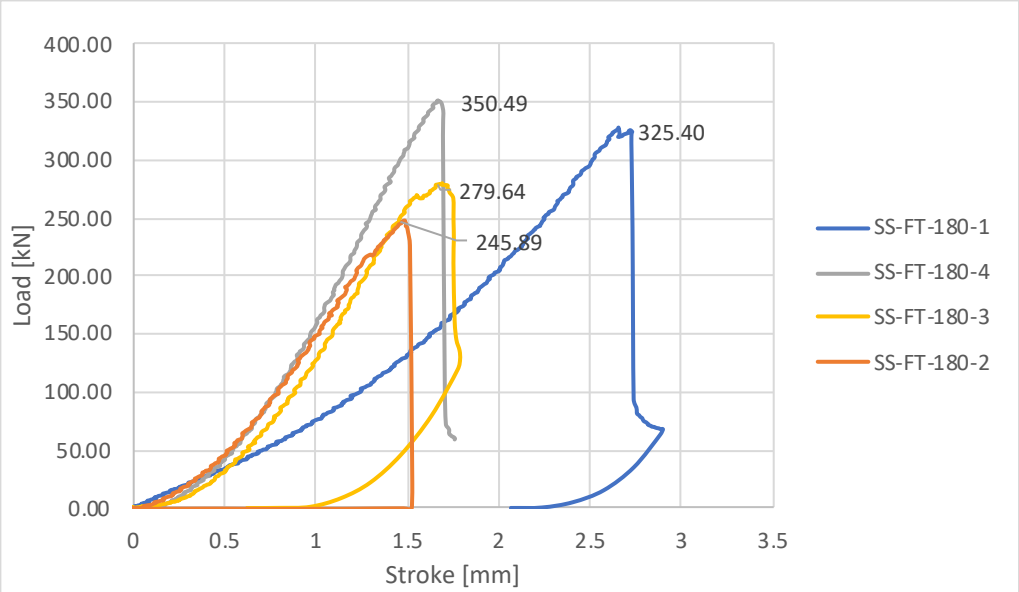

Figure A11.4 Load-stroke diagram for slant shear test after 180 FT cycles

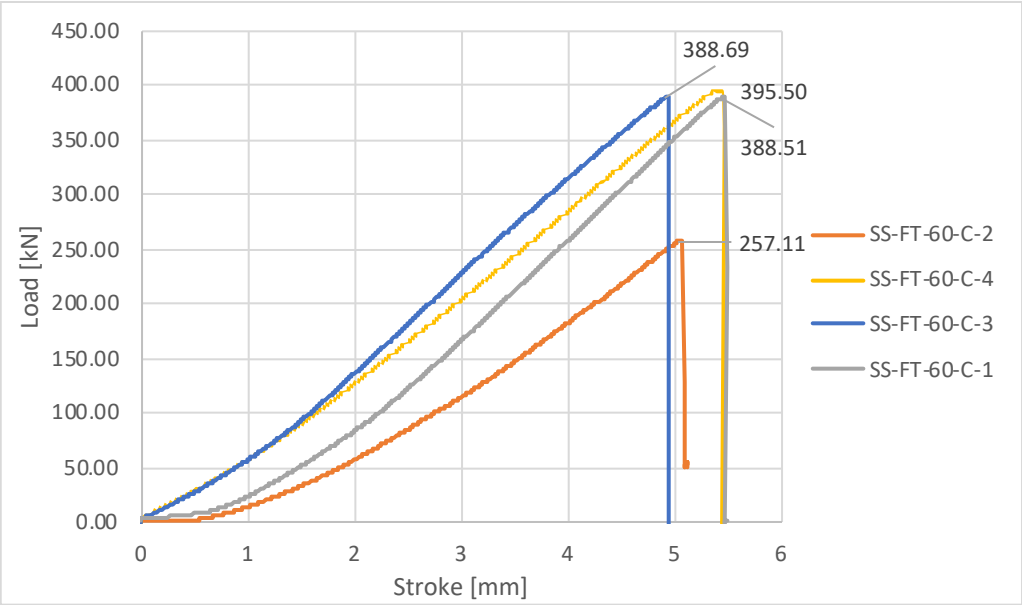

Figure A11.5 Load-stroke diagram for slant shear tested in the chamber after 60 FT cycles

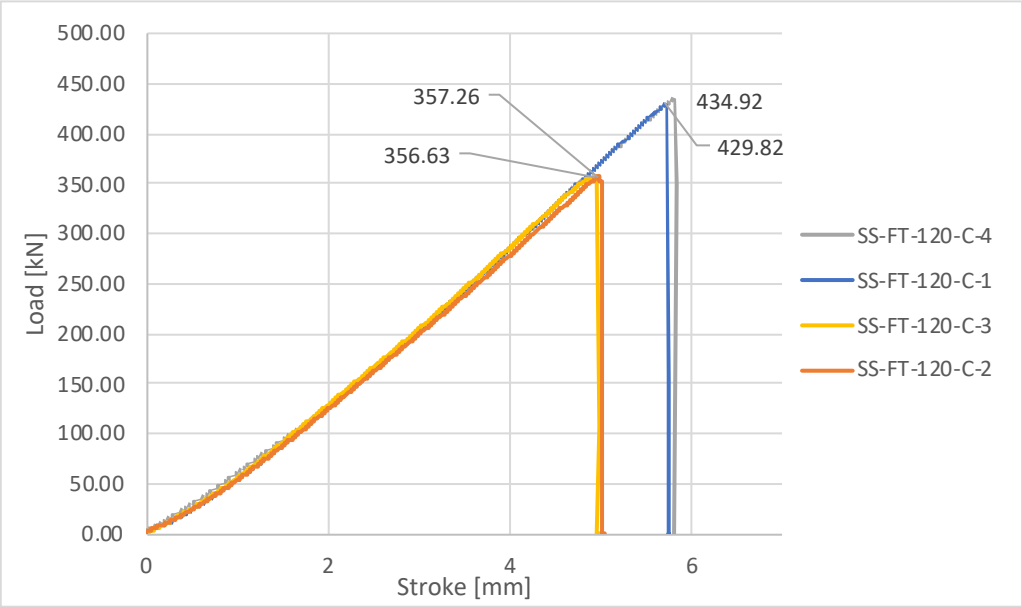

Figure A11.6 Load-stroke diagram for slant shear tested in the chamber after 120 FT cycles

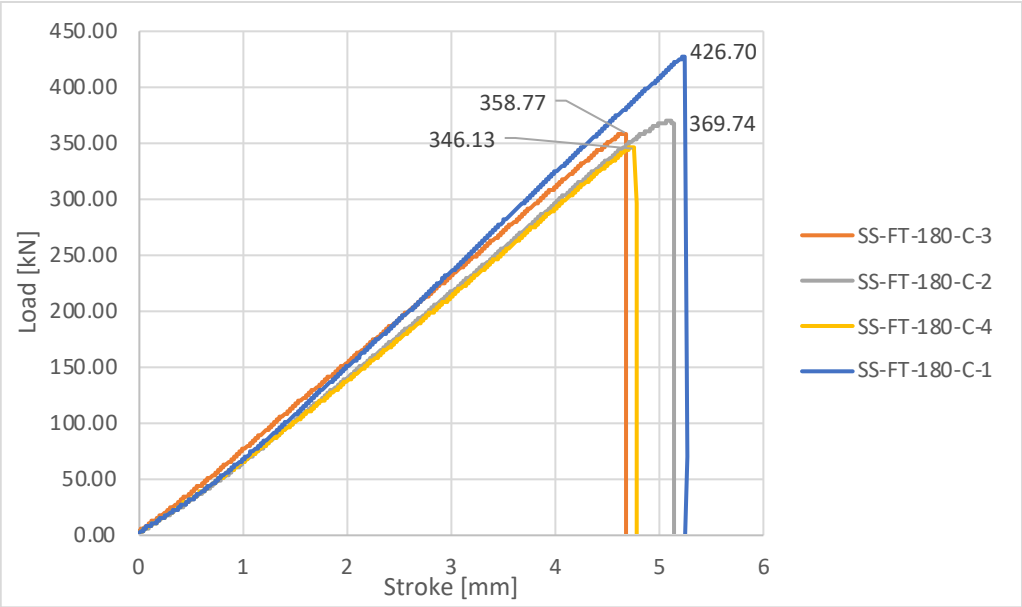

Figure A11.7 Load-stroke diagram for slant shear tested in the chamber after 180 FT cycles

12. Durability Bi-Shear Tests Results

Table A12.1 Summary of bi-shear test results after FT cycles

Specimen	Shear Strength (MPa)	Average Shear (MPa)	STD (MPa)	COV
FT-60	8.55	6.64	1.89	29%
	4.74			
	5.45			
	8.16			
FT-120	8.53	8.80	2.08	24%
	9.62			
	6.07			
	10.98			
FT-180	7.15	6.46	1.29	20%
	7.92			
	5.17			
	5.62			
Control	9.77	7.68	1.77	23%
	5.81			
	8.44			
	6.70			
FT-60-C	6.91	6.91	1.36	20%
	4.99			
	7.79			
	7.94			
FT-120-C	9.86	10.33	1.80	17%
	11.43			
	12.03			
	8.01			
FT-180-C	11.43	9.05	3.43	38%
	12.55			
	6.44			
	5.79			

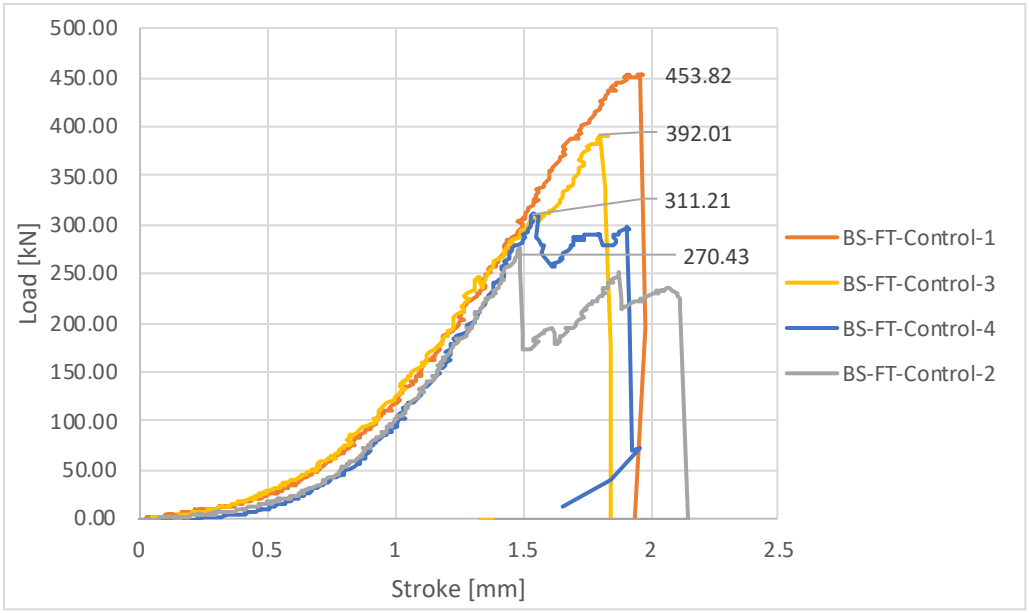

Figure A12.1 Load-stroke diagram for control bi-shear test

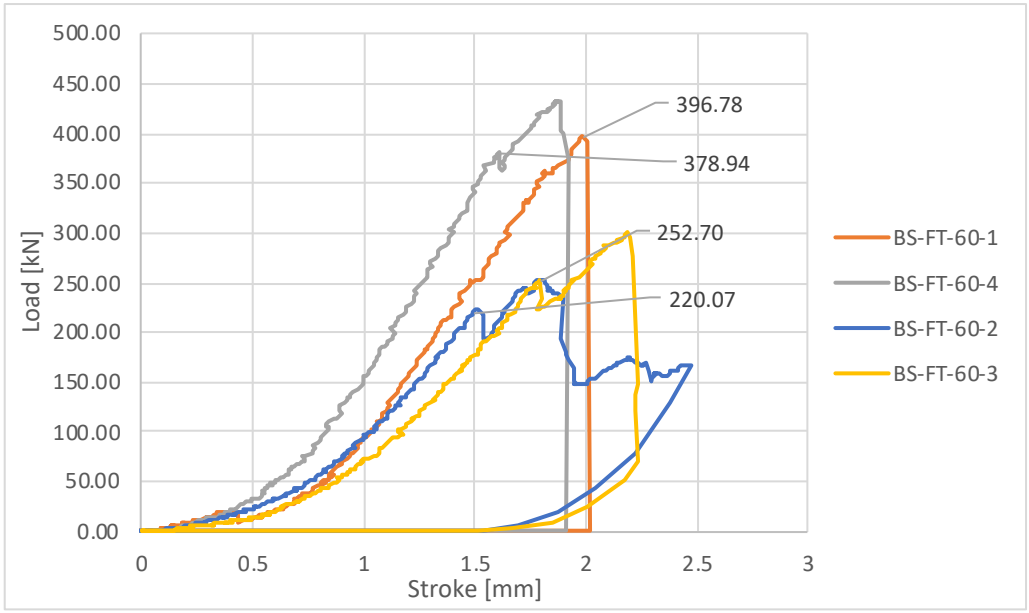

Figure A12.2 Load-stroke diagram for bi-shear test after 60 FT cycles

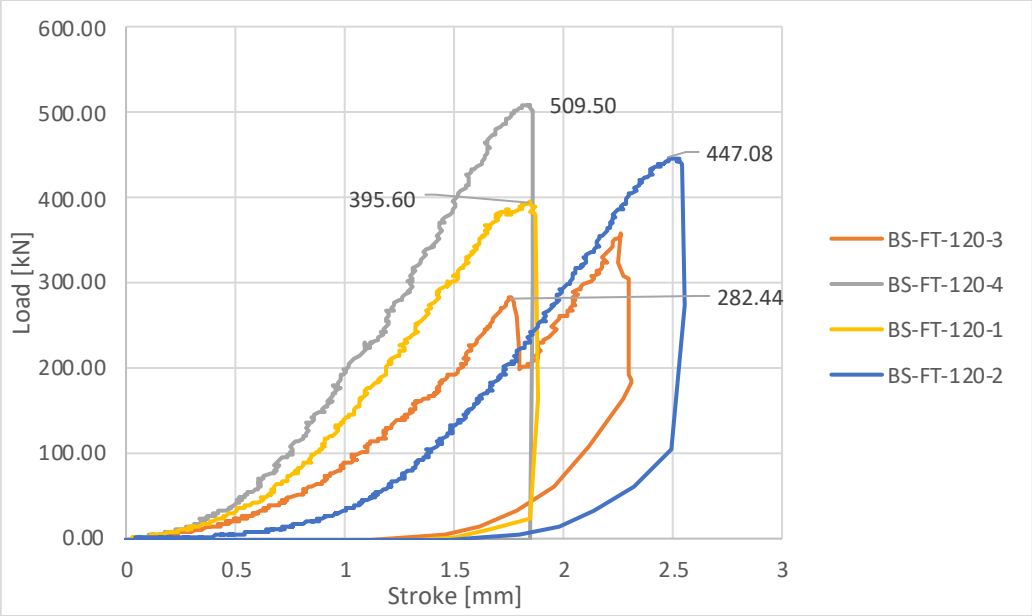

Figure A12.3 Load-stroke diagram for bi-shear test after 120 FT cycles

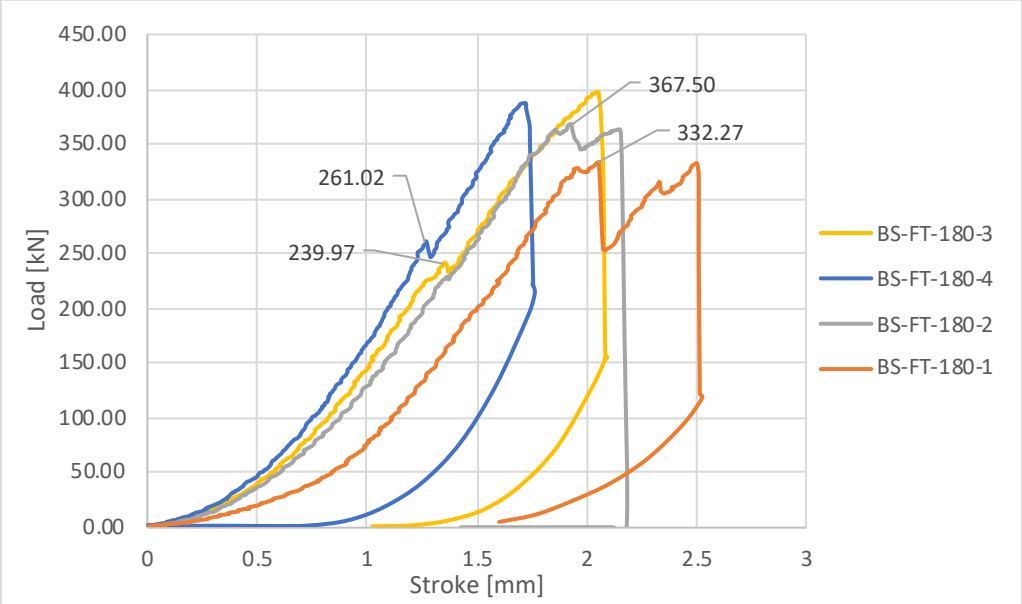

Figure A12.4 Load-stroke diagram for bi-shear test after 180 FT cycles

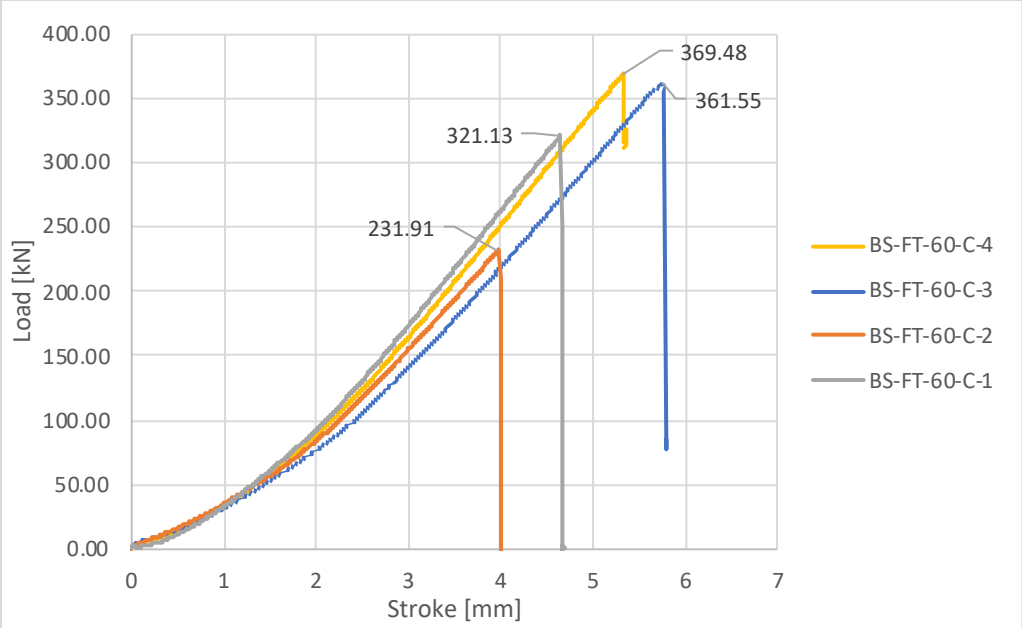

Figure A12.5 Load-stroke diagram for bi-shear tested in the chamber after 60 FT cycles

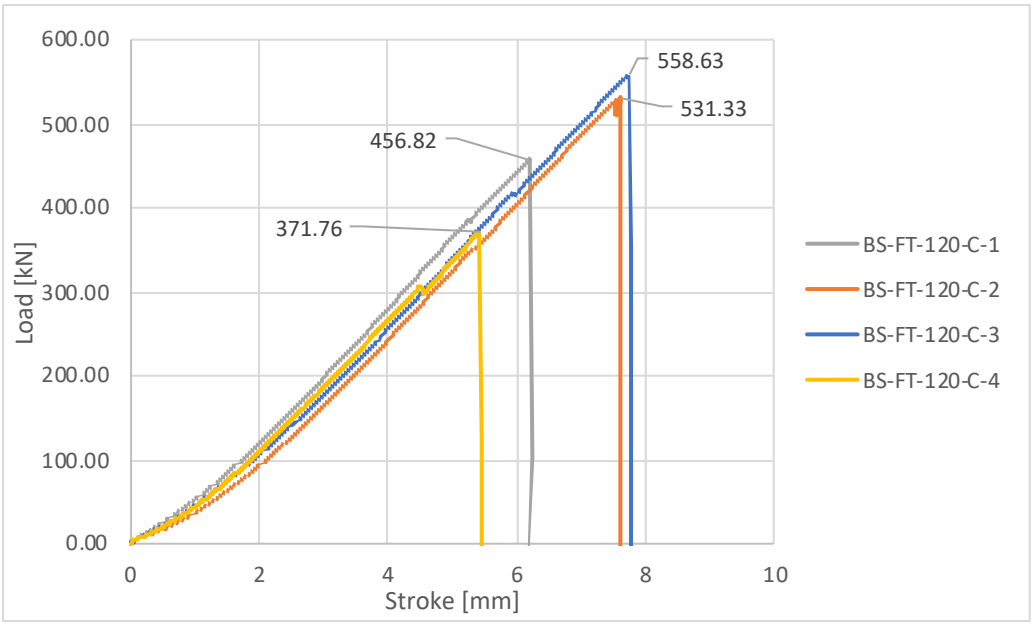

Figure A12.6 Load-stroke diagram for bi-shear tested in the chamber after 120 FT cycles

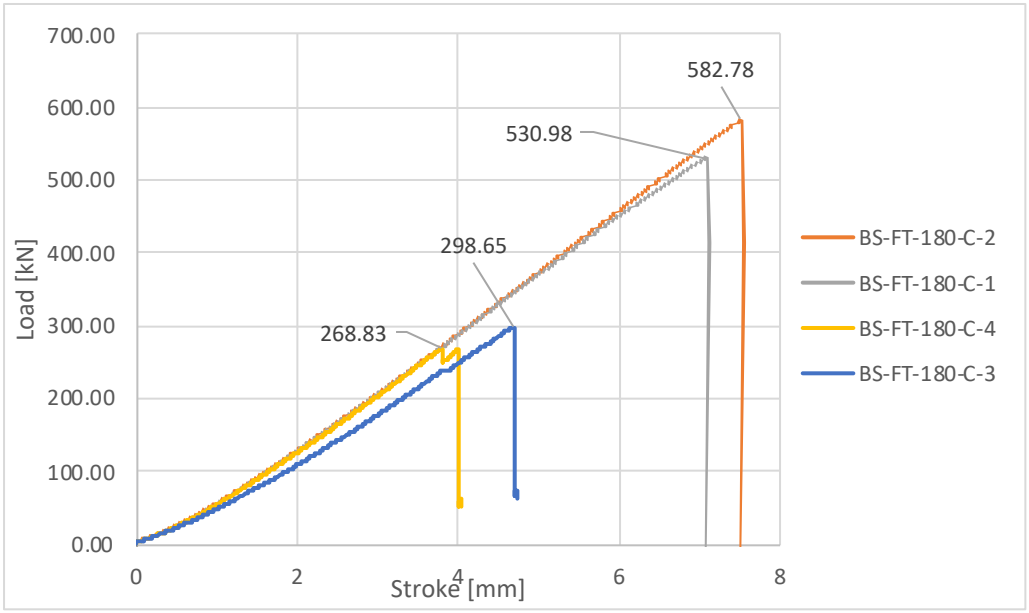

Figure A12.7 Load-stroke diagram for bi-shear tested in the chamber after 180 FT cycles

13. Early Age Bond Tests Cohesion and Friction Coefficient – Using 5th Percentile Values

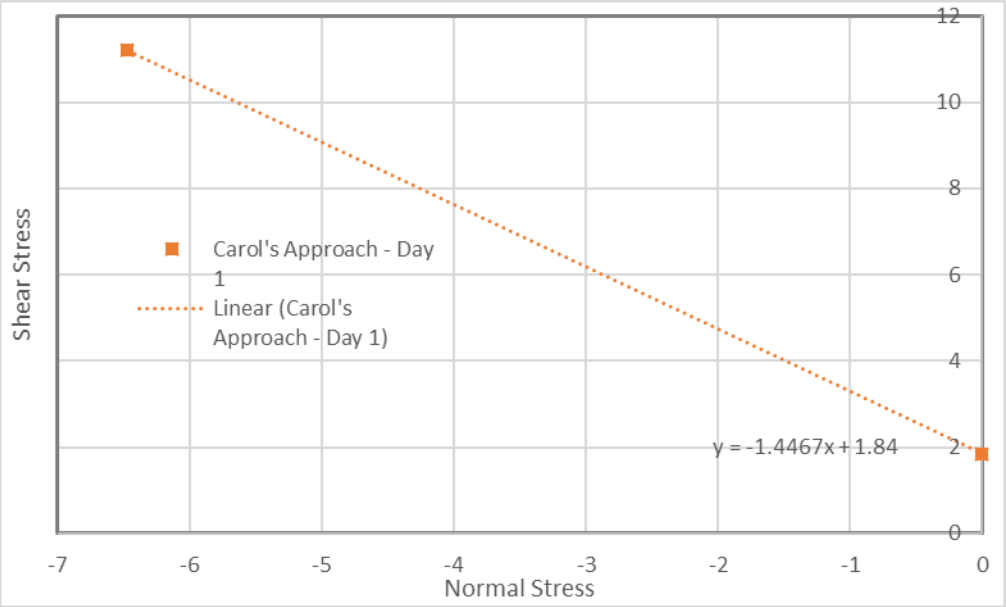

Figure A13.1 Day 1 cohesion and friction coefficient linear analysis

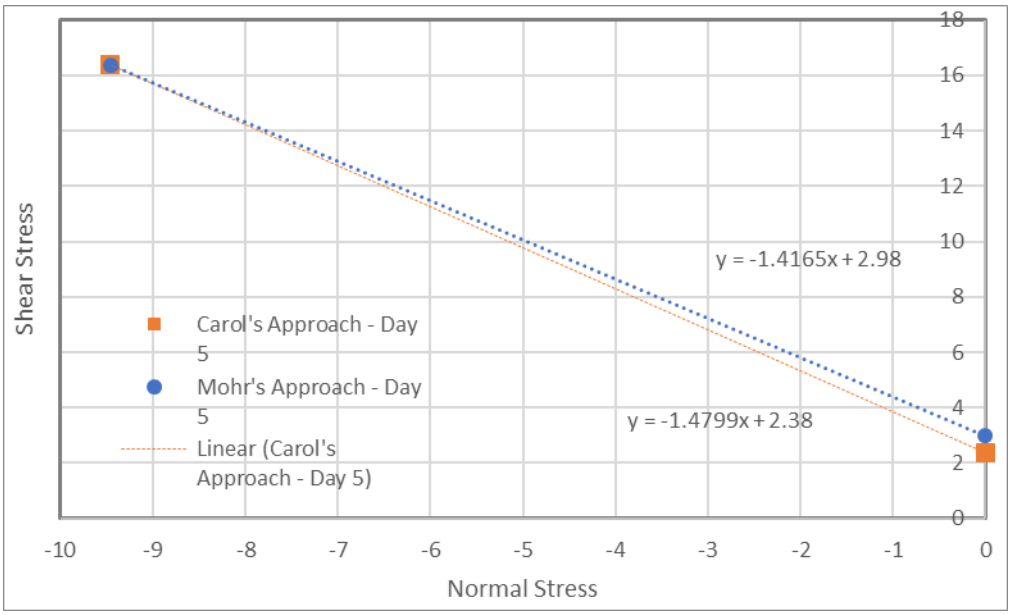

Figure A13.2 Day 5 cohesion and friction coefficient linear analysis

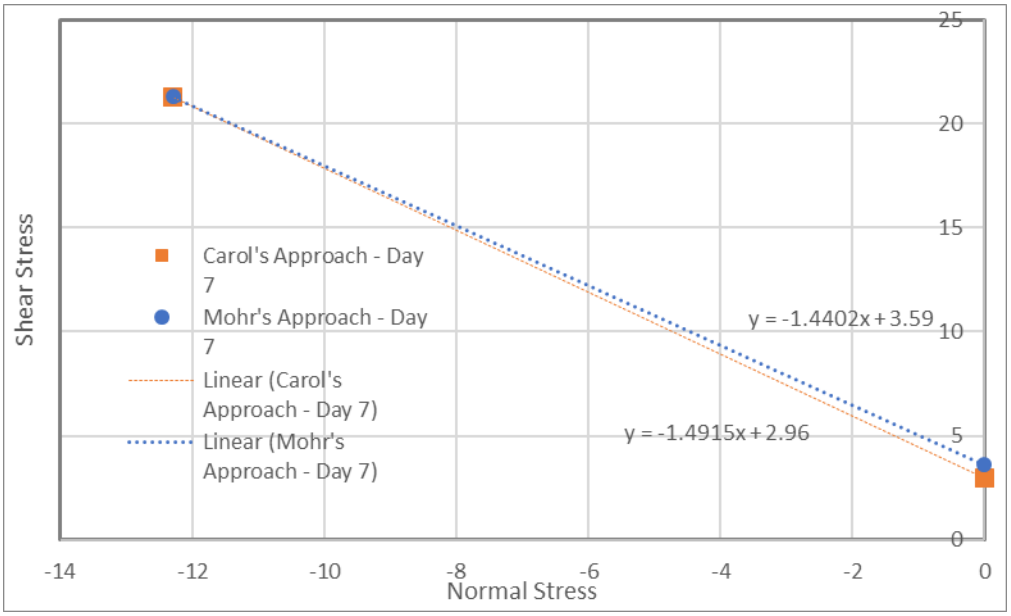

Figure A13.3 Day 7 cohesion and friction coefficient linear analysis

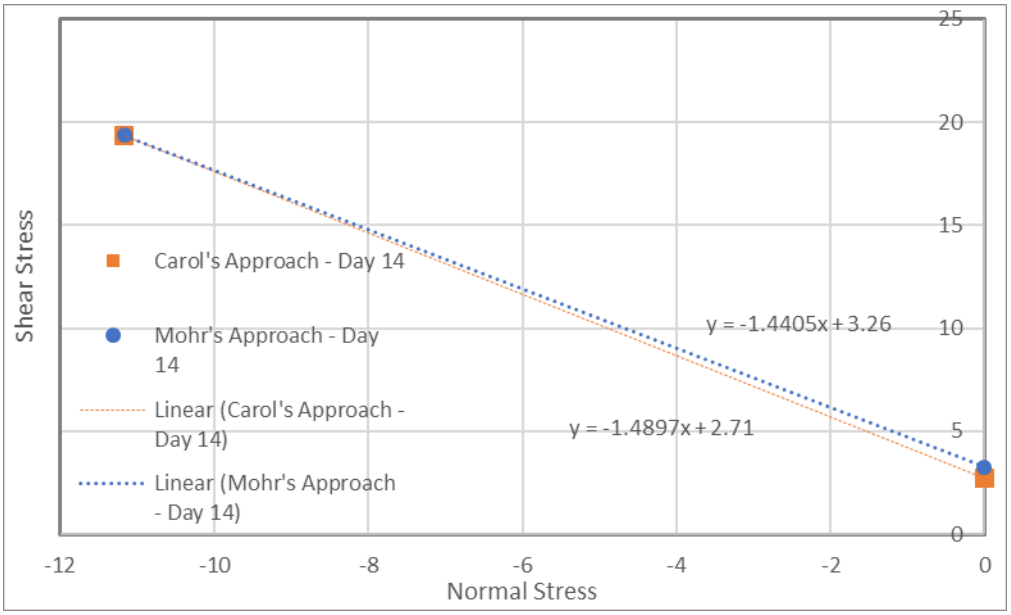

Figure A13.4 Day 14 cohesion and friction coefficient linear analysis

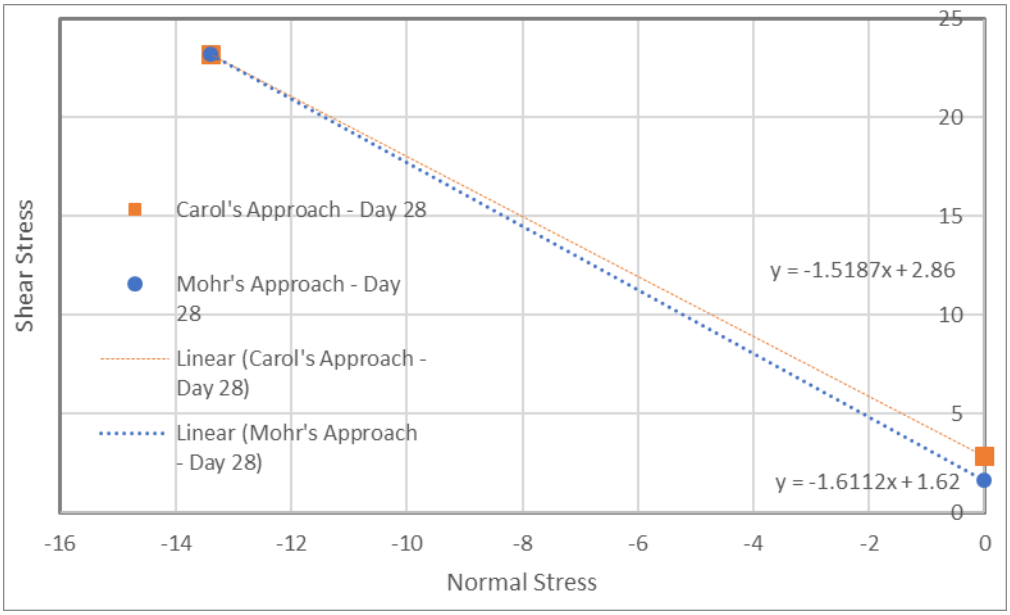

Figure A13.5 Day 28 cohesion and friction coefficient linear analysis

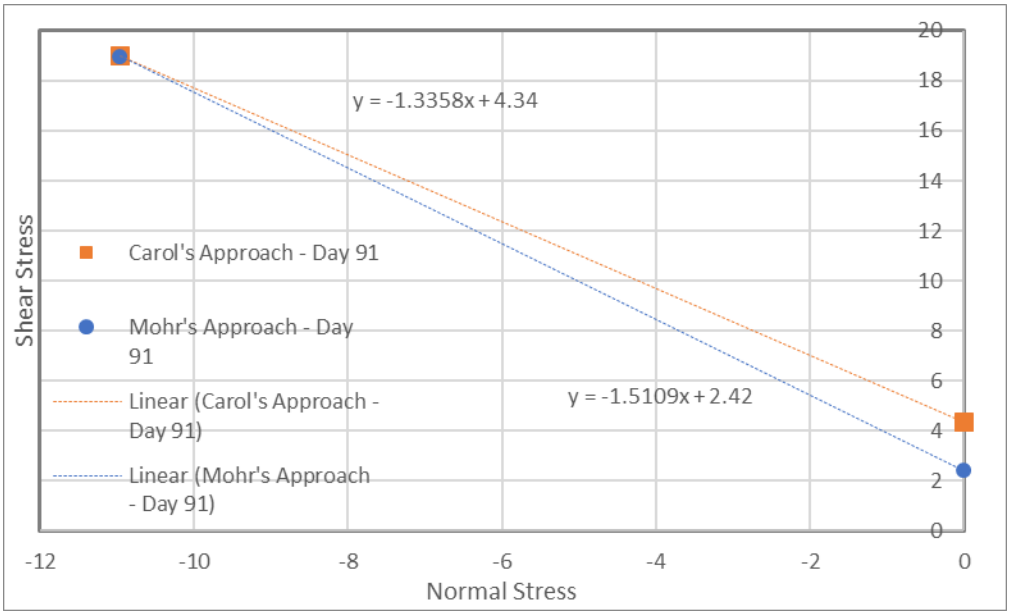

Figure A13.6 Day 91 cohesion and friction coefficient linear analysis

14. Durability Bond Tests Cohesion and Friction Coefficient – Using 5th Percentile Values

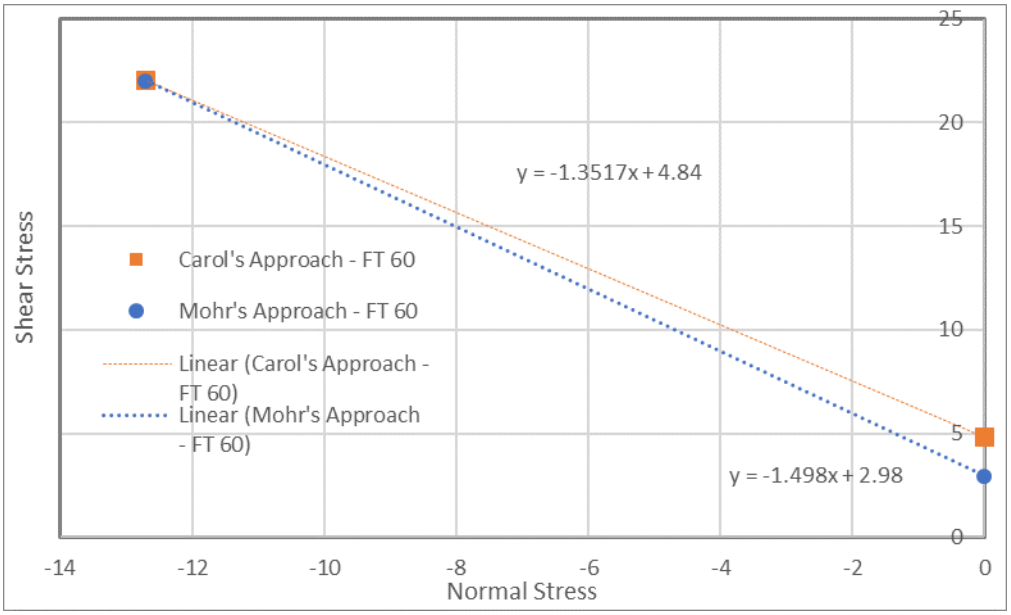

Figure A14.1 FT-60 cohesion and friction coefficient linear analysis

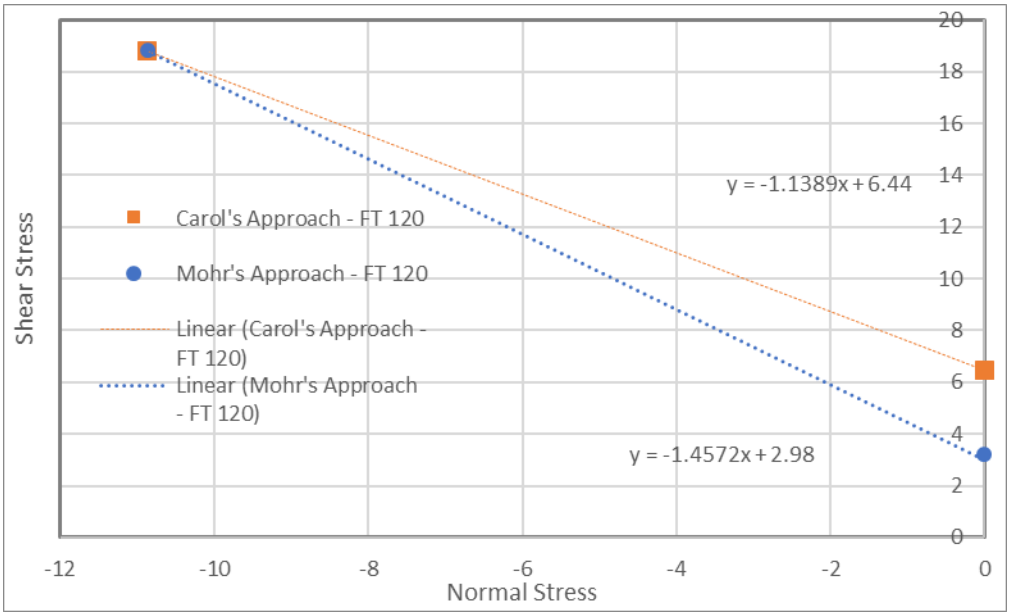

Figure A14.2 FT-120 cohesion and friction coefficient linear analysis

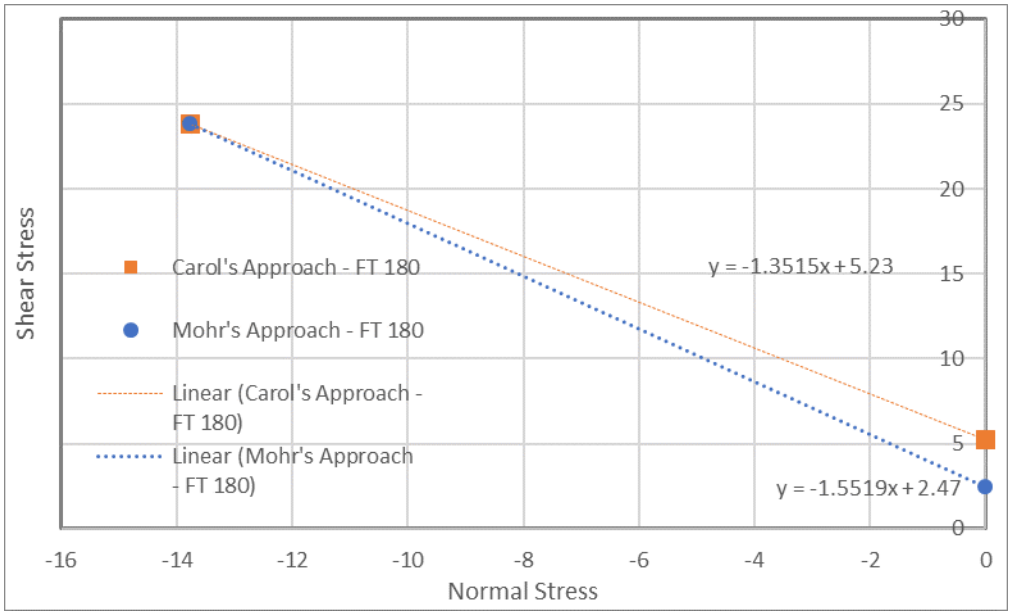

Figure A14.3 FT-180 cohesion and friction coefficient linear analysis

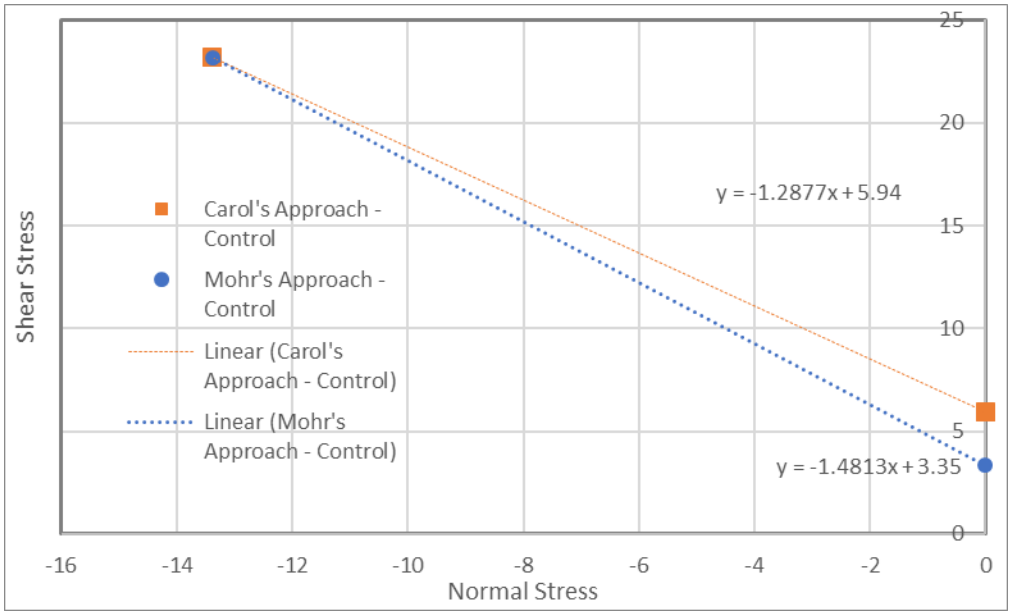

Figure A14.4 Control sample cohesion and friction coefficient linear analysis

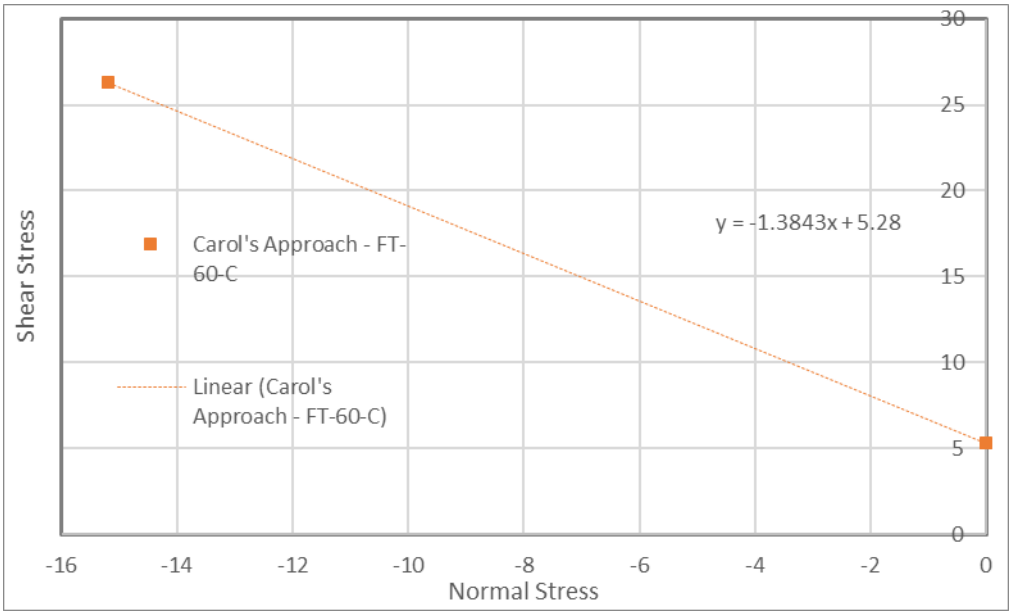

Figure A14.5 FT-60-C cohesion and friction coefficient linear analysis

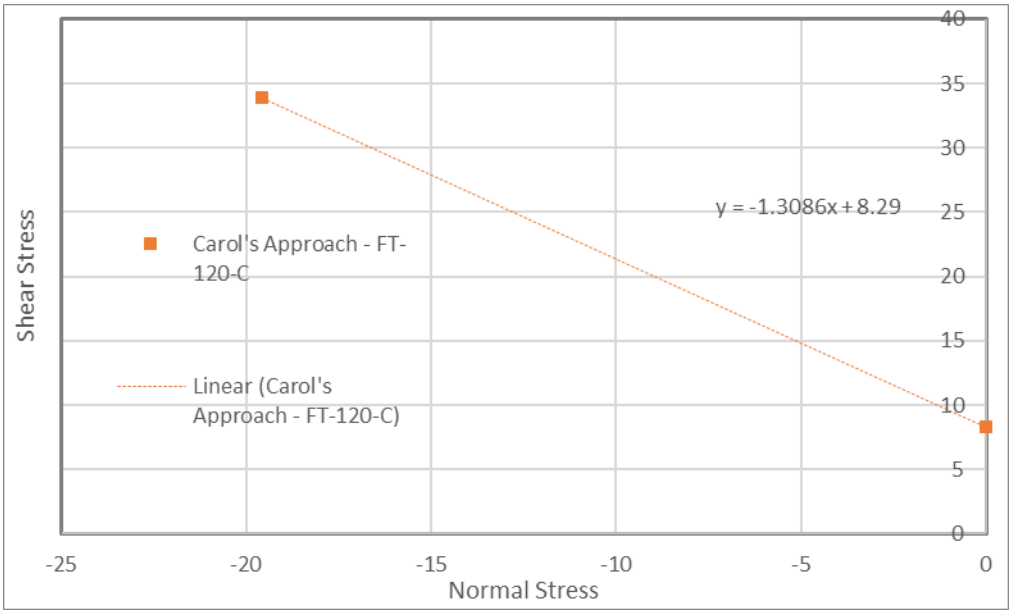

Figure A14.6 FT-120-C cohesion and friction coefficient linear analysis

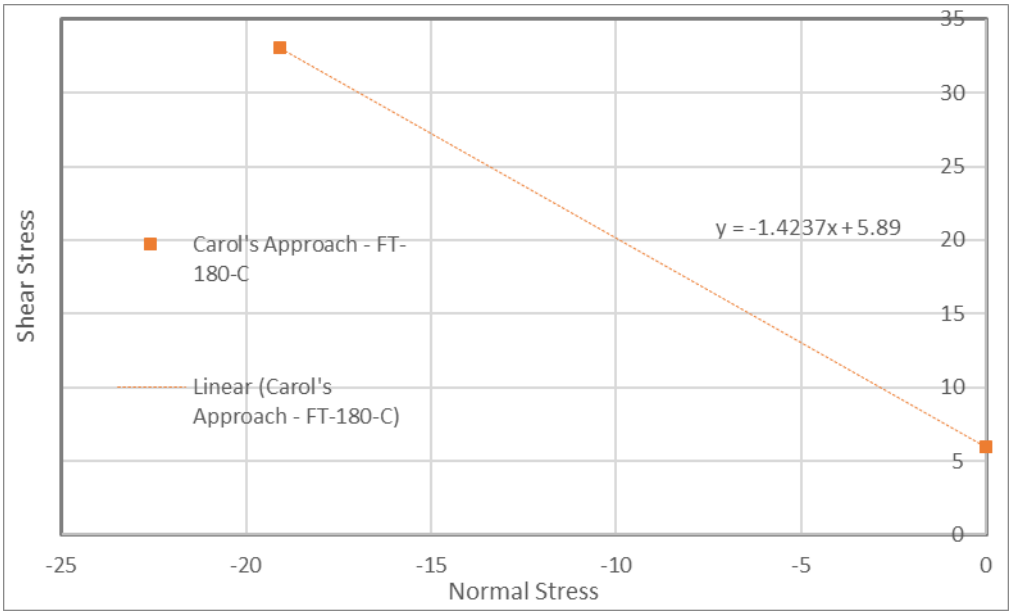

Figure A14.7 FT-180-C cohesion and friction coefficient linear analysis

15. Beam 5 Direct Tension Test Specimen Interface Parameters

Table A15.1 Direct Tension Test Specimen Interface Parameters

Specimen ID	R_a (mm)	MTD (mm)	MPD (mm)	Plane Surface Area (mm^2)	True Surface Area (mm^2)	Interfacial Area Ratio
1	1.49	3.31	1.84	3612.06	8323.01	1.3
2	1.81	3.35	2.06	3549.37	8020.56	1.26
3	1.73	3.11	2.20	3519.84	8426.98	1.39
4	1.28	2.52	1.59	3541.98	8106.6	1.29
5	1.72	3.14	2.23	3380.98	7907.33	1.34
6	1.65	2.80	1.98	3591.62	8733.65	1.43
7	1.67	3.38	2.05	3291.55	7640.7	1.32
8	1.36	3.14	1.96	3391.38	7732.17	1.28
9	1.07	2.46	1.53	3547.25	7619.85	1.15
10	1.59	2.91	1.88	3462.22	8188.79	1.37
11	2.06	3.28	2.55	3546.17	8612.53	1.43
12	1.16	2.38	1.60	3454.28	7440.98	1.15
13	1.16	2.54	1.58	3565.19	7776.21	1.18
14	1.94	3.44	2.29	3422.12	8405.99	1.46
15	1.36	2.80	1.77	3394.64	7905.87	1.33
16	1.54	2.92	1.80	3372.34	7869.33	1.33
17	1.41	2.66	1.77	3509.88	8042.66	1.29
18	1.36	2.63	1.85	3575.82	8101.7	1.27
19	1.42	2.67	1.99	3576.83	8138.99	1.28
20	2.12	3.76	2.35	3412.66	8343.63	1.44
21	1.20	2.44	1.66	3551.48	7541.34	1.12
22	1.19	2.33	1.67	3473.79	7568.7	1.18
23	1.31	2.72	1.74	3537.24	8133.09	1.3
24	1.67	2.52	1.83	3535.95	8349.49	1.36
25	1.69	2.78	1.99	3575.27	8092.62	1.26
26	1.32	2.98	1.83	3563.63	8353.36	1.34
27	1.33	2.54	1.73	3551.91	7912.53	1.23
28	1.38	2.76	1.67	3345.34	7792.47	1.33
29	1.24	2.56	1.71	3573.07	8009.4	1.24
30	1.49	2.36	1.76	3577.93	8016.8	1.24
31	2.05	3.18	2.15	3446.51	8367.4	1.43
32	1.93	3.79	2.31	3555.18	8549.31	1.4
33	1.98	3.76	2.30	3546.57	8319.58	1.35
34	1.76	2.85	1.94	3475.6	8059.43	1.32

35	2.00	4.10	2.47	3525.12	8578.48	1.43
36	1.68	3.16	1.97	3431.87	7734.2	1.25
37	1.68	3.34	2.32	3589.6	8547.65	1.38
38	1.41	2.58	1.75	3513.99	8358.75	1.38
39	1.48	2.81	2.01	3581.07	8089.96	1.26
40	2.11	3.47	2.36	3390.16	8537.75	1.52
Average	1.57	2.96	1.95	3501.49	8106.25	1.32

16. Beam 4 Bond Direct Tension Test Specimen Interface Parameters

Figure A16.1 Direct Tension Test Specimen Interface Parameters

Specimen ID	R_a (mm)	MTD (mm)	MPD (mm)	Plane Surface Area (mm^2)	True Surface Area (mm^2)	Interfacial Area Ratio
1	1.03	1.95	1.50	3539.86	7594.44	1.15
2	0.88	1.86	1.29	3448.98	6643.63	0.93
3	0.96	2.05	1.45	3646.03	8051.87	1.21
4	0.97	2.17	1.43	3570.82	8456.5	1.37
5	0.89	1.96	1.29	3567.74	6916.84	0.94
6	0.92	1.99	1.43	3624.72	7621.82	1.1
7	0.81	2.05	1.26	3426.6	6991.08	1.04
8	1.02	2.01	1.29	3172.57	6554.1	1.07
9	1.18	2.16	1.51	3510.16	7324.05	1.09
10	0.71	1.94	1.16	3541.9	6777.53	0.91
11	0.87	1.90	1.24	3445.08	6787.62	0.97
12	0.84	1.95	1.29	3433.7	6787.44	0.98
13	0.83	2.01	1.28	3520.81	6625.13	0.88
14	0.93	1.78	1.35	3496.71	6996.47	1
15	0.92	2.35	1.39	3685	8146.26	1.21
16	0.98	2.03	1.33	3580.05	7578.32	1.12
17	1.11	2.24	1.45	3563.08	7034.81	0.97
18	1.13	2.06	1.60	3542.79	7618.49	1.15
19	0.95	1.95	1.61	3511.03	7564.01	1.15
20	0.84	1.77	1.33	3502.17	7292.8	1.08
21	1.06	2.03	1.40	3446.5	7410.45	1.15
22	0.71	1.64	1.18	3463.04	7139.26	1.06
23	0.77	1.87	1.17	3514.29	7289.46	1.07
24	0.92	2.01	1.45	3543.51	7421.07	1.09
25	1.05	2.09	1.47	3494	7588.07	1.17
26	0.92	2.17	1.34	3551.4	7566.54	1.13
27	1.10	2.02	1.55	3577.28	7728.57	1.16
28	0.94	1.98	1.43	3535.69	7614.24	1.15
29	0.79	1.94	1.39	3492.55	7363.17	1.11
30	0.75	1.82	1.20	3526.07	7338.03	1.08
31	0.80	1.67	1.20	3537.47	7518.42	1.13
32	0.80	1.85	1.35	3594.31	7654.23	1.13
33	0.85	1.87	1.28	3449.16	7260.6	1.11

34	0.89	1.95	1.58	3538.77	7497.26	1.12
35	1.11	2.28	1.50	3580.94	7817.14	1.18
36	0.97	2.34	1.42	3440.11	7525.06	1.19
37	0.90	1.76	1.33	3507.7	7476.01	1.13
38	0.99	1.81	1.37	3585.85	7774.97	1.17
39	1.07	1.90	1.43	3589.59	7768.05	1.16
40	0.86	2.20	1.25	3632.2	7832.4	1.16
Average	0.93	1.98	1.37	3523.26	7398.66	1.10